Escola de Camins
Escola Tècnica Superior d'Enginyeria de Camins, Canals i Ports
UPC BARCELONATECH

TREBALL FINAL DE MÀSTER

Model-based evaluation and optimization of high-rate algae ponds for wastewater treatment at demonstrative scale

Treball realitzat per:
Àlvaro Gallego Puerta

Dirigit per:
Rubén Díez Montero
Fabiana Lopes Del Rei Passos
Ivet Ferrer Martí

Màster en:
Enginyeria ambiental

Barcelona, 29 juny 2020

Departament d'Enginyeria Civil i Ambiental

Prefaci

El següent treball ha estat realitzat en el Grup d'Enginyeria i Microbiologia Mediambientals (GEMMA) del Departament d'Enginyeria Civil i Ambiental de la UPC. S'ha portat a terme en col·laboració amb el Departamento de Engenharia Sanitária e Ambiental de la Universidade Federal de Minas Gerais (UFMG, Belo Horizonte, Brasil), en el marc del projecte "Strategies for Enhancing Sustainable Treatment of Wastewater and Food Waste" (2019-B017), gracies al finançament del Centre de Cooperació per al Desenvolupament (CCD) de la UPC. El treball ha estat redactat en format d'article científic i en anglès per tal de facilitar la compressió i l'intercanvi d'idees entre totes les parts involucrades.

Preface

The present Master Thesis was carried out in the Group of Environmental Engineering and Microbiology (GEMMA), at the Civil and Environmental Engineering Department of UPC. It was carried out in collaboration with the Department of Sanitary and Environmental Engineering from Universidade Federal de Minas Gerais (UFMG, Belo Horizonte, Brasil), in the framework of the project "Strategies for Enhancing Sustainable Treatment of Wastewater and Food Waste" (2019-B017), funded by the Centre for Development Cooperation (CCD) of UPC. The report has been prepared as a scientific paper in English to ease comprehension between all the parties involved.

Index

Abstract 4
1. Introduction 5
2. State of the art 6
2.1 Microalgae-based wastewater treatment 6
2.1.1 Removal of organic pollutants 8
2.1.2 Nitrogen and phosphorous removal 8
2.1.3 Removal of heavy metals 9
2.1.4 Removal of pathogens 9
2.1.5 Remediation of emerging contaminants 10
2.2 Anaerobic wastewater treatment 10
2.2.1 Anaerobic digestion 10
2.2.2 Wastewater treatment based on anaerobic digestion 12
2.3 Combined UASB-HRAP systems for wastewater treatment 14
2.4 Modelling of microalgae-based wastewater treatment systems 14
3. Materials and methods 15
3.1 High-Rate Algae Pond at demonstrative scale 15
3.2 BIO_ALGAE 2 model 16
3.2.1 Description 16
3.2.2 Model implementation 19
3.2.3 Stoichiometric and kinetic parameters and model calibration 20
3.2.4 Definition and simulation of scenarios 20
4. Results 21
4.1 Calibration 21
4.2 Results of the simulations 24
4.2.1 Biomass production 24
4.2.2 Nitrogen and phosphorus 26
5. Conclusions 28
6. Acknowledgements 29
7. Bibliography 29
Annex I. Graphs of the simulations for each scenario 33
Total suspended solids (TSS) 33
Nitrogen 39
Phosphorus 45
Annex II. Model components 51
Mathematical description of the processes of the model (processes rates) 51
Matrix of stoichiometric parameters that relates processes and components through stoichiometric coefficients 54
Values of biokinetic, chemical and physic parameters 55
Values of fractions of carbon, hydrogen, oxygen and nitrogen in microalgae and bacteria biomass 57
Mathematical expressions of the stoichiometric coefficients of each process 58

Abstract

High-rate algae ponds (HRAP) for wastewater treatment have received great interest, as they are a microalgae-based treatment system that optimize the growth of microalgae, have less space requirements than facultative and maturation ponds and have proven to successfully treat a variety of wastewaters. A new demonstrative-scale HRAP (45 to 75 m^3) is currently under construction at the Universidade Federal de Minas Gerais, Brazil. In the present study the performance of this HRAP is predicted by simulations employing the BIO_ALGAE 2 model, which has been adapted to the *Reaction Engineering* interface of the modelling software COMSOL. The influence of hydraulic retention time (HRT, from 3 to 8 d) and useful operational depth (0,3 or 0,5 m) was evaluated. The results showed that the best performance of the HRAP is achieved when operating with an HRT of 8 d, being slightly better when the depth was 0,5 m. With these conditions, the results suggest that the HRAP may be capable of accomplish with the Brazilian regulation for sewage treatment. Furthermore, the biomass produced could be harnessed for other purposes (as, for example, in the production of biogas or biofertilizer). However, when reducing the HRT under 8 d, the microalgal concentration in the system drastically decreases.

Keywords: microalgae-based treatment system, HRAP, upflow anaerobic sludge bed reactor, nitrogen and phosphorus removal, biomass growth, mathematical modelling, numerical simulations.

1. Introduction

Conventional wastewater treatment in activated sludge systems is a well stablished technology that achieves excellent results in terms of bioremediation. However, these processes involve high energy consumption, high operational costs and generate an important amount of waste sludge, which also has to be treated. For these reasons, during the last decades there has been and increasing interest in alternative treatments that may result more sustainable. Among these alternatives, microalgae-based treatments have long been studied, as they present several advantages. The photosynthetic activity involves the production of oxygen and the increase of pH, which enhances the conditions in the system for the removal of a variety of pollutants and reduces the aeration energy demand and cost. The activity of bacteria benefits from the presence of the microalgae, existing an exchange of substrates and may even form consortia (Alcántara et al., 2015; Roostaei et al., 2018). Furthermore, the growth of the microalgae involves the fixation of carbon dioxide and the excess biomass can be valorised in diverse ways, as for example the production of biofuels, biogas, bioifertilizers or fish food (Dani et al., 2016; Dineshkumar et al., 2019; Du et al., 2019; Mehrabadi et al., 2015; Park et al., 2011). Among the different reactor configurations, high-rate algae ponds (HRAP) are probably those of greatest interest, as they optimize the growth of microalgae, have less space requirements than facultative and maturation ponds and have proven to successfully treat a variety of wastewater types (Alcántara et al., 2015; de Godos et al., 2010; García et al., 2000; Tarlan et al., 2002).

Another alternative of high interest are anaerobic wastewater treatments, which take profit of anaerobic digestion to both treat the wastewater and produce biogas from the degradation of organic matter performed by microorganism in absence of oxygen (Lier et al., 2008; Meegoda et al., 2018). These systems are capable of treating wastewater with high chemical oxygen demand (COD) rates in a smaller space than conventional treatments and with lower operational cost. The main energy requirement of this type of treatment is for heating the reactor, which is usually required to perform the anaerobic digestion. However, in warm climates with high ambient temperatures, heating could be avoided. The most successful example of anaerobic reactor is the upflow anaerobic sludge bed reactor (UASB), whose configuration allows high sludge retention time and low hydraulic retention time (Daud et al., 2018; Lier et al., 2008).

In the last few years, the combination of both technologies has been proposed and tested. There are a few examples in the bibliography that use UASB-HRAP systems, where the UASB provides a primary treatment and biogas production, leading to a more adequate effluent for the HRAP. It is especially considered a suitable option for developing countries with tropical climate, as the costs involved in their operation and maintenance are lower than those of activated sludge treatments and may even suppose a net profit depending on the biogas production and utilization (Chatterjee and Ghangrekar, 2017; Daud et al., 2018; Vassalle et al., 2020b, 2020a; Villar-Navarro et al., 2018). More extensive information about both technologies can be found in the *State of the art* section.

At the Universidade Federal de Minas Gerais, UFMG (Belo Horizonte, Brazil), the Departamento de Engenharia Sanitária e Ambiental, DESA (Sanitary and Environmental Engineering Department), operates a demonstrative-scale UASB reactor with a working volume of 343 L that receives raw sewage with a flow rate of 49 $L \cdot h^{-1}$. Its performance has already been proved and, further, two pilot-scale HRAPs with an operational volume of 205 L each were tested to treat part of the effluent of the UASB reactor, with a flow rate of 25.5 $L \cdot d^{-1}$. The results obtained for water quality parameters, that can be found summarized in Table 1, comply with the requirements established at the local legislation (Vassalle et al., 2020b).

Parameter	UASB-HRAP removal
Chemical Oxygen Demand	72%
Total nitrogen	30%
Total suspended solids	59%
Volatile suspended solids	58%

Table 1. Removal of wastewater pollutants in the UASB-HRAP system operated at UFMG by Vassalle et al., 2020b.

Currently, the DESA aims at following this line of research and a demonstrative-scale HRAP is under construction to treat the whole effluent from the UASB reactor, with a working volume of 45 m^3 or 75 m^3 depending on the useful operational depth (0,3 or 0,5 m, respectively). Apart from the climatic conditions (solar radiation and temperature), the efficiency of the HRAP drastically depends on the proper design and operation of the ponds. However, conversely to conventional activated sludge reactors, the design and operation procedures of HRAPs are not consolidated and scaling up from lab and pilot experimental results may not be straightforward. Computational modelling and simulations can be used as a tool to assist and verify the design and optimization of wastewater treatment systems, as it is proposed hereby for the optimization of a demonstrative scale HRAP. Through biokinetic modelling, the biological activity of microalgae and bacteria can be analysed, and the treatment efficiency and the biomass production can be predicted (Solimeno et al., 2017).

The objective of the present study is to predict the performance of the demonstrative-scale HRAP and propose strategies to optimize its operation, in order to obtain proper pollutants removal and biomass production, through modelling and simulations. In particular, the performance of the HRAP has been simulated using the BIO_ALGAE 2 model (Solimeno et al., 2019) through COMSOL Multiphysics® software, and the optimum theoretical hydraulic retention time (HRT) and depth to obtain a proper wastewater treatment has been determined. Moreover, the conditions to obtain the maximum biomass production have been established, as it may result of interest to its valorisation (for example for biogas production).

2. State of the art

2.1 Microalgae-based wastewater treatment

Microalgae has been extensively used to remove pollutants in thousands of communities, as facultative and maturation ponds. However, these systems do not focus on optimize algae growth. In this regard, HRAP have been developed and widely studied, resulting efficient for a variety of influents as urban, agricultural and industrial wastewater, and anaerobic digestion effluents (Alcántara et al., 2015; de Godos et al., 2010; García et al., 2000; Tarlan et al., 2002)). HRAP are shallow raceway reactors in which a microalgae-bacteria consortia is developed and the mixed liquor flows through the raceway driven by a paddlewheel (Figure 1).

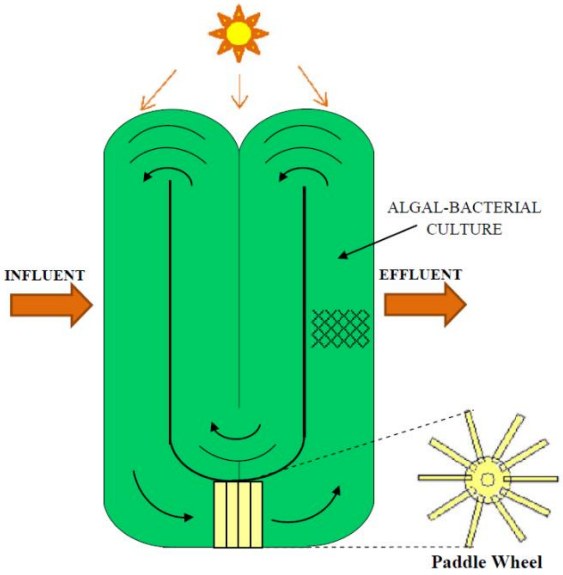

Figure 1. Schematic of a HRAP (Alcántara et al., 2015).

Microalgae biomass can grow using wastewater as feedstock, fixating CO_2 and assimilating the nutrients (mostly nitrogen and phosphorus) present in the influent wastewater. Through photosynthesis, microalgae generate the oxygen needed by heterotrophic and autotrophic bacteria, also present in the mixed liquor, to aerobically degrade the organic matter and ammonium present in the wastewater (Figure 2). The research involving HRAP has increased during the last few years, as can be seen in Figure 3.

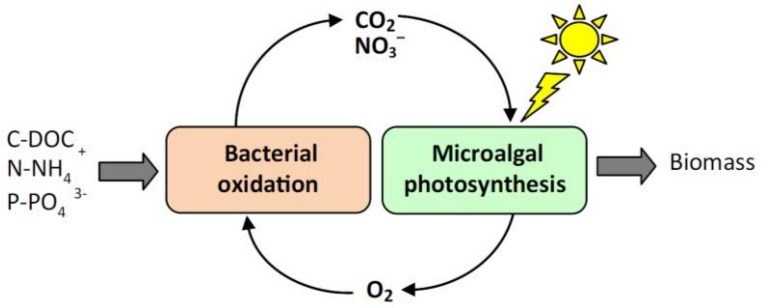

Figure 2. Schematic of photosynthetic oxygenation in microalgal-bacteria consortia. DOC: dissolved organic carbon (Alcántara et al., 2015).

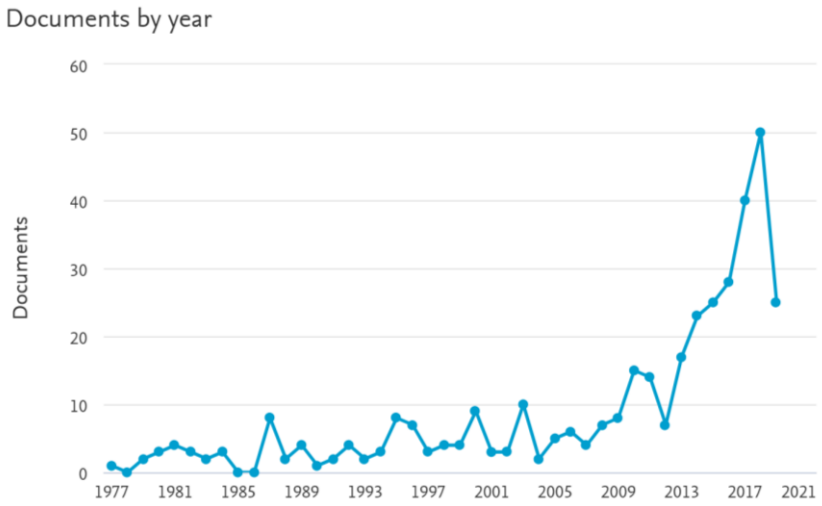

Figure 3. Number of documents published by year (1977 – 2019) found in the bibliographic database *Scopus* about UASB. The method employed was searching 'HRAP OR "High-rate algal pond" OR "High-rate algae pond"' in the field 'Article title, Abstract, Keywords'. Acceded on 24th April 2020.

HRAP, and in general all microalgae-based wastewater treatments, present certain advantages over conventional treatments, due to its versatility, easy operation and low operation and maintenance costs. While the usual biological reactions performed by the diversity of microorganisms take place, microalgae carry out photosynthesis, improving nutrient assimilation and generating oxygen. The latter involves reducing costs in mechanical aeration. Moreover, the high pH together with the oxygen concentrations improve removal of nutrients and heavy metals, and pathogen inactivation (Alcántara et al., 2015). As carbon dioxide is converted into biomass, microalgae-based treatments can be used to mitigate climate change and even be combined with carbon dioxide capture technology. In addition, the biomass produced is of high interest for the recovery of resources from wastewater, and even more considering that, in this specific case, the microalgae growth costs are covered by the wastewater treatment. A few examples of their uses may include co-digestion in anaerobic reactors, production of biofuels and high-value products, biofertilizer and even as fish feed in aquaculture (Dani et al., 2016; Dineshkumar et al., 2019; Du et al., 2019; Mehrabadi et al., 2015; Park et al., 2011).

2.1.1 Removal of organic pollutants

Various microalgae species can grow photoautotrophically, heterotrophically and mixotrophically, being able to consume both inorganic and organic carbon (Alcántara et al., 2015; Roostaei et al., 2018). Moreover, there exists an exchange of substrates between microalgae and the rest of microorganisms, basically with autotrophic and heterotrophic bacteria, with which they can even form consortia (Robles et al., 2020). The whole metabolic activity contributes to the degradation of organic pollutants (Alcántara et al., 2015).

2.1.2 Nitrogen and phosphorous removal

Assimilatory removal of these nutrients in domestic wastewater is mostly carried out by photosynthetic organisms, as far as there is not enough organic carbon to perform it heterotrophically with a sufficient level. Dissimilatory removal of nitrogen consists on a two steps process: nitrification and denitrification. Nitrification consists on the oxidation of ammonium to nitrite and, posteriorly, its oxidation to nitrate, and it is accomplished by chemolitotrophic bacteria and archaea. For its part, denitrification is the reduction of nitrate to nitrogen gas, carried out by heterotrophic bacteria (Figure 4). Both processes, nitrification and

denitrification, happen concurrently as there is a diffusion gradient between the medium and the inside of the biofilms and flocs constituted by algae and bacteria (Alcántara et al., 2015; Delgadillo-Mirquez et al., 2016).

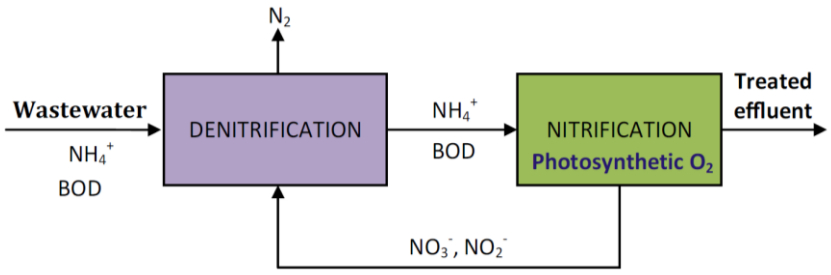

Figure 4. Schematic of denitrification-nitrification process in microalgal-bacteria consortia based treatments (Alcántara et al., 2015).

The photosynthetic activity may cause an increase in the pH of the water when it is limited by carbon availability. That phenomena usually happens at peak sun hours in ponds, and it involves the shift of ammonium/ammonia equilibrium to ammonia formation, which can volatilize. At the same time, and the pH increase can lead to the precipitation of phosphate by its combination with calcium (Alcántara et al., 2015; Delgadillo-Mirquez et al., 2016).

The whole mechanisms can achieve the removal of nitrogen and phosphorus up to 98% and 95%, respectively (Alcántara et al., 2015).

2.1.3 Removal of heavy metals

There are several mechanisms involved in heavy metal removal by microalgae-based treatments, directly related with their strategies to consume them or avoid their toxicity. They comprise immobilization, gene regulation, exclusion or chelation, among other processes. Passively, heavy metals are initially reversibly retained in cell surface by physical adsorption, ion exchange and chemisorption, and later irreversibly retained by covalent bonding and surface precipitation. All these mechanisms are due to the cell wall composition, that includes polysaccharides, lipids and organic proteins, macromolecules rich in functional groups. Microalgae can also, above a determinate metal concentration, excrete metalchelating exopolysaccharides, decreasing their toxicity and promoting their adsorption to cell surface. They can also bioaccumulate some metals by slow intracellular positive diffusion (Alcántara et al., 2015; Leong and Chang, 2020).

As previously described for other pollutants, the pH increase can contribute to heavy metal removal too. Concretely, it provokes their precipitation (Alcántara et al., 2015; Leong and Chang, 2020).

2.1.4 Removal of pathogens

The microalgae activity has been demonstrated to enhance pathogen deactivation, together with solar irradiation. The mechanisms that contribute to this are pH, temperature and dissolved oxygen concentration increase, as well as competition for nutrients, the release of algal toxins. Moreover, pathogens can get attached to algae, directly exposing them to high pH and dissolved oxygen production sites, in addition to increasing their capacity of sedimentation. In some cases, the removal can achieve values higher than 90% depending on the climatic and operational conditions and the algae species, among other factors (Alcántara et al., 2015; Dar et al., 2019).

2.1.5 Remediation of emerging contaminants

It has been shown that microalgae-based treatments can decrease the concentration of several emerging contaminants, basically pharmaceuticals and care products, through diverse mechanisms: bioadsorption to the cell wall or their secretions, bio-uptake via passive diffusion, passive-facilitated diffusion or active uptake, photodegradation, and biodegradation through enzymatic activity. The latest is the most convenient process as, differently to the other two processes, the contaminant is degraded through catalytic metabolism, eliminating the problems associated to the subsequent disposal of the biomass (Sutherland and Ralph, 2019).

2.2 Anaerobic wastewater treatment

2.2.1 Anaerobic digestion

Anaerobic digestion is a well-established technology, that allow to transform biodegradable organic matter, into biogas by cause of its degradation by the action of microorganisms in absence of oxygen. At the same time, it involves a reduction of the waste volume, which results in a more stable configuration, the digestate. That digestate can be used as soil conditioner, for example. Biogas can be used for producing electric and thermal energy, and also be treated to directly fed the natural gas grid (Lin et al., 2013). Other possible substrates typically used are sewage sludge and active sludge from wastewater treatment plants, municipal solid residues or manure.

Four sequential stages take place during anaerobic digestion: hydrolysis, acidogenesis, acetogenesis, methanogenesis (Figure 5). These processes depend on the interaction of a variety of metabolic processes carried out by diverse microorganisms (Meegoda et al., 2018).

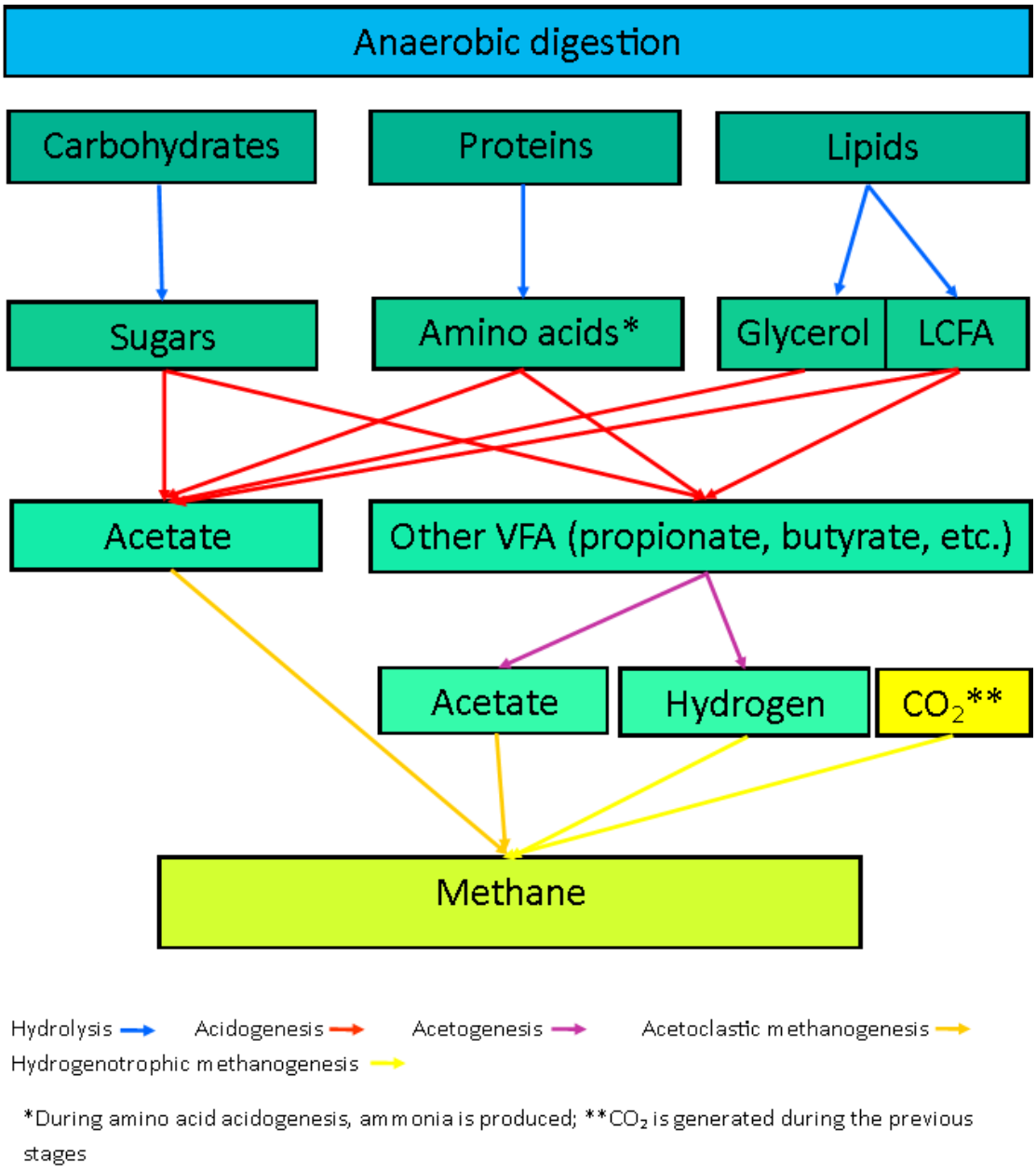

Figure 5. Schematic of anaerobic digestion stages.

2.2.1.1 Hydrolysis

The substrates for anaerobic digestion are typically formed by complex organic compounds which need a previous hydrolysis to be internally metabolized by microorganisms. Hydrolytic bacteria secrete enzymes extracellularly which can hydrolyse carbohydrates, lipids and proteins into sugars, long chain fatty acids (LCFA) and amino acids, respectively. However, some compounds, as cellulose and hemicellulose, are difficult to degrade. In order to enhance this process, enzymes can be added. Hydrolysis has a determinant influence in anaerobic digestion rate, and it exists an enormous interest in pre-treatments focused on optimizing that step. The optimum temperature and pH ranges for hydrolysis are 30-50 ºC and 5-7, respectively (Gujer and Zehnder, 1983; Lier et al., 2008; Meegoda et al., 2018).3.2.1.2 Acidogenesis

Acidogenic microorganisms can internalize hydrolysis products and generate volatile fatty acids (VFA), between other products. The most abundant constituents are acetate, propionate and butyrate, usually found in varying proportions from 75:15:10 to 40:40:20. Their production is

dependent on pH. Acidogenesis is the fastest stage, involving the rapid accumulation of VFA and the consequent acidification in the digester and being the main cause of process failure. Apart from VFA, the amino acid degradation results in the production of ammonia that, at high concentrations, has an inhibitory effect over anaerobic digestion (Meegoda et al., 2018).

2.2.1.3 Acetogenesis

The acetate produced in the previous step is conducted directly through acetoclastic methanogenesis. However, the other VFA produced may be metabolized by acetogenic microorganisms, which convert them and other intermediates into acetate and hydrogen. Hydrogen could be detrimental for acetogenesis, but it is soon consumed by hydrogenotrophic methanogens (Meegoda et al., 2018).

At their part, lipids follow a separate pathway of acetogenesis. Glycerol is transformed in acetate through acidogenesis, while long chain fatty acids are metabolized to it via β-oxidation(Meegoda et al., 2018).

2.2.1.4 Methanogenesis

Methanogenesis represents the last step of the anaerobic digestion process. This stage is performed by methanogenic archaea, which are strictly anaerobic. Two third parts of methane are produced via acetoclastic methanogenesis, while most of the remaining is generated via hydrogenotrophic methanogenesis. There are other minor pathways as, for example, methanogenesis from methanol. Methanogenesis takes approximately 40 days in batch reactors (Meegoda et al., 2018).

Methanogenic microorganisms have, in general, a slow regeneration time and are sensitive to low pH and high redox potential, in contrast with the optimum conditions for the previous stages (Meegoda et al., 2018). For this reason, it has been suggested that a two stages operation, separating methanogenesis from the previous steps, could step to an increased methane production (Yun et al., 2016).

2.2.2 Wastewater treatment based on anaerobic digestion

The most conventional and widely applied wastewater treatment process is activated sludge, which aerobically transforms organic matter into biomass and CO_2. The activated sludge is a versatile process, requires reduced volume and land occupation and can achieve low concentration of pollutants in the effluent. However, it presents an elevated operational cost due to the energy requirements for mixing and aeration, and involves high sludge yields. In this respect, anaerobic treatments show several advantages. They generate up to 90% less sludge and they require low energy supply to operate. Furthermore, as exposed above, methane is generated and can be used as a biofuel for energy production (Lier et al., 2008). They are capable of treating high COD loads in lower space than aerobic treatments and tolerate fluctuations.(Daud et al., 2018).

2.2.2.1 Upflow anaerobic sludge bed reactor

Among anaerobic treatments, anaerobic sludge bed reactors are the most widely used for wastewater treatment, especially for industrial wastewater, but also for municipal wastewater. In this kind of reactor, sludge is constituted by aggregates which can easily settle. Moreover, they count with inner gas-liquid-solids separation systems (Daud et al., 2018; Lier et al., 2008).

The most commonly found configuration for that kind of reactors is UASB, which have a plain design and are capable of successfully retain high concentrations of sludge and properly separated the different phases. In these reactors, wastewater flows upwards through an

activated anaerobic sludge bed, where solids are adsorbed, and the organic part is converted to biogas and biomass. The biogas rises to the top of the reactor dragging solids and water and conducted through baffles to a gas-liquid surface to efficiently separate gas from the other phases (Figure 6). The treated water released through apertures between the baffles and passes to a settling area where the solid particles that was transported settle and slide back to the reactor (Daud et al., 2018; Lier et al., 2008).

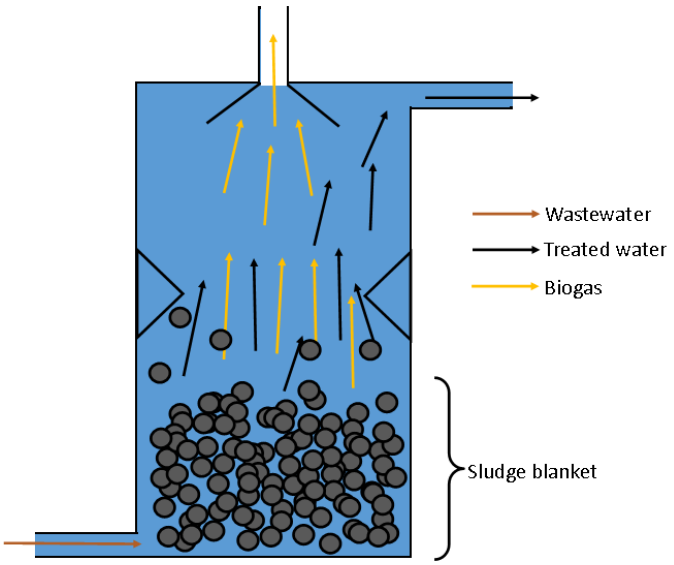

Figure 6. Schematic of an UASB reactor.

UASB can operate with higher rates than complete stirred tank reactors (CSTR) and, therefore, they involve lower hydraulic HRT and can achieve higher sludge retention times, needing to discharge every three or four years. Moreover, it has low implementation and operating cost, and requires simple maintenance and low operating costs (Daud et al., 2018). For these reasons, there has been a growing interest in this technology over the last decades since it was developed in the seventies (Lier et al., 2008), as can be seen in Figure 7.

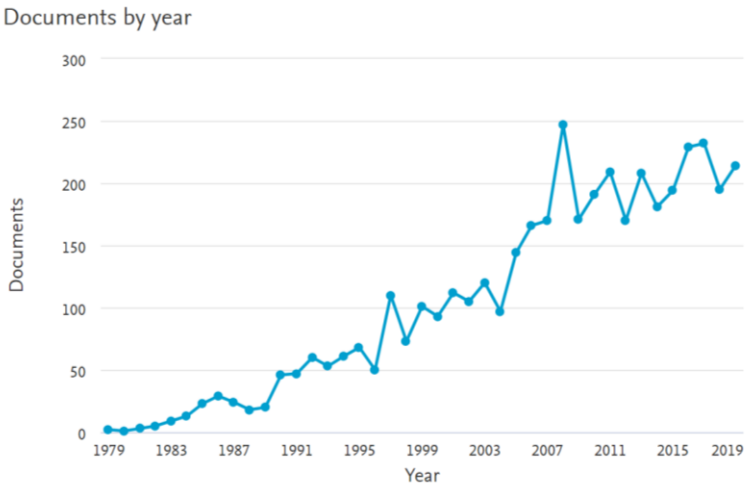

Figure 7. Number of documents published by year (1979 – 2019) found in the bibliographic database *Scopus* about UASB. The method employed was searching 'UASB OR "Upflow Anaerobic Sludge Blanket" OR "Upflow Anaerobic Sludge Bed Reactor"' in the field 'Article title, Abstract, Keywords'. Acceded on 24th April 2020.

2.3 Combined UASB-HRAP systems for wastewater treatment

In general, UASB reactors can perform successfully in the removal of organic matter, but the nutrients removal efficiencies are low or even negligible. Therefore, treated water from the effluent of UASB reactors are nutrient-rich, and has shown to be proper to promote microalgal growth. However, there are few cases or studies of the combination of UASB reactors and HRAP for wastewater treatment. Concretely, 8 articles have been found in the literature resulting of searching '["upflow anaerobic sludge bed reactors" OR UASB] AND [HRAP OR "high-rate algae pond"]' in the section *Documents* of the bibliographic database *Scopus* in the field *Article title, Abstract, Keywords* (acceded on 24th April 2020). From these papers, 7 refer directly to their combination to treat wastewater (Chatterjee and Ghangrekar, 2017; Gutiérrez-Alfaro et al., 2018; Santiago et al., 2013; Vargas e Silva and Monteggia, 2015; Vassalle et al., 2020a, 2020b; Villar-Navarro et al., 2018), as a more sustainable alternative to conventional treatments, which is capable of achieve proper removal rates for organic matter, nutrient (85,1±2,4% for ammonia and 91±1% for phosphate according to Chatterjee & Ghangrekar, 2017), pathogens and, even, it has shown to be effective to remove micropollutants (Chatterjee and Ghangrekar, 2017; Vassalle et al., 2020b, 2020a; Villar-Navarro et al., 2018). It is considered a low-cost treatment compared with ordinary ones, which can also involve a net gain if considering biogas production, biomass valuation and treated water reuse. Therefore, it may be a suitable alternative to be implemented, especially in developing countries from tropical areas with high ambient temperatures that can facilitate the mesophilic methanogenic activity (Chatterjee and Ghangrekar, 2017; Daud et al., 2018; Vassalle et al., 2020b). Furthermore, it has been demonstrated that it is possible to improve the methane yields of the UASB by co-digesting the wastewater with the biomass surplus from the HRAP, taking a direct profit of it in the same system (Vassalle et al., 2020a).

2.4 Modelling of microalgae-based wastewater treatment systems

While mechanistic bacteria mathematical models for wastewater treatments has been properly developed, validated and implemented, most of those regarding microalgae are simple steady-state models, based on deterministic biological kinetics and designed to respond to a single variating factor. In the last years, more complex dynamic models, which consider multiple substrates and physical factors limitations, have been developed, basically following Droop's or Monod kinetics. For instance, growth limited simultaneously by nitrogen and light intensity. There exist some mathematical models focused on characterise the interactions between bacteria and microalgae (Solimeno et al., 2015).

With regarding to bacteria growth model, the most extended are the activated sludge models (ASM) which were promoted by the International Water Association (IWA) The first version included organic matter oxidation, nitrification and denitrification, with the kinetics and stoichiometry based on Monod formulation. The following versions of this model were developed to included phosphorus removal and a more realistic description of decay processes, as well as a better description of cell internal storage compounds. The ASM presents some limitations. For instance, as it was calibrated from data obtained at experimenting at a temperature range of 8-23ºC and pH 6,5-7,5. When out of this ranges, the model results may not be representative of the real behaviour of the system. Moreover, the coefficients related to bacteria processes were set as constant for all types of wastewater. However, the ASM has been extended in different ways in literature in order to improve it or include new processes, so it can be employed as a base to generate new and more complex models (Solimeno et al., 2015).

Among the microalgae-bacteria models, the river water quality model no.1, RWQM1, may be considered as a reference for subsequent models. It was also developed by the IWA, and it is based on mass balance of chemical elements, which are expressed as biochemical oxygen demand (BOD), and incorporates the chemical equilibrium of nitrogen, carbon and phosphorus species. Its kinetic expressions refer to functions of nutrient availability, temperature and light. One of the models which has took as reference the RWQM1, as well as the ASM3, is the BIO_ALGAE model. Furthermore, it incorporates the carbon limitation for microalgae and nitrifying bacteria, in addition to the dependence for microalgae and bacteria, the effect of light intensity on the photosynthesis, light attenuation, pH dynamics and the effect of excess of dissolved oxygen (Solimeno et al., 2015).

3. Materials and methods

3.1 High-Rate Algae Pond at demonstrative scale

The new HRAP (Figure 8, A), which is currently under construction, will have a total depth of 0,7m, and an adjustable useful operational depth of 0,5m or 0,3, corresponding to a working volume of 75m^3 and 45m^3, respectively. The design contemplates a velocity of mixture of 0,15m·s^{-1}, performed by stainless steel paddles. The construction is carried out by masonry and waterproofed with high density polyethylene.

As presented in the introduction, experimentation with two pilot-scale HRAPs with a working volume of 205L has been carried out in previous studies to test their capability of treating the effluent of a UASB (Figure 8, B) in Minas Gerais, as part of a domestic wastewater treatment (Vassalle et al., 2020a, 2020b). Photographs of the pilot HRAPs and the UASB reactors are shown in Figure 9. The data obtained during a campaign of measurements of approximately one year (8500 hours) were employed in this study to calibrate the model. Moreover, the characteristics of the influent, water temperature and irradiance were also used during the simulations for predicting the functionality of the new HRAP.

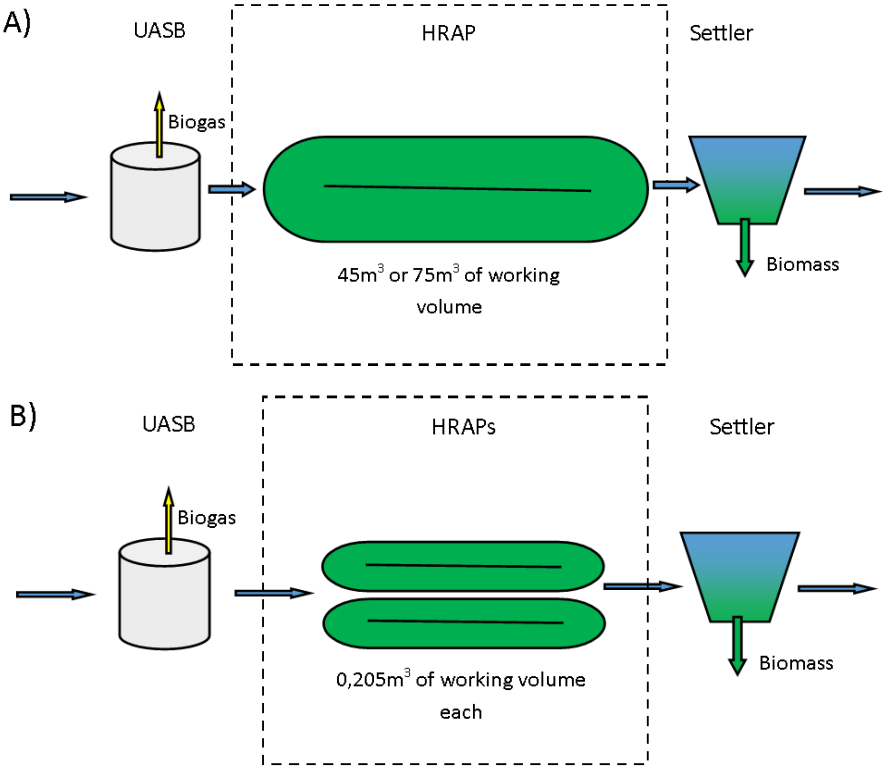

Figure 8. Diagram of the whole treatment system for the new HRAP (A) and the pilot-scale HRAPs (B).

Figure 9. Photographs of the UASBs (left) and HRAPs (right) operated by the DESA (UFMG).

3.2 BIO_ALGAE 2 model

3.2.1 Description

BIO_ALGAE 2 is one of the most recent mechanistic model that describes the physical, chemical and biological interactions occurring in algal-bacterial systems (Solimeno et al., 2019, 2017; Solimeno and García, 2017). It is the result of combining a microalgae activity model (Solimeno et al., 2015), the modified River Water Quality Model 1, RWQM1, and Activated Sludge Model No.3, ASM3 (Iacopozzi et al., 2007), together with the addition of new elements, as the limitation of carbon availability for the growth of microalgae and the growth of autotrophic bacteria (Solimeno et al., 2017). Moreover, this second version of the BIO_ALGAE model includes the variation of microalgae and bacteria activity as a function of pH, temperature and dissolved oxygen in the culture, as well as the possibility of establishing CO_2 injection for pH control (Solimeno et al., 2019). The components and processes are briefly described in the followings (and schematically represented in Figure 10). Further details can be found in *Annex II*. For the whole description of the model, the reader is referred to Solimeno et al., 2015, 2017, 2019.

3.2.1.1 Components

There are 19 components included in the model which can be divided as dissolved (a total of 13) and particulate (the remaining 6), and their nomenclature follows the commonly used by the IWA, models (Solimeno et al., 2019, 2017, 2015).

3.2.1.1.1 Particulate components

1. Microalgae biomass, X_{ALG} [g COD m^{-3}]: its value increases with those processes that promotes microalgae growth, while it decreases because of endogenous respiration and decay of microalgae.
2. Heterotrophic bacteria, X_H [g COD m^{-3}]: its growth is dependent on the organic matter availability, as it is the source of carbon and energy of that microorganisms, that can grow both aerobically and anoxically. It decreases by endogenous respiration and decay.
3. Ammonium oxidizing bacteria, X_{AOB} [g COD m^{-3}]: it corresponds to the fraction of the bacterial biomass which performs the firsts step of the nitrification, the oxidation of ammonium to nitrite. They grow under aerobic conditions and decrease by endogenous respiration and decay.
4. Nitrite oxidizing bacteria, X_{NOB} [g COD m^{-3}]: these bacteria are responsible for the second step of nitrification, oxidizing nitrite to nitrate. As the previous microorganisms, they grow aerobically, and their value declines by endogenous respiration and decay.
5. Slowly biodegradable particulate organic matter, X_S [g COD m^{-3}]: it is conformed by the part of particulate organic matter which is hydrolysable and convertible into readily biodegradable organic matter or inert organic matter (both dissolved components explained below). A fraction of it is present in the influent, while the other one is originated from the decay of the biomass.
6. Inert particulate organic matter, X_I [g COD m^{-3}]: it is the fraction that remains after the hydrolysis of particulate organic matter. It is assumed to be present in the influent and it increases by the decay of microorganisms.

3.2.1.1.2 Dissolved components

1. Ammonium nitrogen, S_{NH4} [g NH_4^+-N m^{-3}]: it enters the system in the influent and it is also generated by all the microorganisms because of the endogenous respiration and decay. It decreases by consumption by microalgae, heterotrophic bacteria and during nitrification.
2. Ammonia nitrogen, S_{NH3} [g NH_3-N m^{-3}]: it exists in acid-base equilibrium with ammonium, and only works as a gaseous component in the model. Its volatilization depends on pH, temperature and mixing conditions.
3. Nitrate nitrogen, S_{NO3} [g NO_3^--N m^{-3}]: it usually arrives in negligible concentration with the influent, so it is assumed that it is only generated inside the pond by nitrification. It is assimilated by microalgae and heterotrophic bacteria, being the latter also capable of employing it as electron acceptor during denitrification, as they are considered facultative.
4. Nitrite nitrogen, S_{NO2} [g NO_2-N m^{-3}]: as in the case of nitrate, it is assumed that it is only produced in the pond, as an intermediate in nitrification. It is consumed by nitrite oxidizing bacteria and heterotrophic bacteria during denitrification.
5. Phosphate phosphorus, S_{PO4} [g PO_4^--P m^{-3}]: it is introduced in the pond with the influent, and released from the oxidation of organic matter. Moreover, it is generated during the respiration and decay of microorganisms, and assimilated by microalgae, heterotrophic bacteria and autotrophic bacteria during their growth.
6. Dissolved oxygen, S_{O2} [g O_2 m^{-3}]: it is produced during photosynthetic growth of microalgae, and there exists transference with the atmosphere. Furthermore, it is consumed during aerobic respiration and decay of the whole biomass.
7. Dissolved carbon dioxide, S_{CO2} [g CO_2-C m^{-3}]: it is in equilibrium with bicarbonate and carbonate, and is generated during the growth of heterotrophic bacteria and during the

respiration and decay of all types of microorganisms. There is also transference with the atmosphere and it is consumed by microalgae and autotrophic bacteria

8. Bicarbonate, S_{HCO3} [g HCO_3^--C m^{-3}]: it is in equilibrium with carbon dioxide and carbonate, and it is consumed by microalgae.
9. Carbonate, S_{CO3} [g CO_3^{2-}-C m^{-3}]: it is in chemical equilibrium with carbon dioxide and bicarbonate, and it is consumed by both microalgae and autotrophic bacteria.
10. Hydrogen ions, S_H [g H^+ m^{-3}]: they are generated by ammonium oxidizing bacteria and heterotrophic bacteria, and their levels decrease during the growth of microalgae and nitrifying bacteria and because of the endogenous respiration and decay of biomass. They are involved in acid-base equilibria including the carbonate, ammonium and phosphate systems.
11. Hydroxide ions, S_{OH} [g OH^--H m^{-3}]: they are in equilibrium with hydrogen ions.
12. Readily biodegradable soluble organic matter, S_S [g COD m^{-3}]: this is the fraction of soluble organic matter which is directly biodegradable by heterotrophic bacteria. It arrives to the ponds in the influent and is generated through the hydrolysis of biodegradable particulate organic matter.
13. Inert soluble organic matter, S_I [g COD m^{-3}]: this is the fraction of soluble organic matter that is not readily biodegradable by heterotrophic bacteria. As in the case of the readily biodegradable soluble organic matter, it enters the pond with the influent and is produced during the hydrolysis of the biodegradable particulate organic matter.

3.2.1.2 Processes

The processes included in the model are those described by Solimeno et al., 2015 for microalgae growth. The bacterial processes were inspired by the River Water Quality Model 1, RWQM1, and the modified ASM3. However, the model neither considers processes related with the storage of readily biodegradable soluble organic matter nor anaerobic biological processes. Likewise, the absorption and desorption of phosphate on particulate matter were neglected.

1. Growth of microalgae: it represents the increment of microalgae biomass per unit of time, being the product of the maximum specific growth rate, the biomass concentration at that precise moment and corrective factors to limit or inhibit the growth. They grow with carbon dioxide and bicarbonate as carbon source and with ammonia, ammonium or nitrate as nitrogen source. Carbon dioxide, ammonia and ammonium have inhibitory effects above certain concentrations. That process is also influenced by the irradiance, temperature and oxygen concentration.
2. Endogenous respiration of microalgae: this process depends on the concentration of microalgae, as well as temperature and oxygen concentration.
3. Inactivation of microalgae: this process is affected by the same parameters as the endogenous respiration.
4. Chemical equilibrium of $CO_2 \leftrightarrow HCO_3^-$: it describes the equilibrium between both species as part of the carbonate system.
5. Chemical equilibrium of $HCO_3^- \leftrightarrow CO_3^{2-}$: it represents the remaining component of the carbonate system.
6. Chemical equilibrium of $NH_4^+ \leftrightarrow NH_3$: it describes the equilibrium between ammonium and ammonia.
7. Chemical equilibrium of $H^+ \leftrightarrow OH^-$: it describes the equilibrium between both ions.
8. Oxygen transfer to atmosphere: it considers the transference of O_2 from the water to the atmosphere.

9. Carbon dioxide transfer to the atmosphere: it considers the transference of CO_2 from the water to the atmosphere.
10. Ammonia transfer to the atmosphere: it considers the transference of NH_3 from the water to the atmosphere.
11. Aerobic and anoxic growth of heterotrophic bacteria: it was developed with Monod kinetics. While both processes use the same parameter and coefficient values, anoxic processes include additionally a reduction factor. When the dissolved oxygen concentration is 0,5 g m^{-3} or higher, heterotrophic bacteria assimilate the readily biodegradable substrate and consume ammonium, ammonia and nitrate as nitrogen source. At lower dissolved oxygen concentration, nitrate is used as electron acceptor and converted to nitrogen gas.
12. Aerobic and anoxic endogenous respiration of heterotrophic bacteria: it includes the endogenous respiration, and it is limited by oxygen (for the aerobic part) and nitrogen (for the anaerobic part). It generates carbon dioxide and transforms biomass into inert organic matter.
13. Decay of heterotrophic bacteria: it prompts the transformation of biomass into slowly biodegradable and inert organic matter.
14. Growth of autotrophic bacteria: it refers to the growth of the bacteria that carry out nitrification, which is established as a process in two steps.
15. Endogenous respiration of autotrophic bacteria: it is modelled as the aerobic respiration of heterotrophic bacteria.
16. Decay of autotrophic bacteria: this process is stablished in the same way as the decay of heterotrophic bacteria but with different decay rates.
17. Hydrolysis: it is the process by which slowly biodegradable particulate organic matter is transformed into readily biodegradable soluble organic matter. It is carried out by heterotrophic bacteria.

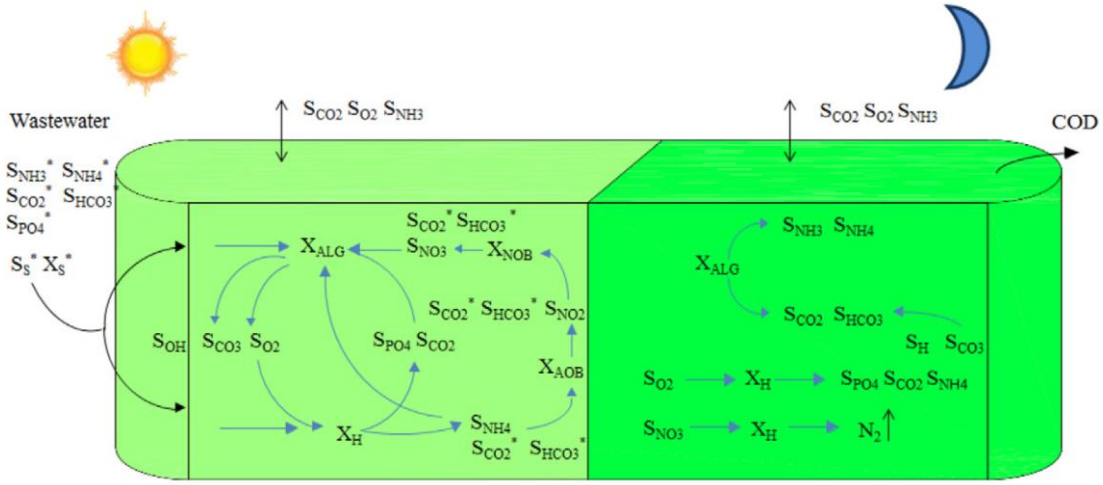

Figure 10. Schematic representation of the BIO_ALGAE model components and processes during day (left) and night (right). * Components which enter the ponds in wastewater (Solimeno et al., 2017).

3.2.2 Model implementation

The model was implemented in COMSOL Multiphysics® software. COMSOL is a platform to perform simulations of designs, devices and processes ("COMSOL Multiphysics® Software - Understand, Predict, and Optimize," n.d.). It has been chosen as it is a suitable tool for the purposes of this study. Furthermore, it was the software employed by the authors of the model to apply it and calibrate it (Solimeno et al., 2019, 2017). Moreover, due to the ability of COMSOL

to combine different physics, the model presented in this study could be the basis for the combination of BIO_ALGAE 2 with the hydrodynamic conditions inside the HRAP.

The computer employed to carry out the simulations was an HP Pavilion x360 Convertible 14-dh1xxx laptop, with an Intel® Core™ i5-10210U CPU @ 1,60GHz 2,11GHz processor and 8GB of RAM.

In this study, the model was performed in a 0D geometry, assuming that the ponds are perfect mixed systems, as it is considered a close approach to reality without high computational requirement. The interface chosen to implement de model was *Reaction Engineering* (RE), which is part of the *Chemical Species Transport* branch. It differs from the option chosen by the authors of the model in previous studies, who selected the *Transport of Diluted Species* (TDS) interface with a 1D geometry instead (note that this interface cannot work with a 0D geometry, so the authors had to select the 1D geometry, although they did not made an spatial study nor obtained any variation along the geometry) RE interface has been proposed in this study in order to assess the feasibility of reducing the computational costs and duration of the simulations. For this reason, a comparison between both interfaces for this case study has been established as a secondary objective.

The input data employed were those obtained during one year of monitoring the influents of the two 250L HRAPs from UFMG.

3.2.3 Stoichiometric and kinetic parameters and model calibration

The model calibration was carried out employing the *Parametric Sweep* tool from COMSOL, which allows for observing how the results are modified when varying specific parameters. The simulations were firstly visually evaluated until satisfactory results were achieved, and subsequently by calculating the minimum quadratic error function, S, in comparison to the real measurements in the HRAPs (Equation 1). As an acceptable match to all the species could not be achieved, priority was given to the total suspended solids (TSS, calculated as the sum of all the particulate species), NH_4^+-N, NO_3^--N and O_2, as they are considered the most relevant parameters to take into account when evaluating the performance of a HRAP.

$$S(\%) = \sqrt{\frac{\sum_i^n \left(\frac{C_{i,exp} - C_{i,sim}}{C_{i,exp}}\right)^2}{n}} \cdot 100\% \qquad \textbf{Equation 1}$$

$C_{i,exp}$: experimental data for an i moment.

$C_{i,sim}$: simulated result for an i moment.

n: total number of data

3.2.4 Definition and simulation of scenarios

Once the model was calibrated, 12 different scenarios were set to evaluate the different combinations of HRT and depth values (Table 2). In this way, it was possible to determine which conditions would be more suitable for an optimal removal of pollutants and biomass production in the new demonstrative HRAP.

Scenario	1	2	3	4	5	6	7	8	9	10	11	12
Depth (m)	0,3	0,5	0,3	0,5	0,3	0,5	0,3	0,5	0,3	0,5	0,3	0,5
HRT (d)	8	8	7	7	6	6	5	5	4	4	3	3

Table 2. Scenarios

4. Results

The model was successfully implemented in the RE interface from COMSOL, taking as a reference the original document in which the BIO_ALGAE 2 was implemented in the TDS interface by its authors (Solimeno et al., 2019, 2017). The final simulation of the calibration process took 22 s of computation to obtain the same results. However, the TDS interface, performed at the same computer and with the same values and parameters, took 3 h 4 min 37 s. Moreover, the use of the RE was, in this case, more intuitive, as it is possible to work directly with HRT and reactor volume values, while TDS involve transforming that parameters into others mathematically equivalents. In this case, it is also conceptually easier to work in a 0D geometry than with a 1D one.

4.1 Calibration

During calibration process, the parameters of the model were adjusted to visually obtain the simulations that better match with the experimental measurements of the priority species (TSS, NH_4^+-N, NO_3^--N and O_2). The comparison between the simulated results for NH_4^+-N, NO_3^--N, O_2 and TSS after calibrating the model and the experimental measurements are shown in Figures 11 to 14, respectively. After this first step, the S parameter for each specie was determined (Table 4).

Table 3 shows the values of the parameters that had been modified with respect to those originally established by Solimeno et al., 2019 (for more details see *Annex II*). As can be seen, the chosen parameters are all involved with the biomass growth and the way the microorganisms interact with the nitrogen and phosphorus species. Moreover, the modification of the optimum temperature value for microalgae contributed to the calibration too. This fact may be related with the species of microalgae growing in the HRAPs, which may be adapted to higher temperatures, as those in Brazil.

Parameter	Original value	Calibrated value	Unit
Maximum growth rate of X_{ALG}	1,45	1,18	d^{-1}
Endogenous respiration constant	0,05	0,1	d^{-1}
Saturation constant of X_{ALG} for S_{HPO4}	0,02	0,001	$g \cdot m^{-3}$ P
Saturation constant of X_H for S_{NO3}	0,5	1	$g \cdot m^{-3}$ N
Saturation constant of X_H for S_{NO2}	0,2	0,62	$g \cdot m^{-3}$ N
Maximum growth rate of X_{AOB}	0,63	0,725	d^{-1}
Maximum growth rate of X_{NOB}	1,1	1,8	d^{-1}
Ammonia inhibition constant of X_{NOB}	5	40	$g \cdot m^{-3}$ N
Optimum temperature value for X_{ALG}	26	30	-

Table 3. Parameters modified during the calibration process.

With regards to NH_4^+-N (Figure 11), a good correspondence was achieved between the simulation and experimental results, with an S of 0.16%, so it can be stated that the model can successfully simulate the evolution of this species over time.
As can be seen in Table 4, NO_3^--N and TSS resulted in an extremely high S value. At Figures 12 and 13, it is observed that, although the simulations achieved a proper range, their values did not match properly with the dynamic variations of experimental data. For this reason, the model should not be taken as a tool to predict the concentration of TSS and NO_3^--N in a specific moment but seems to be realistic to roughly estimate the biomass production during a long period.
çLastly, the simulation for O_2 (Figure 14) did not reach an extremely accurate match with the experimental values. Concretely, there is a peak around t=5000h, which is directly related with the peak in the same period in the TSS simulation, and that were not observed during the experimental measurements. Similarly to TSS and NO_3^--N, the model may not properly predict the concentration of O_2 at a particular time, but it could be used to estimate the average value for long periods.

Specie	TSS	NH_4^+-N	NO_3^--N	O_2
S (%)	137,01	0,16	110,39	30,62

Table 4. S parameter values for the calibrations of the chosen species.

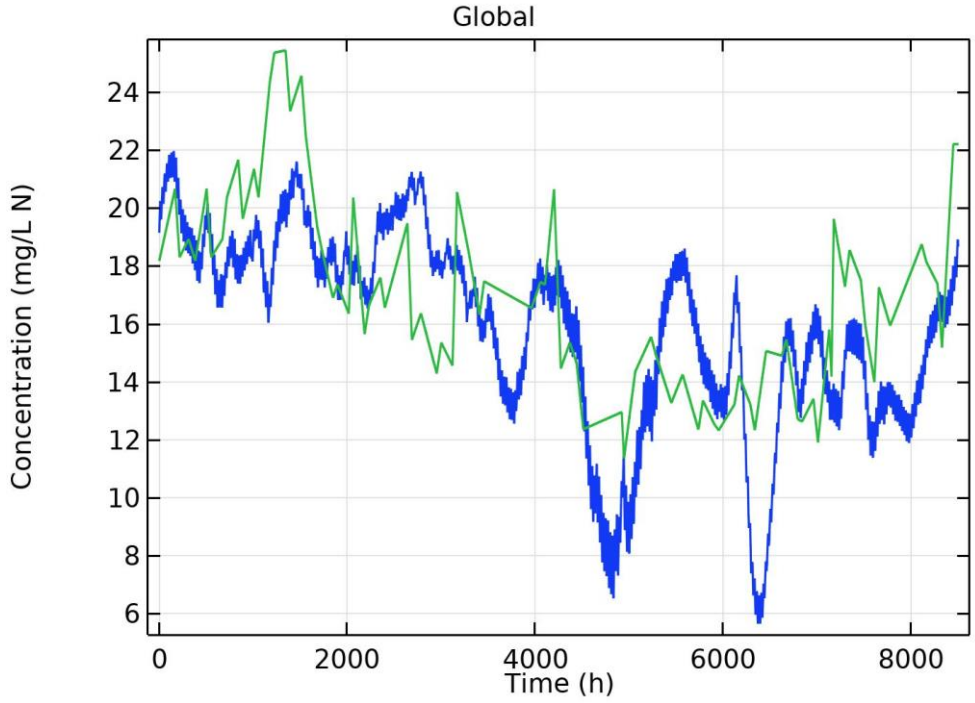

Figure 11. Comparison of the simulated results for NH_4^+-N after calibrating the model (blue) and experimental measurements (green).

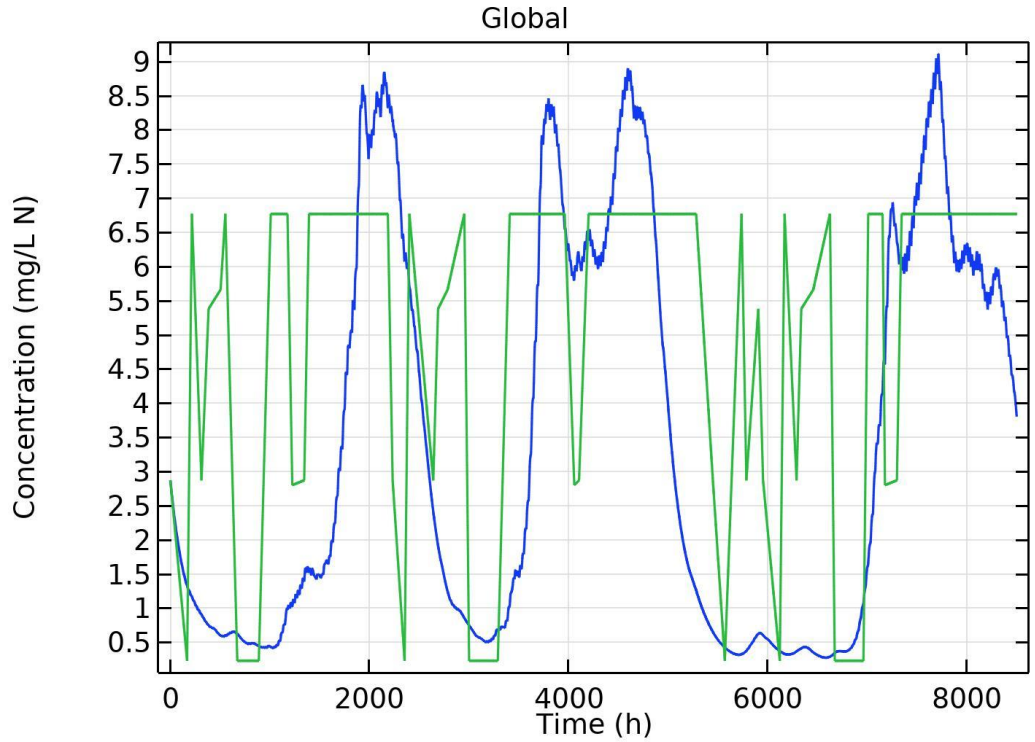

Figure 12. Comparison of the simulated results for NO_3^--N after calibrating the model (blue) and experimental measurements (green).

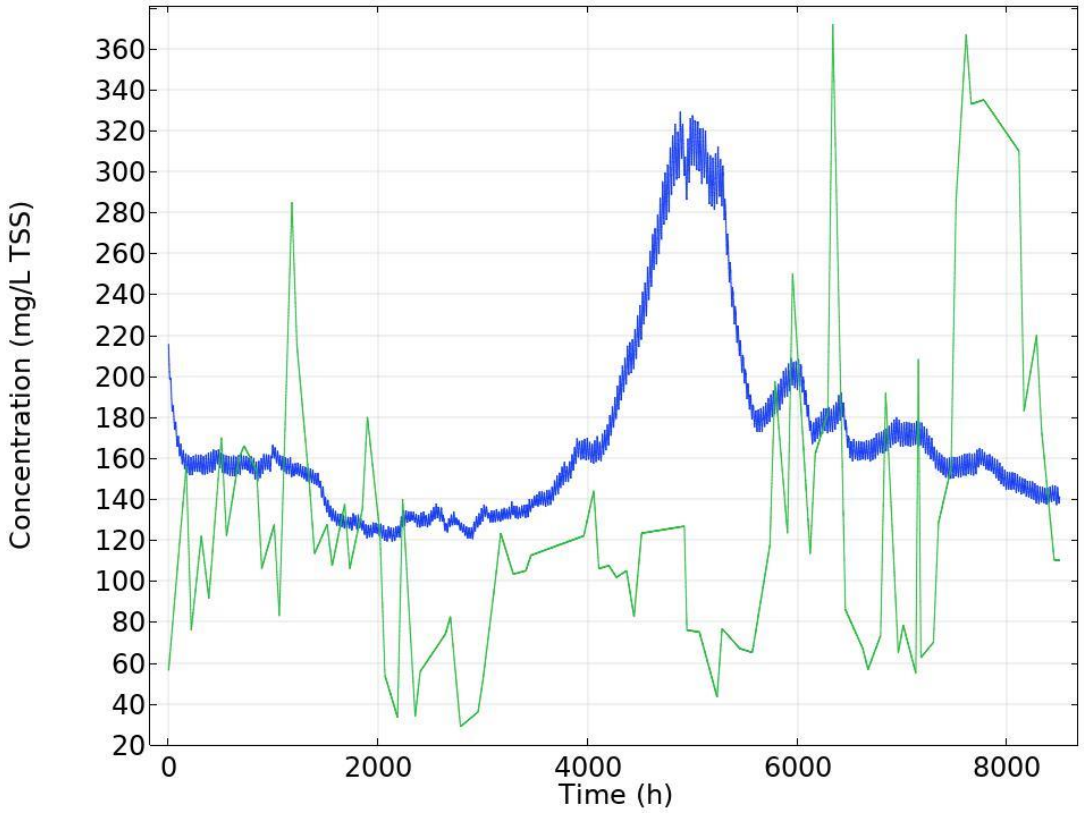

Figure 13. Comparison of the simulated results for TSS after calibrating the model (blue) and experimental measurements (green).

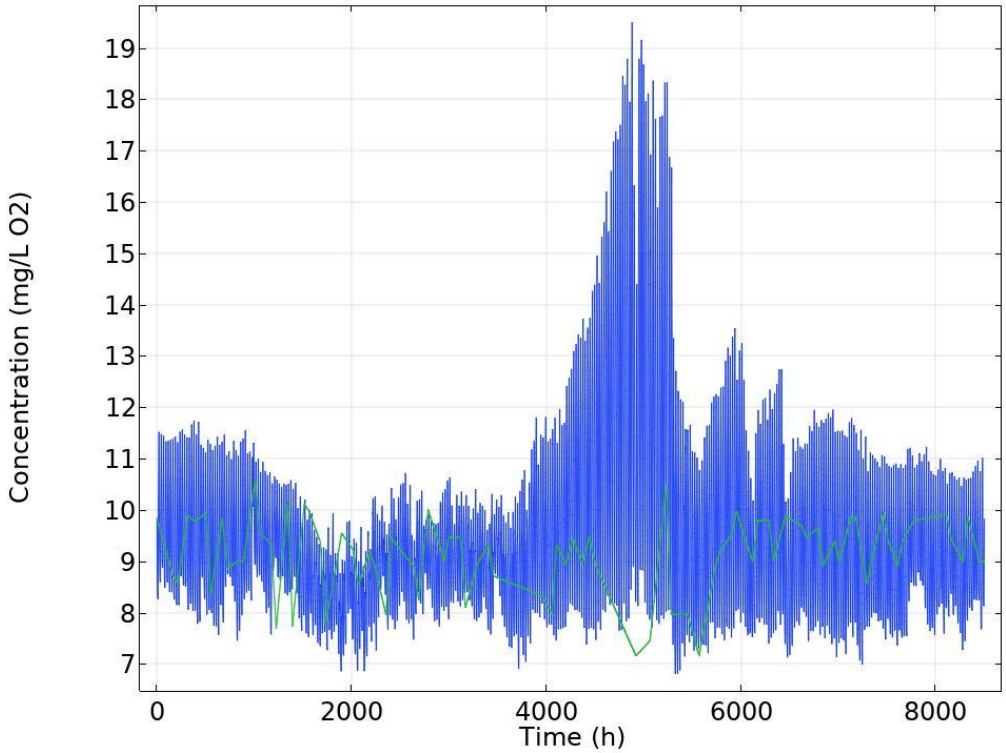

Figure 14. Comparison of the simulated results for O_2 after calibrating the model (blue) and experimental measurements (green).

4.2 Results of the simulations

Once the calibration was considered adequate, the 12 scenarios were simulated variating the HRT and the depth as shown in Table 5. In *Annex I*, the detailed results for the main species are shown.

4.2.1 Biomass production

The biomass concentration in the pond, expressed as concentration of TSS, is summarized in Table 5 for the 12 scenarios simulated. As can be seen, only the scenarios 1 and 2 (which both correspond to HRT of 8 d) generated a high amount of biomass, with a similar concentration to that obtained by Vassalle et al., 2020a in the same location. The biomass production of the 12 scenarios, expressed as grams of TSS per day and per square meter of pond, is also summarized in Table 5.

While the normal values in this kind of systems ranges between 13 and 35 $gTSS \cdot m^{-2} \cdot d^{-1}$ (Park and Craggs, 2011), the results of the simulations ranged between 2,8 and 13,9 $gTSS \cdot m^{-2} \cdot d^{-1}$. The authors of the previous study suggested that the reason of the lower yield may be related with the little availability of CO_2 in the domestic sewage (Vassalle et al., 2020a).

In Scenarios 3 through 12 (HRT from 7 to 3), the concentration of biomass in the HRAP decreased since the beginning of the simulation to low levels and stabilised rapidly at values between 50 and 90 $mgTSS \cdot L^{-1}$, as can be observed in Figure 15. Concretely, the microalgae biomass disappears (see *Annex I*). Generally, with the climatic conditions (temperature and solar irradiation) in Minas Gerais, even low HRT would be guessed to efficiently produce biomass. Therefore, the reason why the model generated these results may be more related with the influent characteristics. The results of the model simulations suggest that low HRT are not suitable for significant microalgal biomass production. However, experiments at low HRT could confirm this model predictions.

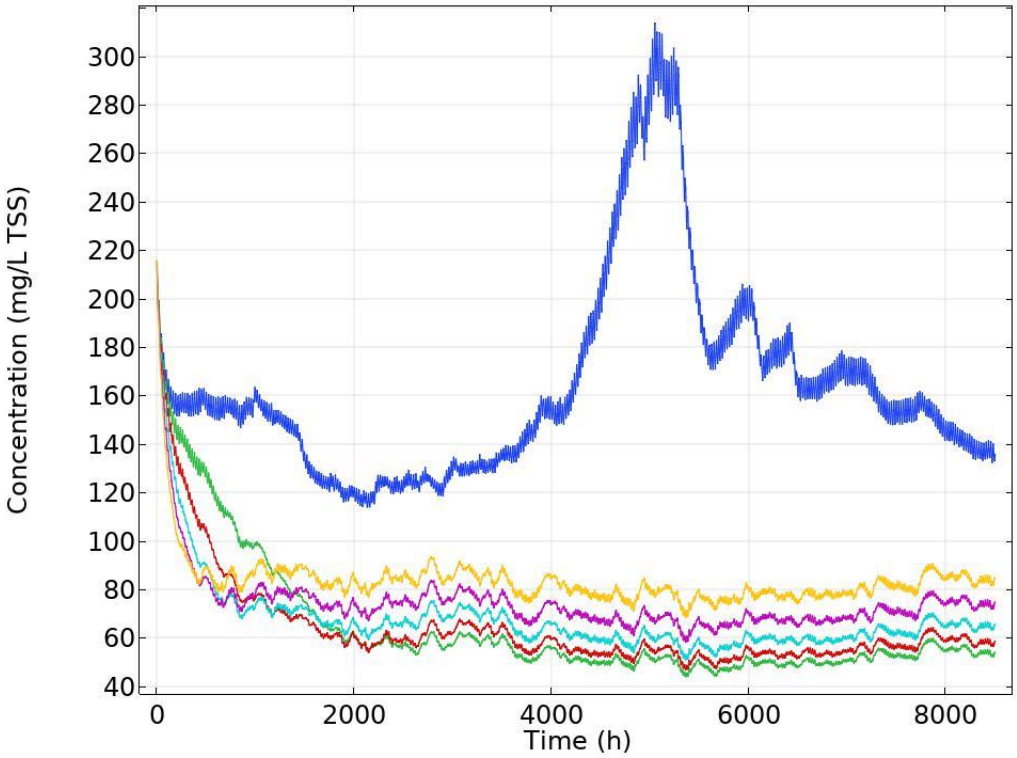

Figure 15. Variation of TSS concentration when varying the HRT. Scenario 1: dark blue; Scenario 3: green; Scenario 5: red; Scenario 7: pale blue; Scenario 9: pink; Scenario 11: yellow.

For HRT of 8 or 7 d, the depth had little influence over the annual average of TSS concentration, with slightly higher values when operating at 0,5 m. Thus, the maximum biomass production was achieved at HRT of 8 d and 0,5 m of depth (Figure 16). For the other cases, the depth had no influence. As lesser depth involves a greater penetration of the solar irradiance, the results suggest that in Minas Gerais it is so elevated that its attenuation when operating at greater depth enhances the microalgae growth.

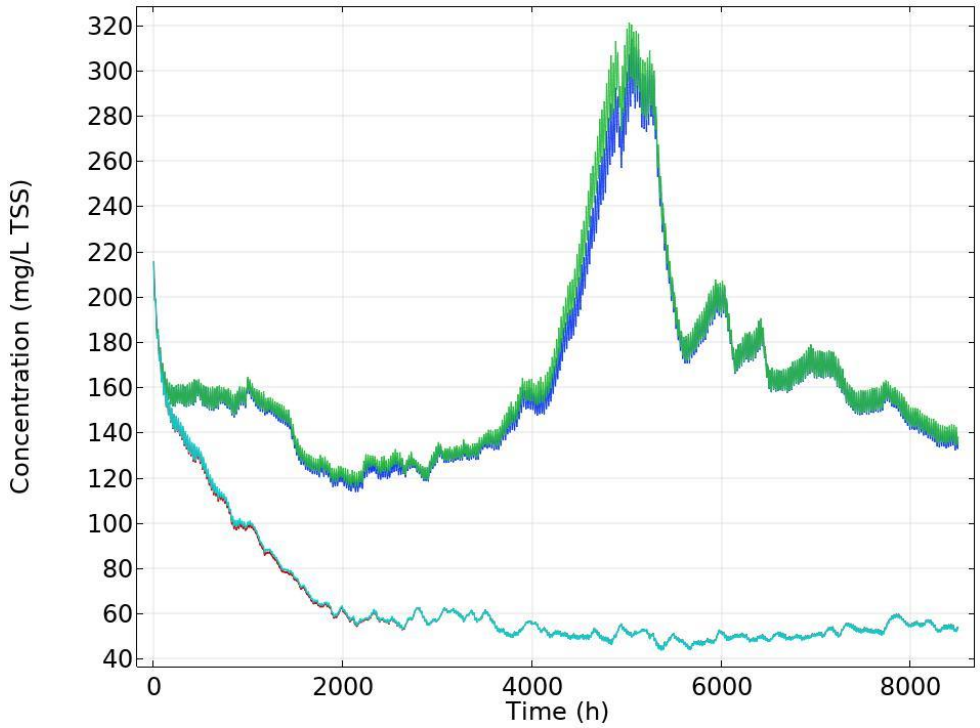

Figure 16. Variation of TSS concentration in function of depth for an HRT of 7 d (0,3 and 0,5 m in red and pale blue respectively) and 8 d (0,3 and 0,5 m in dark blue and green respectively).

Although the TSS concentration increased when using HRT lower than 5 d (Figure 17), it may be related not with the biomass production, but with the lack of consumption of the particulate organic matter that enters in the HRAP.

Considering that the regulation for sewage treatment from Minas Gerais determines that the maximum concentration of TSS allowed in the effluent is 150 mg·L^{-1}, in the scenarios where there is an acceptable biomass generation, the settler placed after the HRAP would have to efficiently remove, at least, 55-60% of the TSS to accomplish with the regulation. An optimum performance of the settler would also enhance the biomass recovery for further valorisation.

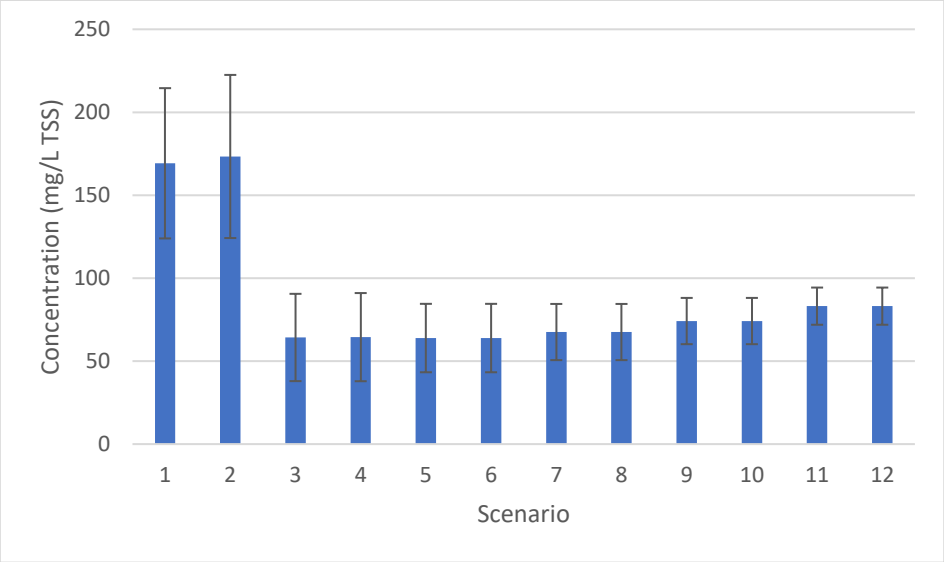

Figure 17. Average concentration of TSS obtained at each scenario.

4.2.2 Nitrogen and phosphorus

The current Brazilian regulation establishes that the limit of ammonium nitrogen (NH_4^+-N) is 20 mg·L^{-1} N. When only considering ammonium nitrogen obtained in the simulation, the annual average exceeded the maximum value when operating with an HRT lower than 7 d, for both depths (Figure 18). However, this limit may be surpassed punctually at higher HRT. The lowest levels corresponded to those obtained when employing an HRT of 8 d, which may be attributed to the higher biomass production and, thus, to its activity treating the wastewater. In Europe, the regulation specifies that the annual average concentration of total nitrogen (TN) cannot be higher than 15 mg·L^{-1} N (in populations from 10.000 to 100.000 equivalent inhabitants). Considering TN as the sum the different species of inorganic nitrogen (not taking into account the organic nitrogen, whose concentration would depend on the efficiency of the settler) no scenario would comply with the requirement. This simulated removal efficiency is higher than the reported by Vassalle et al., 2020b (Tables 1 and 5).

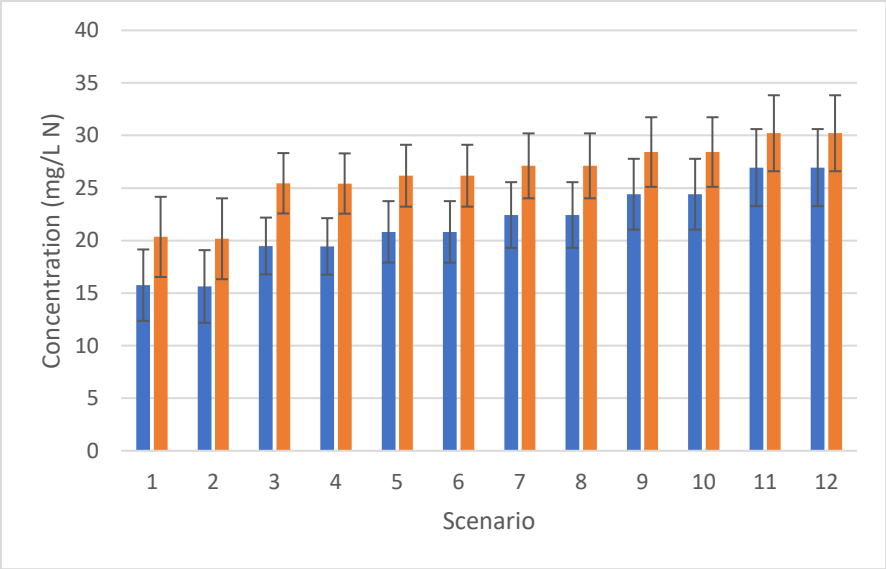

Figure 18. Average concentration and standard deviation of ammonium nitrogen (blue) and TN (orange) at each scenario.

With regards to phosphorus, neither Brazil nor Minas Gerais have any specification in their regulation. Regarding the European regulation, it establishes that the maximum annual average concentration of total phosphorus (TP) is 2 $mg \cdot L^{-1}$ P (in populations from 10.000 to 100.000 population equivalent). It can be seen in Figure 19 that, at least when omitting the organic phosphorus (as in the case of total nitrogen), the requirement was fulfilled only at scenarios 1 and 2. The lower values for phosphorus in these scenarios can also be attributed to the higher microalgal growth.

It can be observed that, at lower HRT, the annual average levels of phosphorus and nitrogen increase. That phenomenon can be associated with the lack of microalgae in the HRAP.

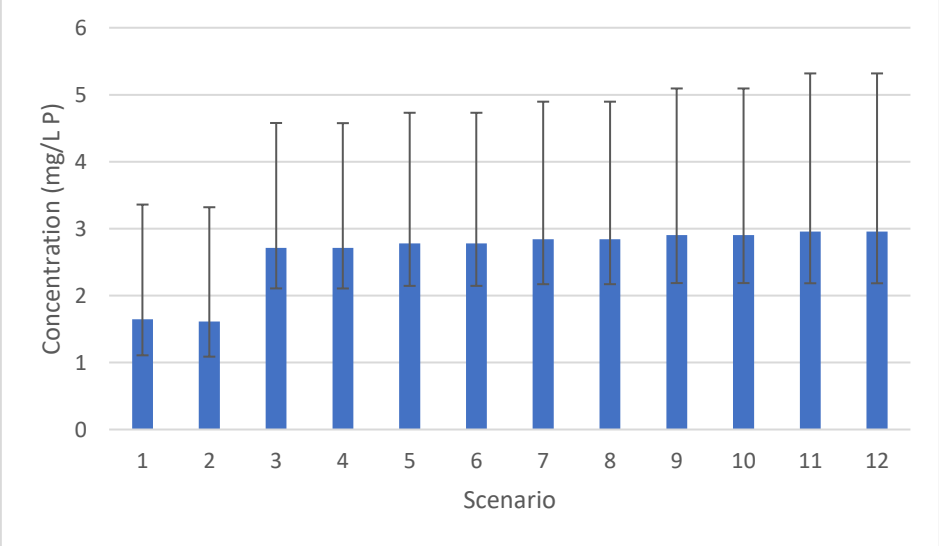

Figure 19. Average concentration and standard deviation of TP obtained at each scenario.

As for TSS, for HRT of 8 and 7 d, a little difference can be seen between operating with a depth of 0,3 or 0,5 m. In both cases, the simulation showed that at 0,5 m the levels of phosphorus and nitrogen were slightly lower. Once again, it can be correlated with the fact that the biomass is subtly higher at that depth, especially for HRT of 8 d. However, it does not seem to be an

extremely relevant factor in that case. In the rest of scenarios, the variation of the depth did not suppose any difference in the average concentrations.

Scenario	Depth (m)	HRT (d)	Computation time (s)	Annual average concentration ($mg \cdot L^{-1}$)				Annual average removal (%)			TSS production ($g \cdot m^{-2} \cdot d^{-1}$)
				NH_4^+-N	TN	TP	TSS	NH_4^+-N	TN	TP	
1	0,3	8	36	15,8	20,3	1,6	169,2	60,6	50,1	50,2	6,4
2	0,5	8	24	15,6	20,2	1,6	173,3	60,9	50,5	51,1	10,9
3	0,3	7	18	19,5	25,5	2,7	64,3	51,2	37,6	17,8	2,8
4	0,5	7	9	19,4	25,4	2,7	64,5	51,3	37,6	17,8	4,6
5	0,3	6	10	20,8	26,2	2,8	63,9	47,9	35,8	15,8	3,2
6	0,5	6	10	20,8	26,2	2,8	63,9	47,9	35,8	15,8	5,3
7	0,3	5	9	22,4	27,1	2,8	67,5	43,9	33,5	14,0	4,1
8	0,5	5	9	22,4	27,1	2,8	67,5	43,9	33,5	14,0	6,8
9	0,3	4	10	24,4	28,4	2,9	74,2	38,9	30,3	12,1	5,6
10	0,5	4	11	24,4	28,4	2,9	74,2	38,9	30,3	12,1	9,3
11	0,3	3	11	26,9	30,2	3,0	83,1	32,6	25,9	10,5	8,3
12	0,5	3	11	26,9	30,2	3,0	83,1	32,6	25,9	10,5	13,9

Table 5. Results for the simulation of the 12 scenarios.

5. Conclusions

In this study, the BIO_ALGAE 2 model was employed to predict the performance of a demonstrative-scale HRAP which is currently under construction in Belo Horizonte, Brazil, and that will be operated by the UFMG. Twelve scenarios were defined to evaluate the influence of the HRT and the depth in the results of the wastewater treatment and the microalgal biomass production.

The use of RE interface with a 0D geometry instead of the TDS interface with a 1D geometry in the software COMSOL provided an approximately 500 times faster simulation, which was also easier to operate, giving rise to the same results.

The simulations for the 12 defined scenarios combining different HRT and depths in the demonstrative HRAP, showed that the only HRT that promoted a proper biomass growth was 8 d, being slightly higher with a depth of 0,5 m. Moreover, these scenarios had the best performances removing nitrogen and phosphorus, evidencing the clear relation between the biomass production and the pollutants elimination, and achieving values in accordance with the current regulation for sewage treatment and discharge in Brazil and, specifically, in Minas Gerais. However, to ensure that these regulations are accomplished, efficient settling or biomass harvesting following the HRAP must be ensured to minimize the organic fraction of nitrogen and phosphorus (that have not been considered in this study), as well as the TSS, in the final effluent. That would also enhance the biomass recovery for its valorisation.

As far as calibration is concerned, for some of the main species, an adequate fitting was not achieved. Indeed, the model can basically be implemented to estimate the global performance of the HRAP for long periods, but it cannot properly predict the dynamic variations or state of the system at punctual moments. It would be appropriate to carry out a future study to check if a better calibration could be achieved. Moreover, it is highly recommended to complement this study with experimental campaigns, especially at low HRT, in order to confirm the predictions of the model. Once the HRAP is operating, the effects of varying the HRT and depth could be experimentally evaluated. In this way, the accuracy of the model and its calibration for that case could be tested and validated.

6. Acknowledgements

This thesis has been developed during the 2020 Covid-19 pandemic, so first of all I would want to express my gratitude to all the people that continued working during that crisis, in such a risky situation, to keep us safe.

I would also want to thank my tutors, Rubén Díez, Ivet Ferrer (GEMMA) and Fabiana Passos (DESA) who were extremely supportive during all the process, including when the initial project in Brazil had to be cancelled due to the whole situation and we had to start from zero. Fortunately, I could keep collaborating with the UFMG with this new work. I also want to express my gratitude to Lucas Vassalle (DESA) and Estel Rueda (GEMMA) for their helpful advices on data treatment and comprehension of the COMSOL software, respectively.

I must include in this appreciation to the CCD for funding the project "Strategies for Enhancing Sustainable Treatment of Wastewater and Food Waste" (2019-B017) and, especially, to Eva Vendrell, who attentively assisted us during the whole period.

Finally, I would want to thank my family, that were encouraging all the time, even in the hardest moments.

7. Bibliography

Alcántara, C., Posadas, E., Guieysse, B., Muñoz, R., 2015. Microalgae-based Wastewater Treatment. Handb. Mar. Microalgae Biotechnol. Adv. 439–455. https://doi.org/10.1016/B978-0-12-800776-1.00029-7

Chatterjee, P., Ghangrekar, M.M., 2017. Biomass granulation in an upflow anaerobic sludge blanket reactor treating 500 m3/day low-strength sewage and post treatment in high-rate algal pond. Water Sci. Technol. 76, 1234–1242. https://doi.org/10.2166/wst.2017.269

COMSOL Multiphysics® Software - Understand, Predict, and Optimize [WWW Document], n.d. URL https://www.comsol.com/comsol-multiphysics (accessed 4.12.20).

Dani, D., Thirugnanamurthy, S., Kandasamy, S., Shalini, B., Baruah, A., R, K., Dam Roy, S., 2016. A Review on Microalgae as Potential Fish Feed Ingredient. J. Andaman Sci. Assoc. 21, 140–144.

Dar, R.A., Sharma, N., Kaur, K., Phutela, U.G., 2019. Feasibility of Microalgal Technologies in Pathogen Removal from Wastewater, Feasibility of Microalgal Technologies in Pathogen Removal from Wastewater. https://doi.org/10.1007/978-3-030-13913-1

Daud, M.K., Rizvi, HinaDaud, M. K., Rizvi, H., Akram, M. F., Ali, S., Rizwan, M., Nafees, M., & Jin, Z. S. (2018). Review of upflow anaerobic sludge blanket reactor technology: Effect of different parameters and developments for domestic wastewater treatment. Journal, 2018. https://doi.org/10.1155/2018/1596319, Akram, M.F., Ali, S., Rizwan, M., Nafees, M., Jin, Z.S., 2018. Review of upflow anaerobic sludge blanket reactor technology: Effect of different parameters and developments for domestic wastewater treatment. J. Chem. 2018. https://doi.org/10.1155/2018/1596319

de Godos, I., Blanco, S., García-Encina, P.A., Becares, E., Muñoz, R., 2010. Influence of flue gas sparging on the performance of high rate algae ponds treating agro-industrial wastewaters. J. Hazard. Mater. 179, 1049–1054. https://doi.org/10.1016/j.jhazmat.2010.03.112

Delgadillo-Mirquez, L., Lopes, F., Taidi, B., Pareau, D., 2016. Nitrogen and phosphate removal

from wastewater with a mixed microalgae and bacteria culture. Biotechnol. Reports 11, 18–26. https://doi.org/10.1016/j.btre.2016.04.003

Dineshkumar, R., Subramanian, J., Gopalsamy, J., Jayasingam, P., Arumugam, A., Kannadasan, S., Sampathkumar, P., 2019. The Impact of Using Microalgae as Biofertilizer in Maize (Zea mays L.). Waste and Biomass Valorization 10, 1101–1110. https://doi.org/10.1007/s12649-017-0123-7

Du, X., Tao, Y., Li, H., Liu, Y., Feng, K., 2019. Synergistic methane production from the anaerobic co-digestion of Spirulina platensis with food waste and sewage sludge at high solid concentrations. Renew. Energy 142, 55–61. https://doi.org/10.1016/j.renene.2019.04.062

García, J., Mujeriego, R., Hernández-Mariné, M., 2000. High rate algal pond operating strategies for urban wastewater nitrogen removal. J. Appl. Phycol. 12, 331–339. https://doi.org/10.1023/A:1008146421368

Gujer, W., Zehnder, A.J.B., 1983. Conversion processes in anaerobic digestion. Water Sci. Technol. 15, 127–167. https://doi.org/10.2166/wst.1983.0164

Gutiérrez-Alfaro, S., Rueda-Márquez, J.J., Perales, J.A., Manzano, M.A., 2018. Combining sun-based technologies (microalgae and solar disinfection) for urban wastewater regeneration. Sci. Total Environ. 619–620, 1049–1057. https://doi.org/10.1016/j.scitotenv.2017.11.110

Iacopozzi, I., Innocenti, V., Marsili-Libelli, S., Giusti, E., 2007. A modified Activated Sludge Model No. 3 (ASM3) with two-step nitrification-denitrification. Environ. Model. Softw. 22, 847–861. https://doi.org/10.1016/j.envsoft.2006.05.009

Leong, Y.K., Chang, J.S., 2020. Bioremediation of heavy metals using microalgae: Recent advances and mechanisms. Bioresour. Technol. 303, 122886. https://doi.org/10.1016/j.biortech.2020.122886

Lier, J.B. van, Mahmoud, N., Zeeman, G., 2008. Anaerobic wastewater treatment, Environmental Science and Technology. https://doi.org/10.1021/es00154a002

Lin, C.S.K., Pfaltzgraff, L.A., Herrero-Davila, L., Mubofu, E.B., Abderrahim, S., Clark, J.H., Koutinas, A.A., Kopsahelis, N., Stamatelatou, K., Dickson, F., Thankappan, S., Mohamed, Z., Brocklesby, R., Luque, R., 2013. Food waste as a valuable resource for the production of chemicals, materials and fuels. Current situation and global perspective. Energy Environ. Sci. 6, 426–464. https://doi.org/10.1039/c2ee23440h

Meegoda, J.N., Li, B., Patel, K., Wang, L.B., 2018. A review of the processes, parameters, and optimization of anaerobic digestion. Int. J. Environ. Res. Public Health 15. https://doi.org/10.3390/ijerph15102224

Mehrabadi, A., Craggs, R., Farid, M.M., 2015. Wastewater treatment high rate algal ponds (WWT HRAP) for low-cost biofuel production. Bioresour. Technol. 184, 202–214. https://doi.org/10.1016/j.biortech.2014.11.004

Park, J.B.K., Craggs, R.J., 2011. Algal production in wastewater treatment high rate algal ponds for potential biofuel use. Water Sci. Technol. 63, 2403–2410. https://doi.org/10.2166/wst.2011.200

Park, J.B.K., Craggs, R.J., Shilton, A.N., 2011. Wastewater treatment high rate algal ponds for biofuel production. Bioresour. Technol. 102, 35–42. https://doi.org/10.1016/j.biortech.2010.06.158

Robles, Á., Capson-Tojo, G., Galès, A., Ruano, M.V., Sialve, B., Ferrer, J., Steyer, J.P., 2020. Microalgae-bacteria consortia in high-rate ponds for treating urban wastewater: Elucidating the key state indicators under dynamic conditions. J. Environ. Manage. 261. https://doi.org/10.1016/j.jenvman.2020.110244

Roostaei, J., Zhang, Y., Gopalakrishnan, K., Ochocki, A.J., 2018. Mixotrophic Microalgae Biofilm: A Novel Algae Cultivation Strategy for Improved Productivity and Cost-efficiency of Biofuel Feedstock Production. Sci. Rep. 8, 1–10. https://doi.org/10.1038/s41598-018-31016-1

Santiago, A.F., Calijuri, M.L., Assemany, P.P., Calijuri, M.D.C., Reis, A.J.D. Dos, 2013. Algal biomass production and wastewater treatment in high rate algal ponds receiving disinfected effluent. Environ. Technol. (United Kingdom) 34, 1877–1885. https://doi.org/10.1080/09593330.2013.812670

Solimeno, A., García, J., 2017. Microalgae-bacteria models evolution: From microalgae steady-state to integrated microalgae-bacteria wastewater treatment models – A comparative review. Sci. Total Environ. 607–608, 1136–1150. https://doi.org/10.1016/j.scitotenv.2017.07.114

Solimeno, A., Gómez-Serrano, C., Acién, F.G., 2019. BIO_ALGAE 2: improved model of microalgae and bacteria consortia for wastewater treatment. Environ. Sci. Pollut. Res. 26, 25855–25868. https://doi.org/10.1007/s11356-019-05824-5

Solimeno, A., Parker, L., Lundquist, T., García, J., 2017. Integral microalgae-bacteria model (BIO_ALGAE): Application to wastewater high rate algal ponds. Sci. Total Environ. 601–602, 646–657. https://doi.org/10.1016/j.scitotenv.2017.05.215

Solimeno, A., Samsó, R., Uggetti, E., Sialve, B., Steyer, J.P., Gabarró, A., García, J., 2015. New mechanistic model to simulate microalgae growth. Algal Res. 12, 350–358. https://doi.org/10.1016/j.algal.2015.09.008

Sutherland, D.L., Ralph, P.J., 2019. Microalgal bioremediation of emerging contaminants - Opportunities and challenges. Water Res. 164, 114921. https://doi.org/10.1016/j.watres.2019.114921

Tarlan, E., Dilek, F.B., Yetis, U., 2002. Effectiveness of algae in the treatment of a wood-based pulp and paper industry wastewater. Bioresour. Technol. 84, 1–5. https://doi.org/10.1016/S0960-8524(02)00029-9

Vargas e Silva, F., Monteggia, L.O., 2015. Pyrolysis of algal biomass obtained from high-rate algae ponds applied to wastewater treatment. Front. Energy Res. 3, 1–6. https://doi.org/10.3389/fenrg.2015.00031

Vassalle, L., Díez-Montero, R., Machado, A.T.R., Moreira, C., Ferrer, I., Mota, C.R., Passos, F., 2020a. Upflow anaerobic sludge blanket in microalgae-based sewage treatment: Co-digestion for improving biogas production. Bioresour. Technol. 300, 122677. https://doi.org/10.1016/j.biortech.2019.122677

Vassalle, L., García-Galán, M.J., Aquino, S.F., Afonso, R.J. de C.F., Ferrer, I., Passos, F., R Mota, C., 2020b. Can high rate algal ponds be used as post-treatment of UASB reactors to remove micropollutants? Chemosphere 248. https://doi.org/10.1016/j.chemosphere.2020.125969

Villar-Navarro, E., Baena-Nogueras, R.M., Paniw, M., Perales, J.A., Lara-Martín, P.A., 2018. Removal of pharmaceuticals in urban wastewater: High rate algae pond (HRAP) based

technologies as an alternative to activated sludge based processes. Water Res. 139, 19–29. https://doi.org/10.1016/j.watres.2018.03.072

Yun, Y.M., Sung, S., Choi, J.S., Kim, D.H., 2016. Two-stage co-fermentation of lipid-extracted microalgae waste with food waste leachate: A viable way to reduce the inhibitory effect of leftover organic solvent and recover additional energy. Int. J. Hydrogen Energy 41, 21721–21727. https://doi.org/10.1016/j.ijhydene.2016.07.096

Annex I. Graphs of the simulations for each scenario

Total suspended solids (TSS)

The following graphs show the evolution of the concentration of TSS (blue) and its microalgal biomass portion (green).

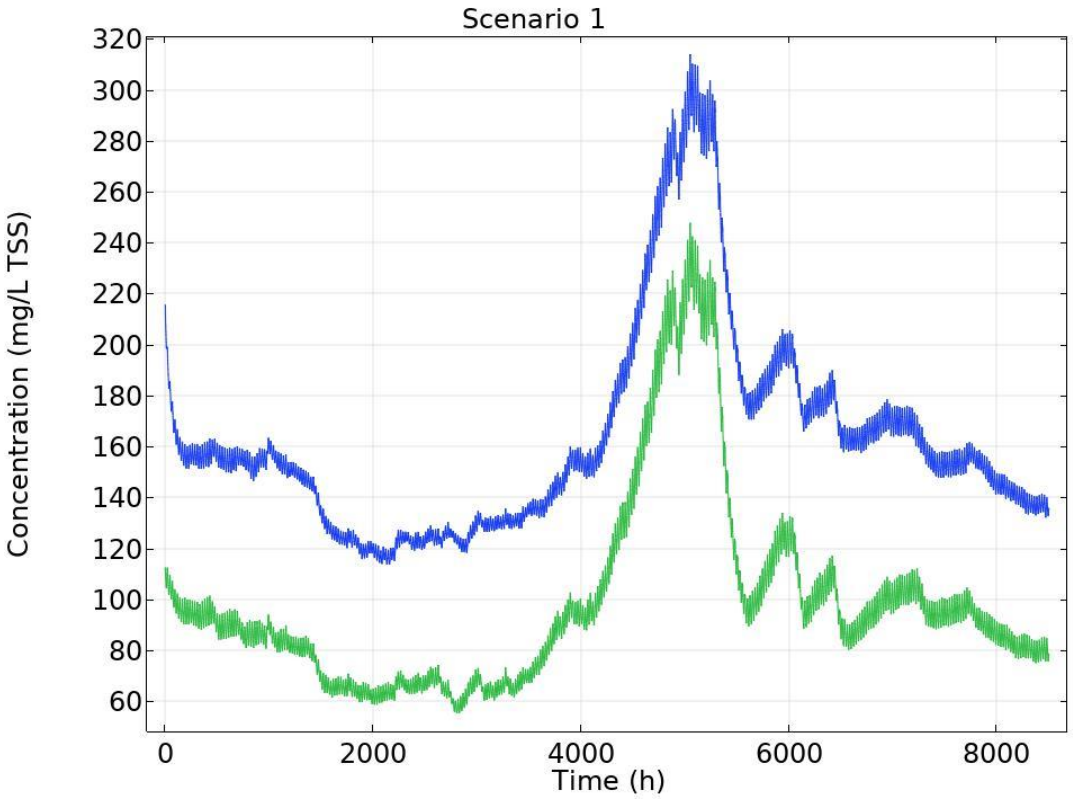

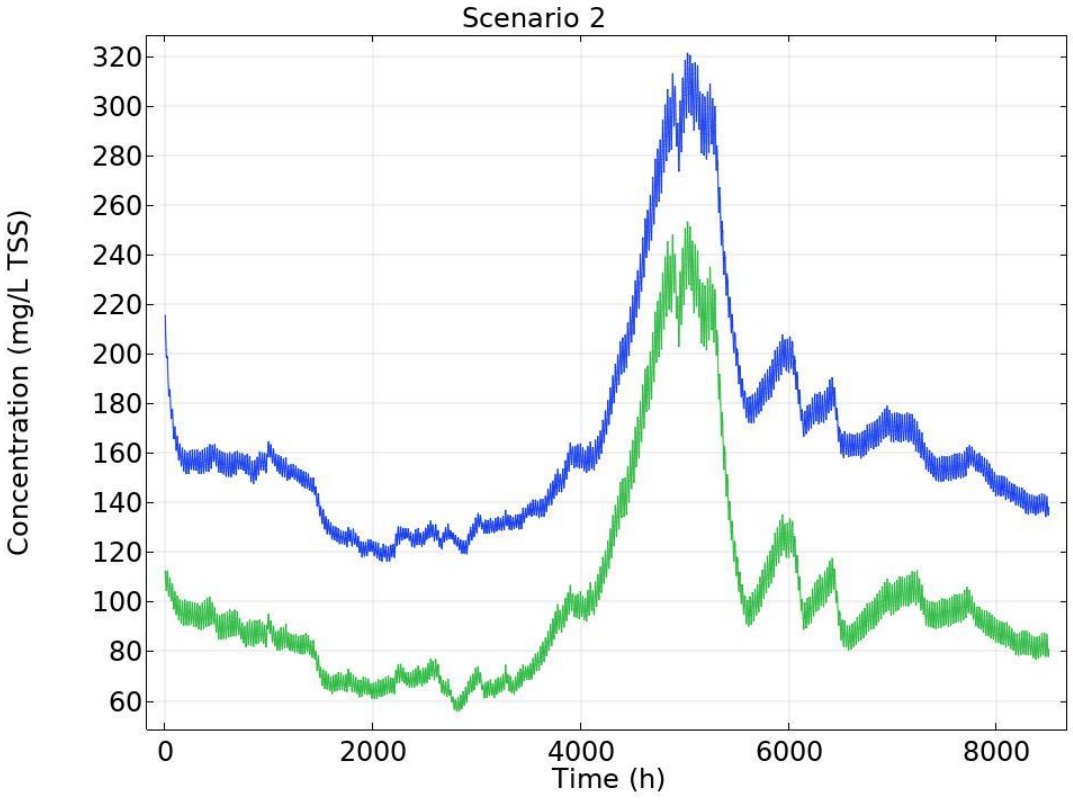

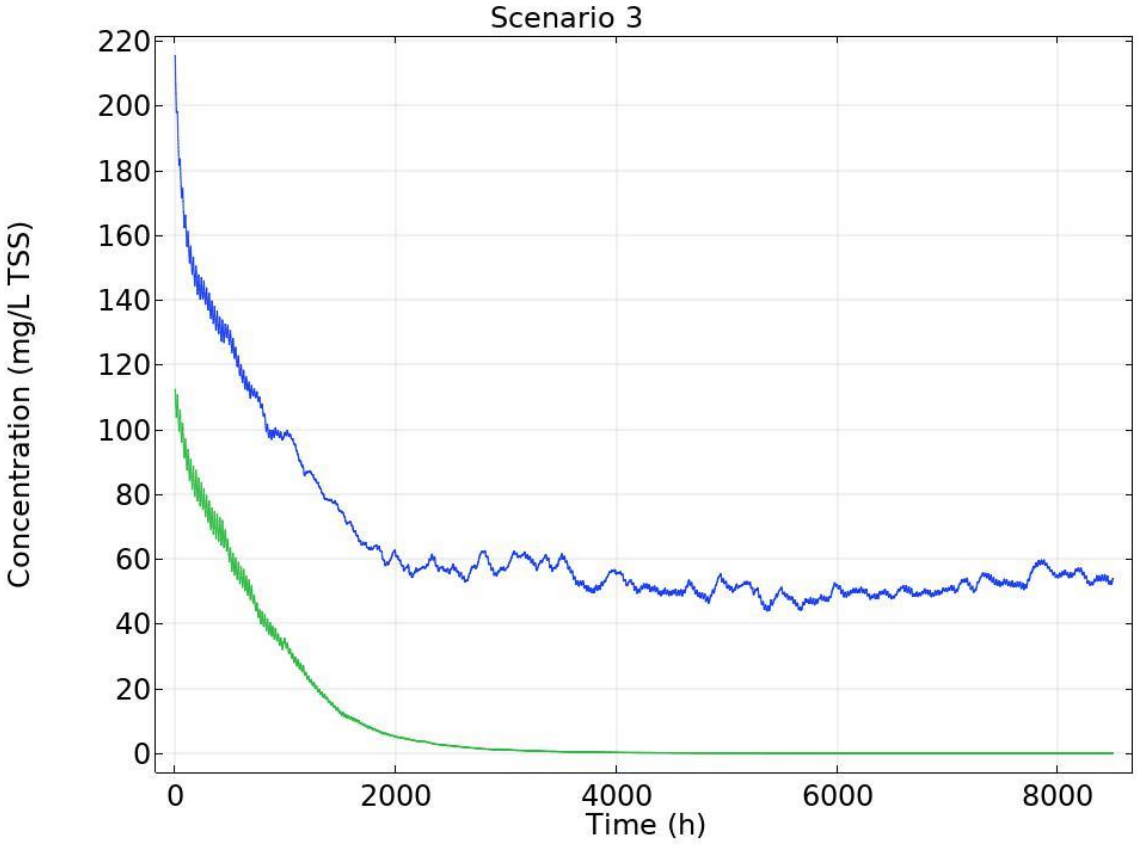
Scenario 3
Concentration (mg/L TSS)
Time (h)
0
20
40
60
80
100
120
140
160
180
200
220
0
2000
4000
6000
8000

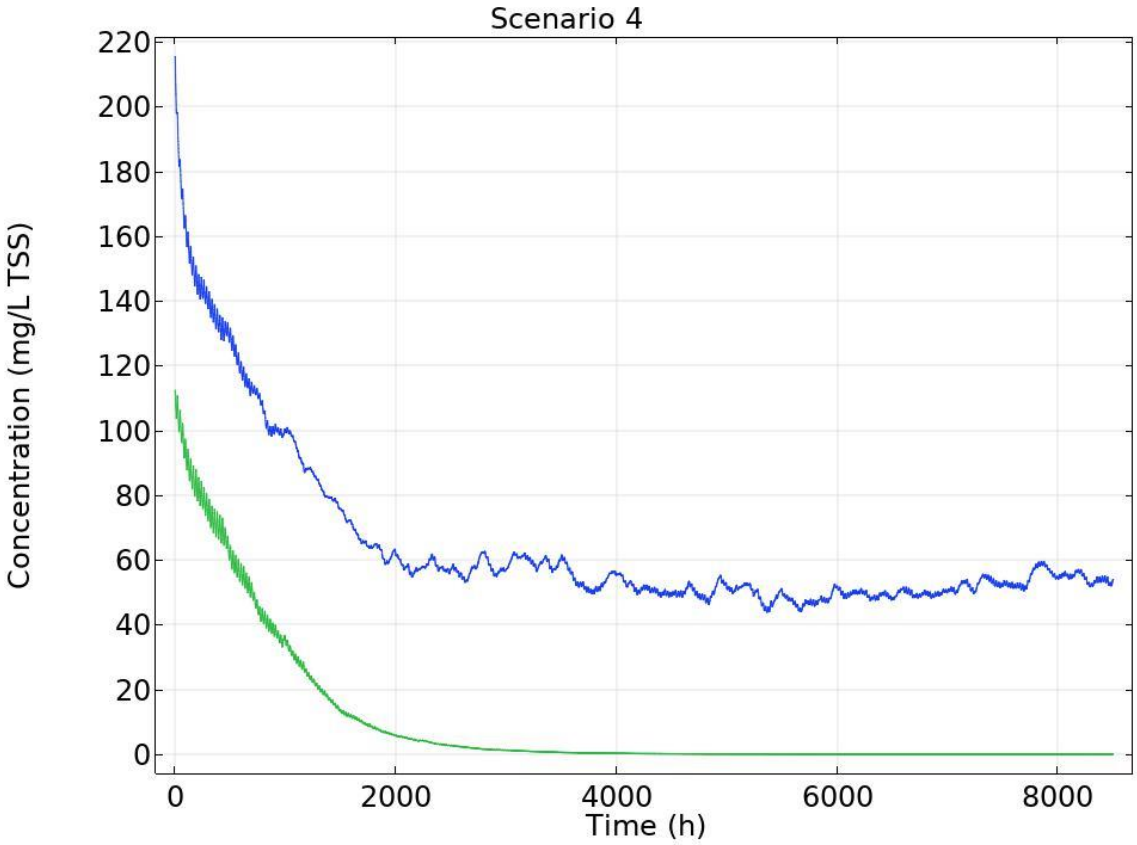
Scenario 4
Concentration (mg/L TSS)
Time (h)
0
20
40
60
80
100
120
140
160
180
200
220
0
2000
4000
6000
8000

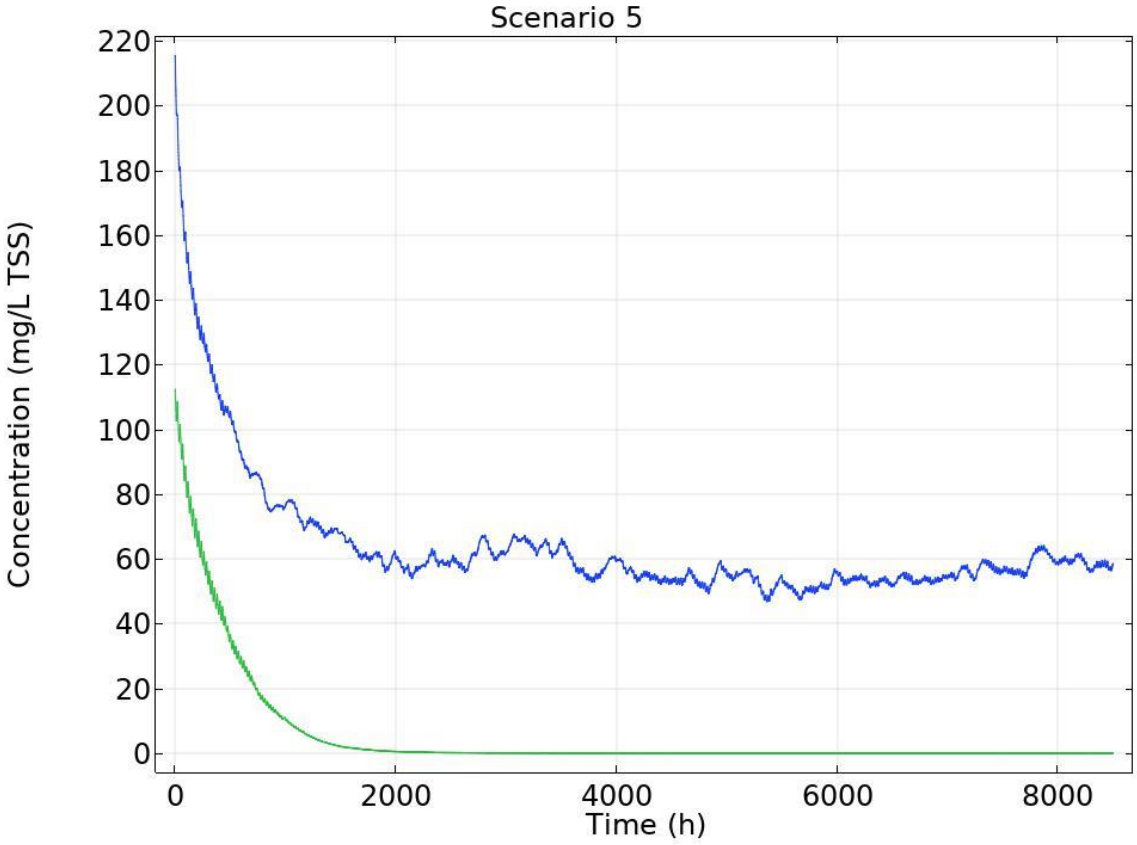
Scenario 5
Concentration (mg/L TSS)
220
200
180
160
140
120
100
80
60
40
20
0
0
2000
4000
6000
8000
Time (h)

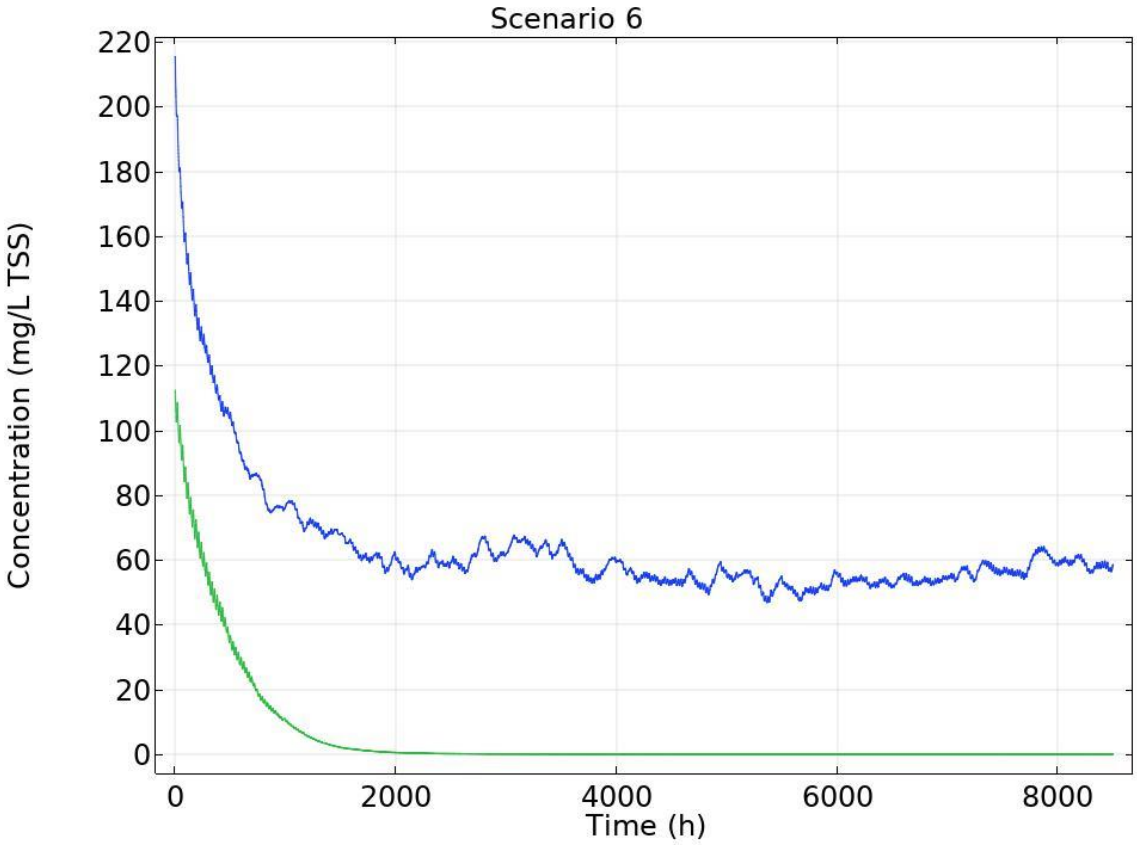
Scenario 6
Concentration (mg/L TSS)
220
200
180
160
140
120
100
80
60
40
20
0
0
2000
4000
6000
8000
Time (h)

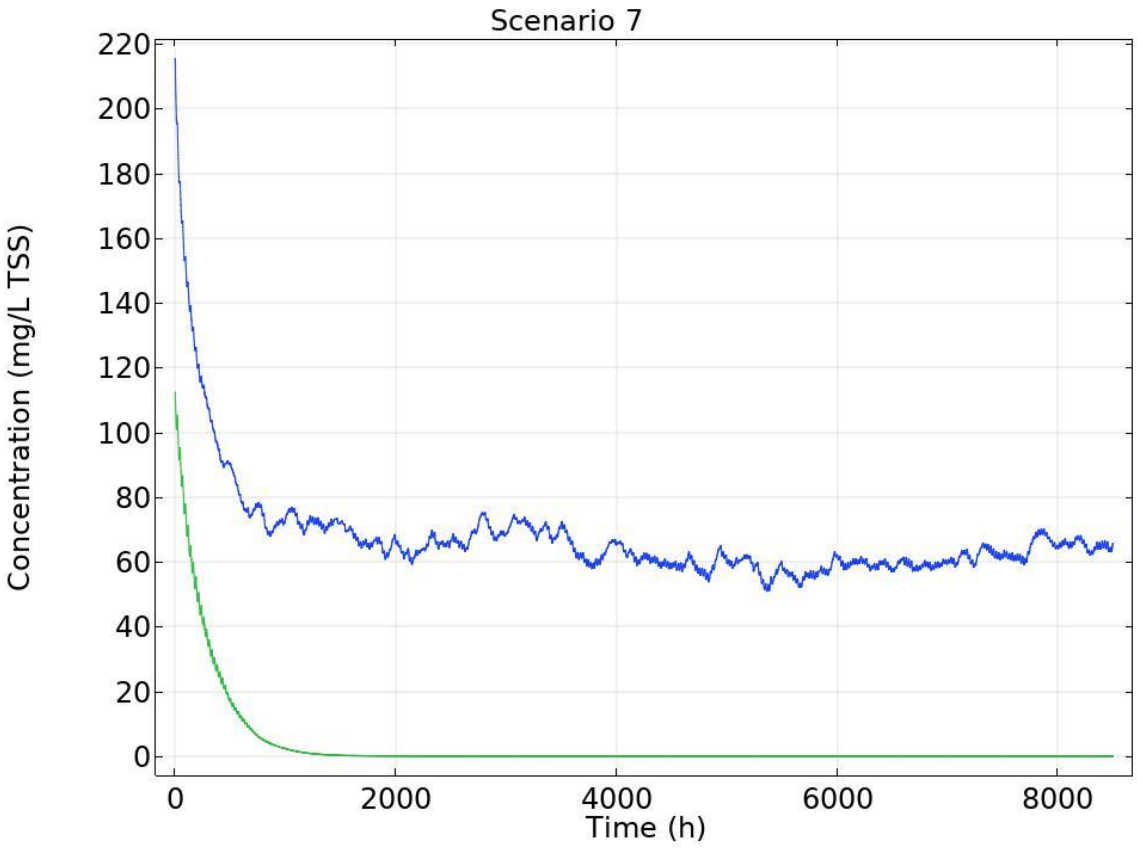
Scenario 7
Concentration (mg/L TSS)
220
200
180
160
140
120
100
80
60
40
20
0
0
2000
4000
6000
8000
Time (h)

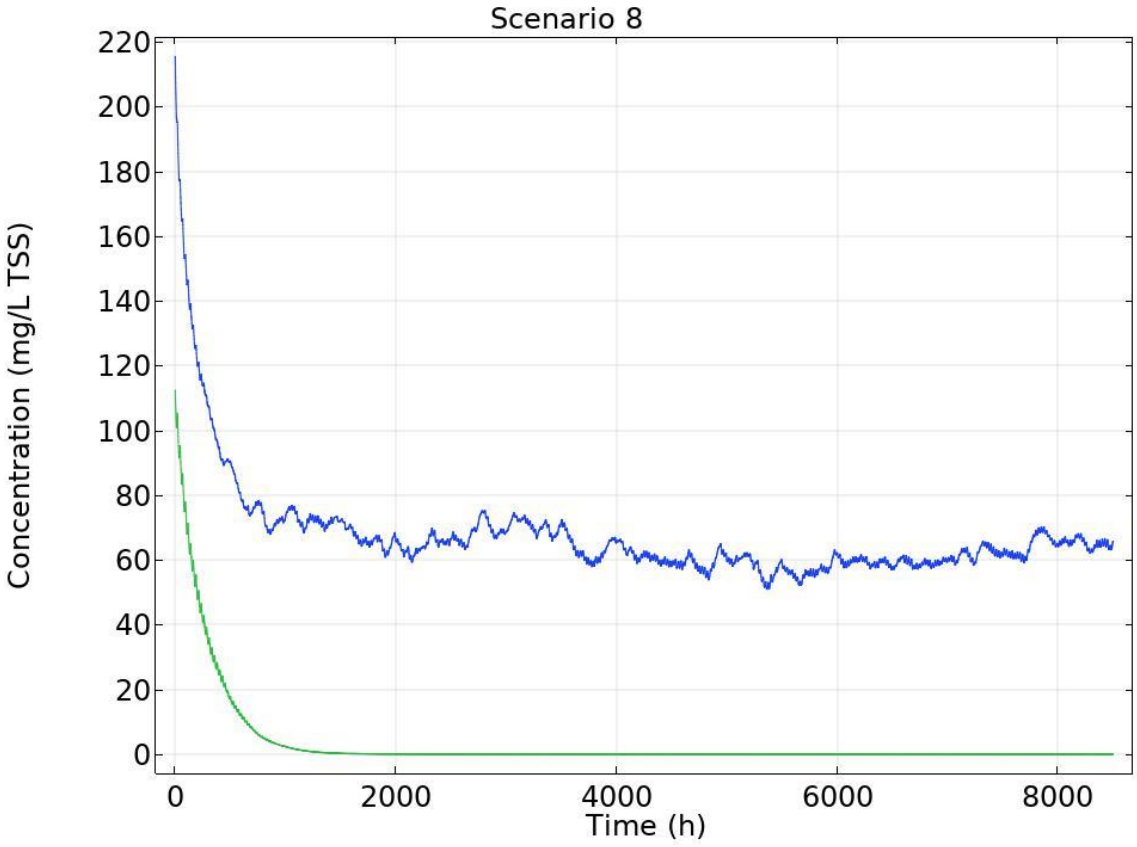
Scenario 8
Concentration (mg/L TSS)
220
200
180
160
140
120
100
80
60
40
20
0
0
2000
4000
6000
8000
Time (h)

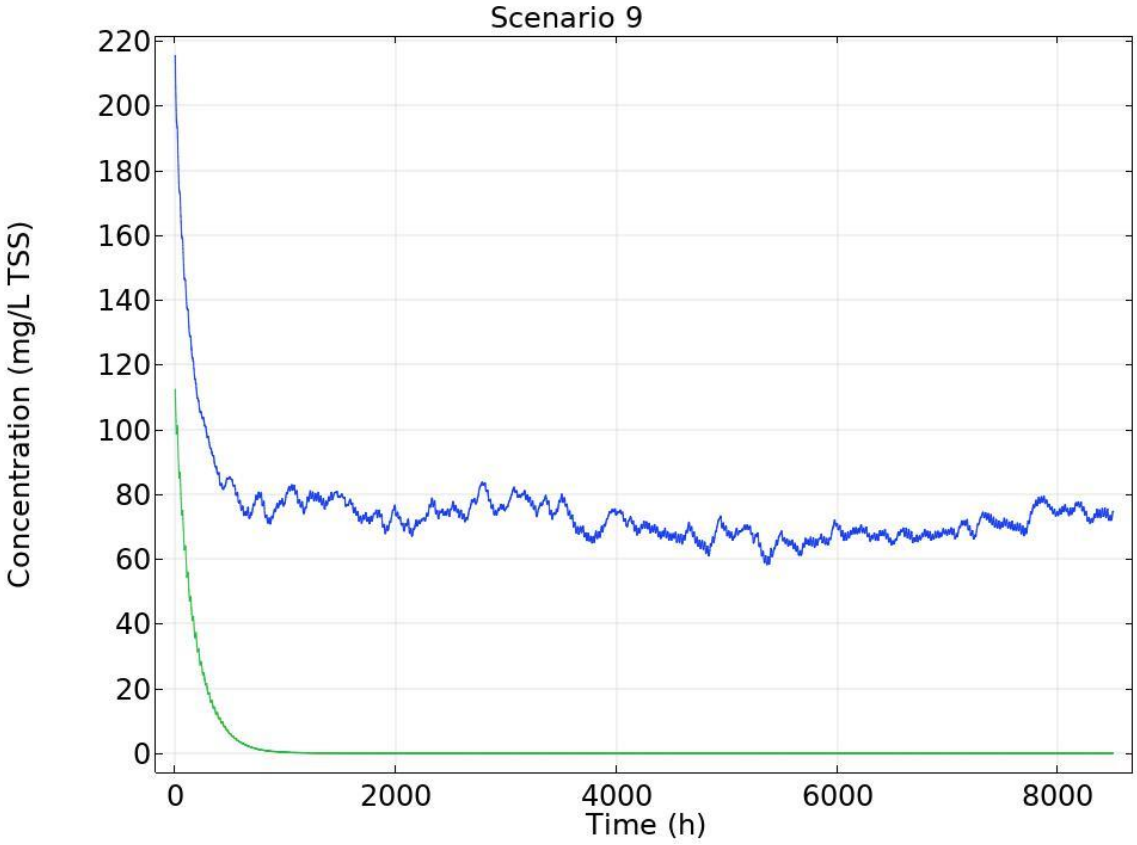
Scenario 9
Concentration (mg/L TSS)
220
200
180
160
140
120
100
80
60
40
20
0
0
2000
4000
6000
8000
Time (h)

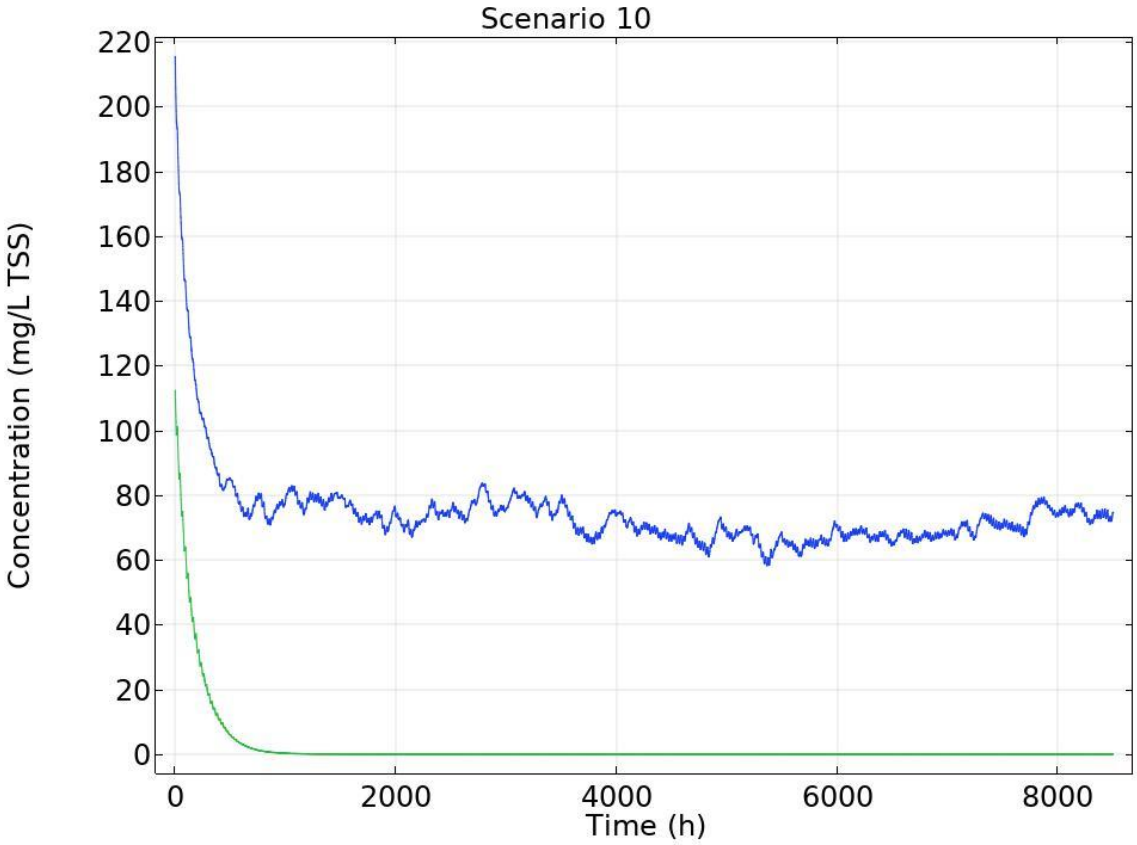
Scenario 10
Concentration (mg/L TSS)
220
200
180
160
140
120
100
80
60
40
20
0
0
2000
4000
6000
8000
Time (h)

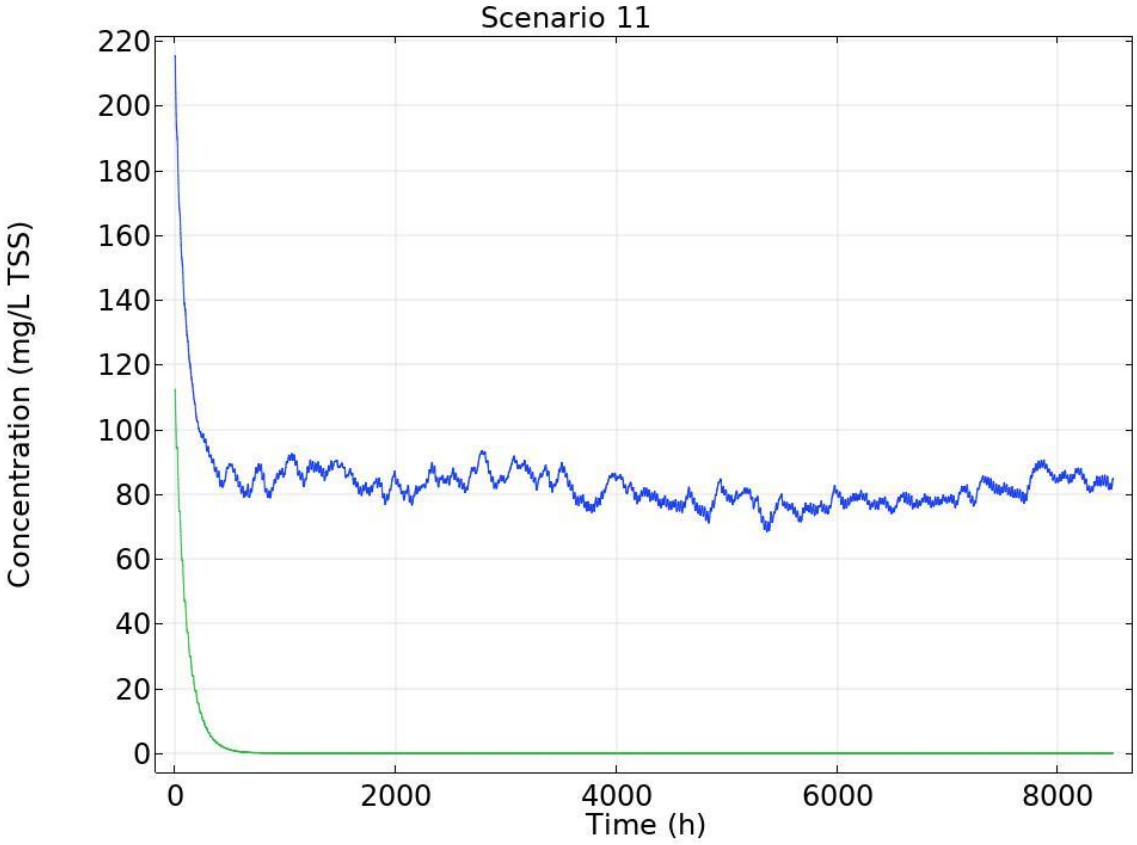
Scenario 11
Concentration (mg/L TSS)
220
200
180
160
140
120
100
80
60
40
20
0
0
2000
4000
6000
8000
Time (h)

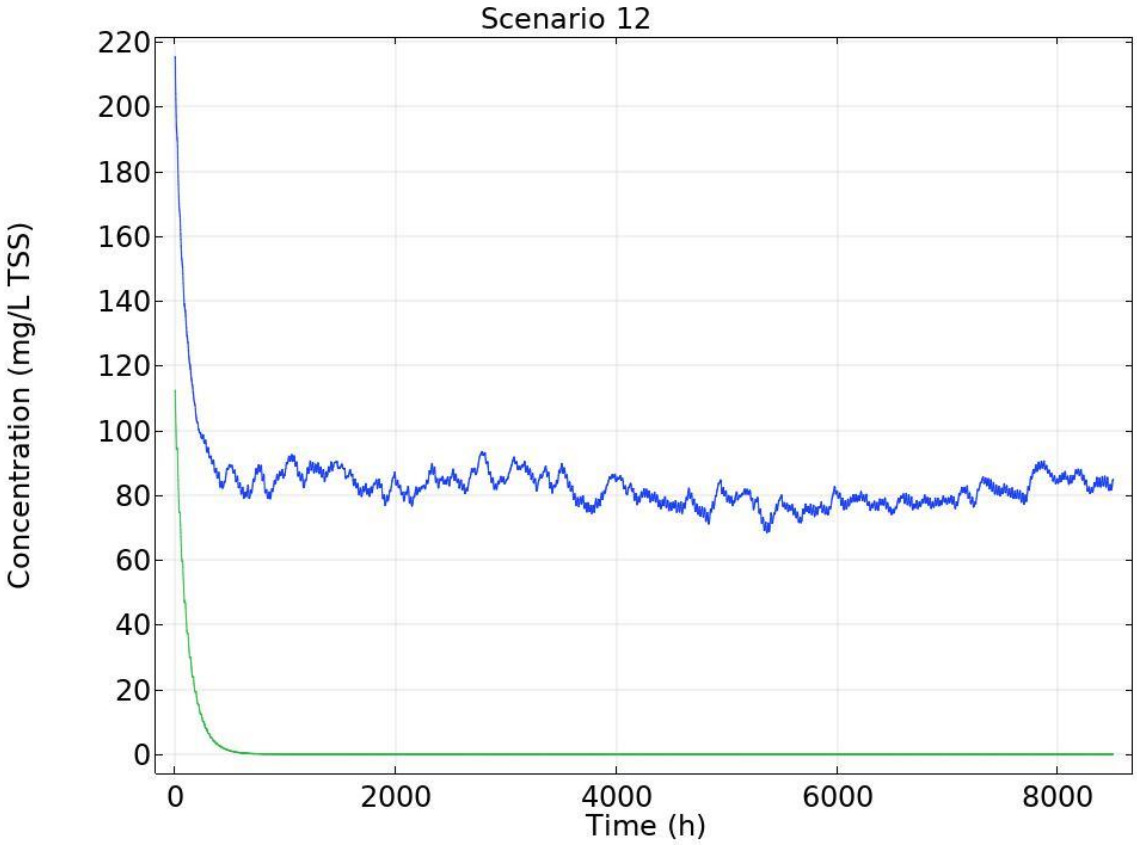
Scenario 12
Concentration (mg/L TSS)
220
200
180
160
140
120
100
80
60
40
20
0
0
2000
4000
6000
8000
Time (h)

Nitrogen

The following graphs show the evolution of the concentration of total nitrogen (blue) and ammonium nitrogen (green). Note that for total nitrogen, organic nitrogen was omitted.

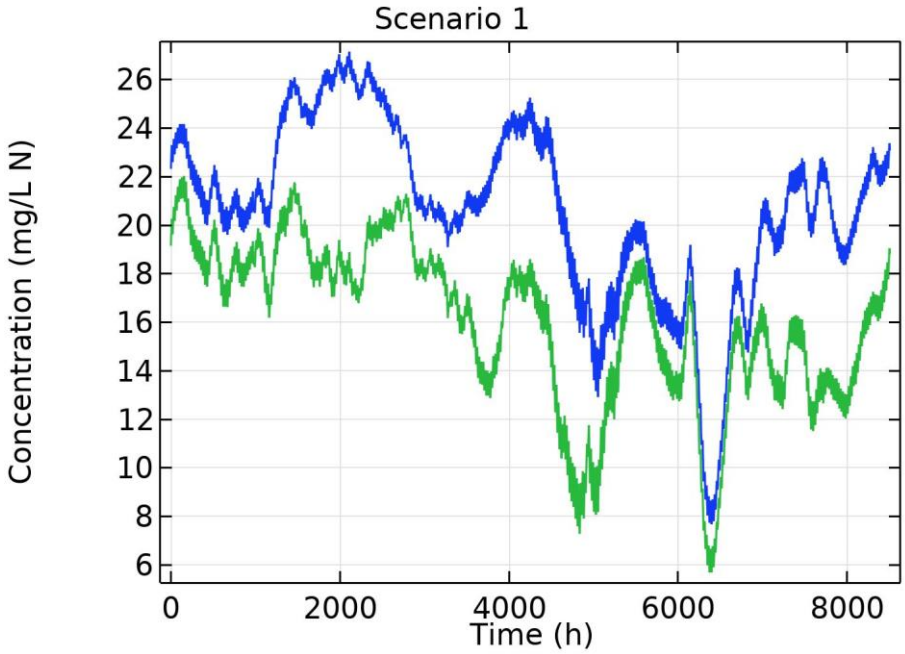

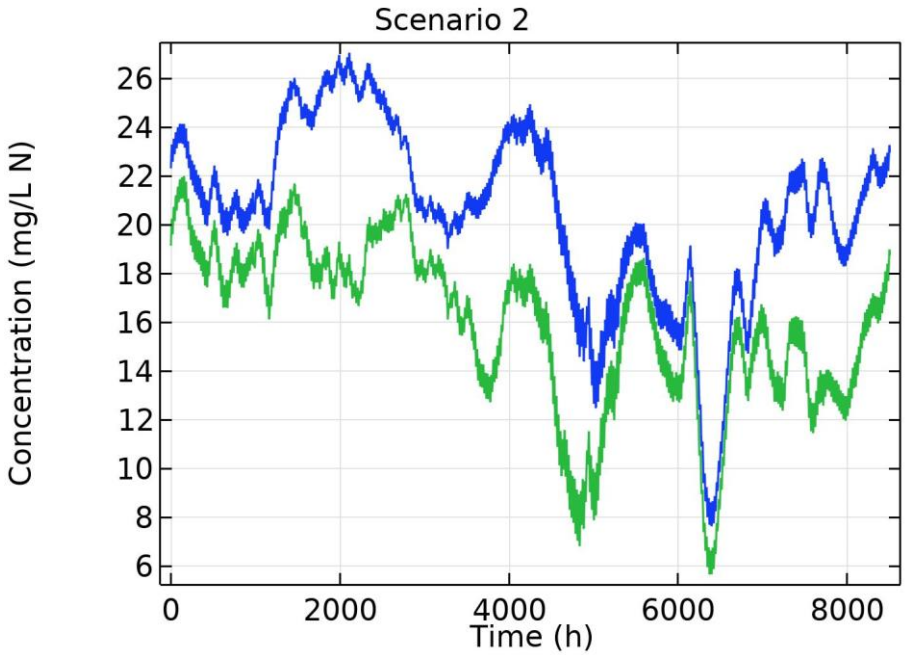

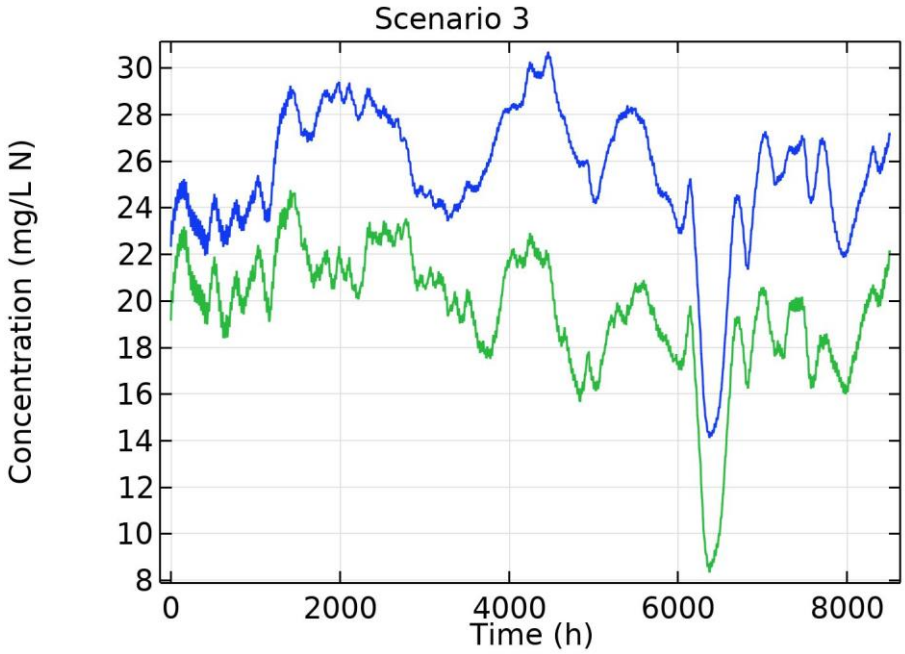
Scenario 3
Concentration (mg/L N)
30
28
26
24
22
20
18
16
14
12
10
8
0
2000
4000
6000
8000
Time (h)

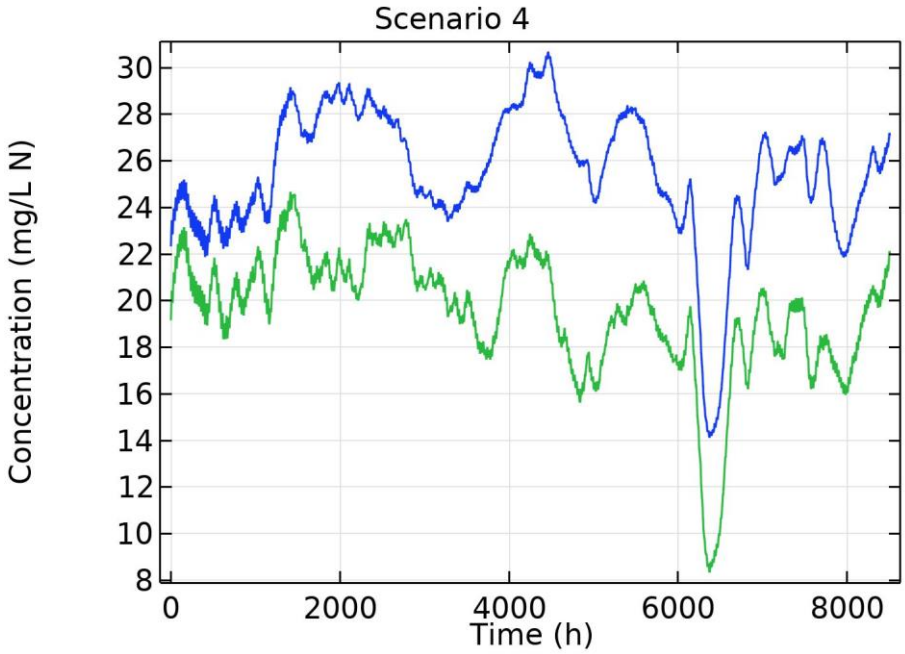
Scenario 4
Concentration (mg/L N)
30
28
26
24
22
20
18
16
14
12
10
8
0
2000
4000
6000
8000
Time (h)

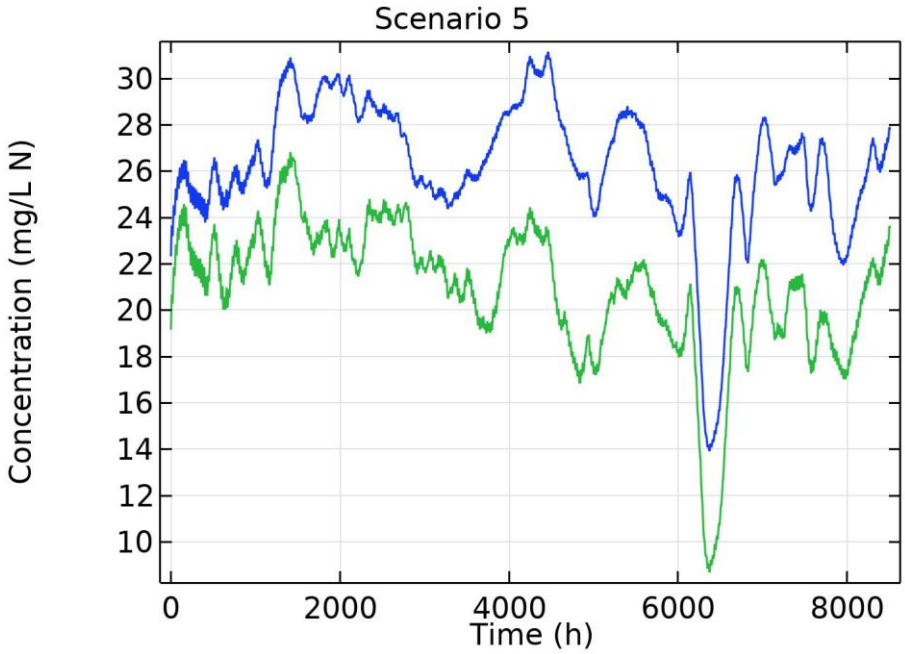
Scenario 5
Concentration (mg/L N)
30
28
26
24
22
20
18
16
14
12
10
0
2000
4000
6000
8000
Time (h)

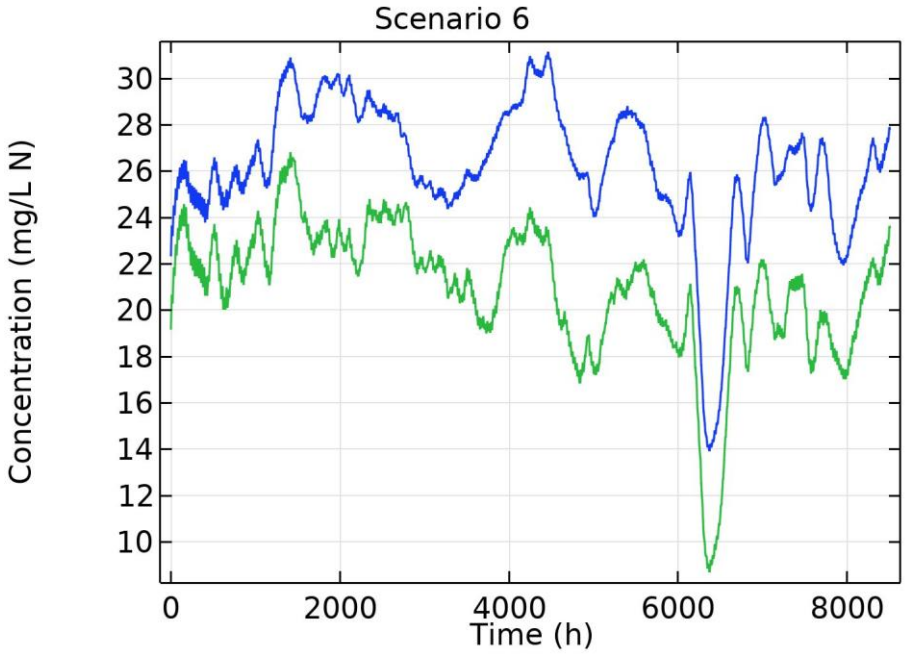
Scenario 6
Concentration (mg/L N)
30
28
26
24
22
20
18
16
14
12
10
0
2000
4000
6000
8000
Time (h)

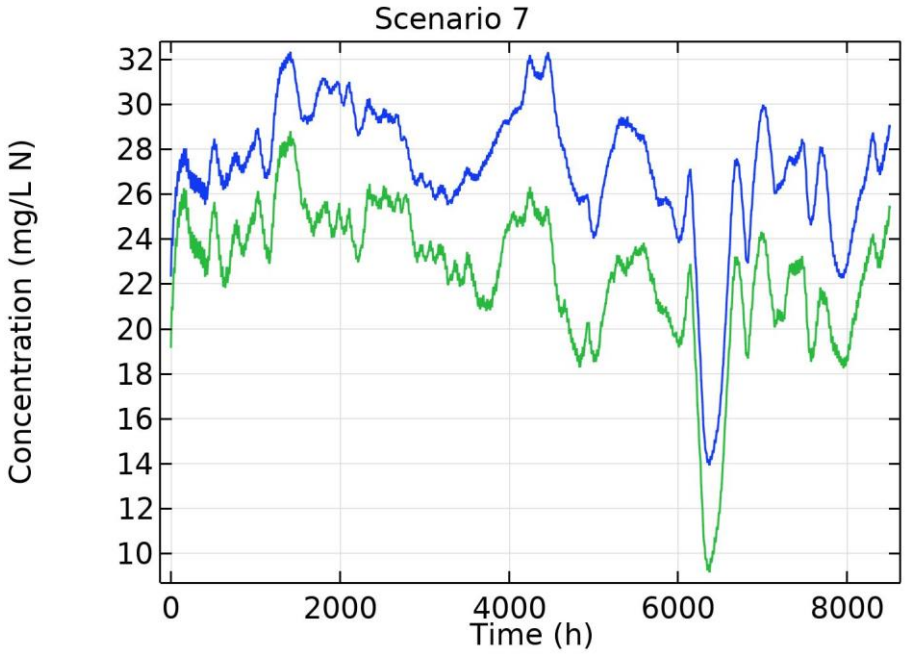
Scenario 7
Concentration (mg/L N)
32
30
28
26
24
22
20
18
16
14
12
10
0
2000
4000
6000
8000
Time (h)

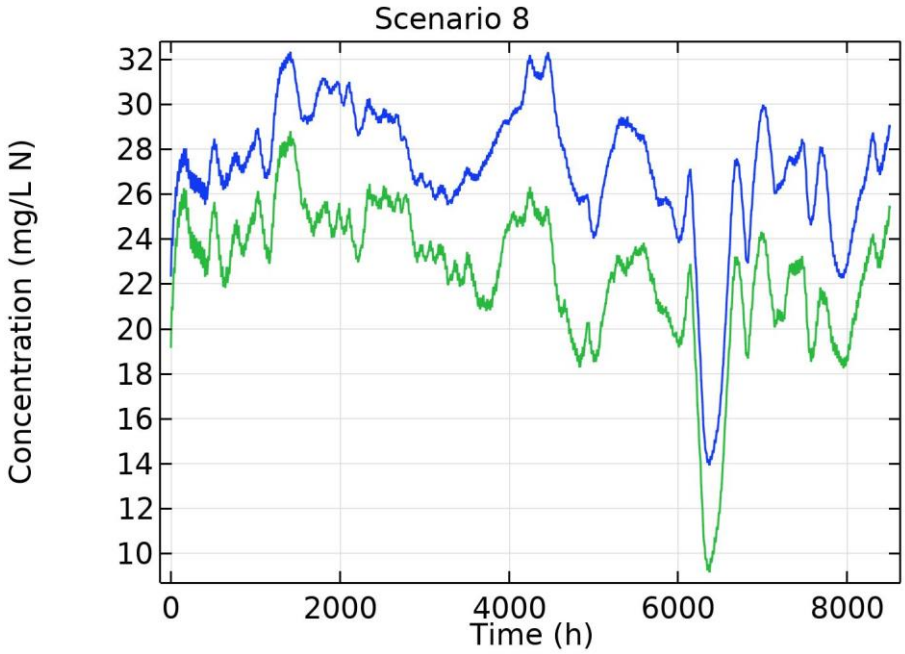
Scenario 8
Concentration (mg/L N)
32
30
28
26
24
22
20
18
16
14
12
10
0
2000
4000
6000
8000
Time (h)

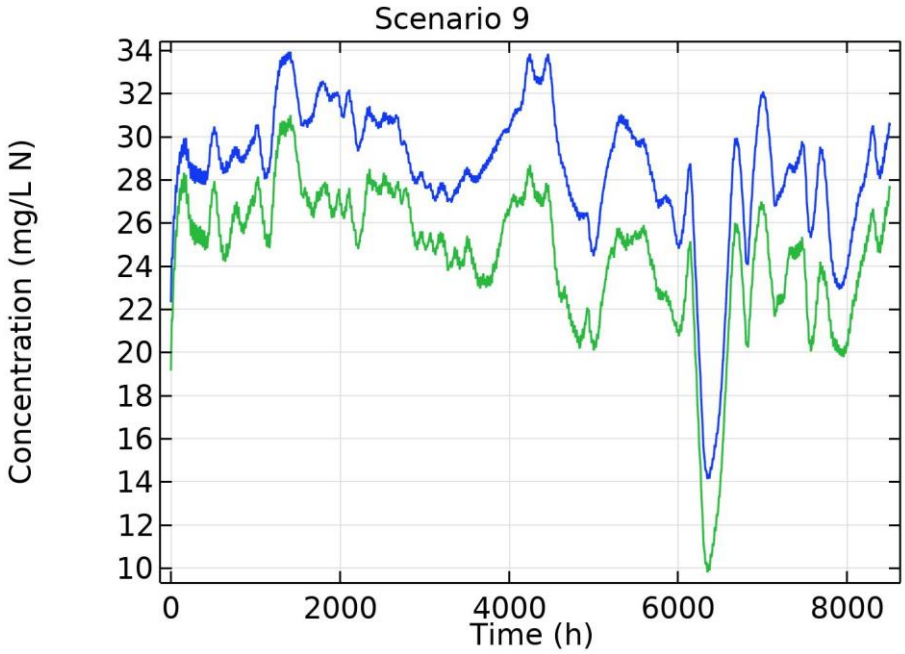
Scenario 9
Concentration (mg/L N)
34
32
30
28
26
24
22
20
18
16
14
12
10
0
2000
4000
6000
8000
Time (h)

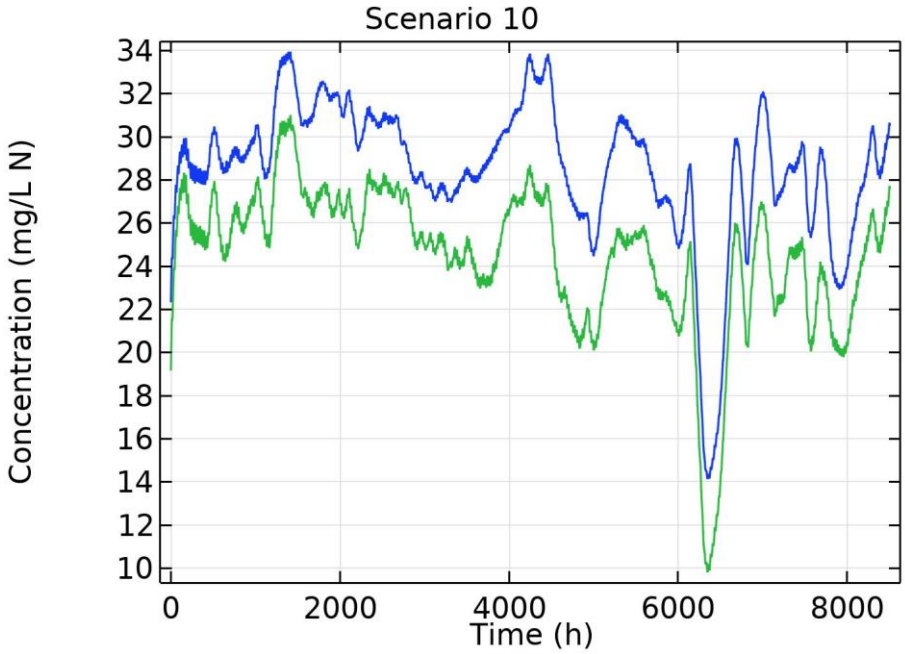
Scenario 10
Concentration (mg/L N)
34
32
30
28
26
24
22
20
18
16
14
12
10
0
2000
4000
6000
8000
Time (h)

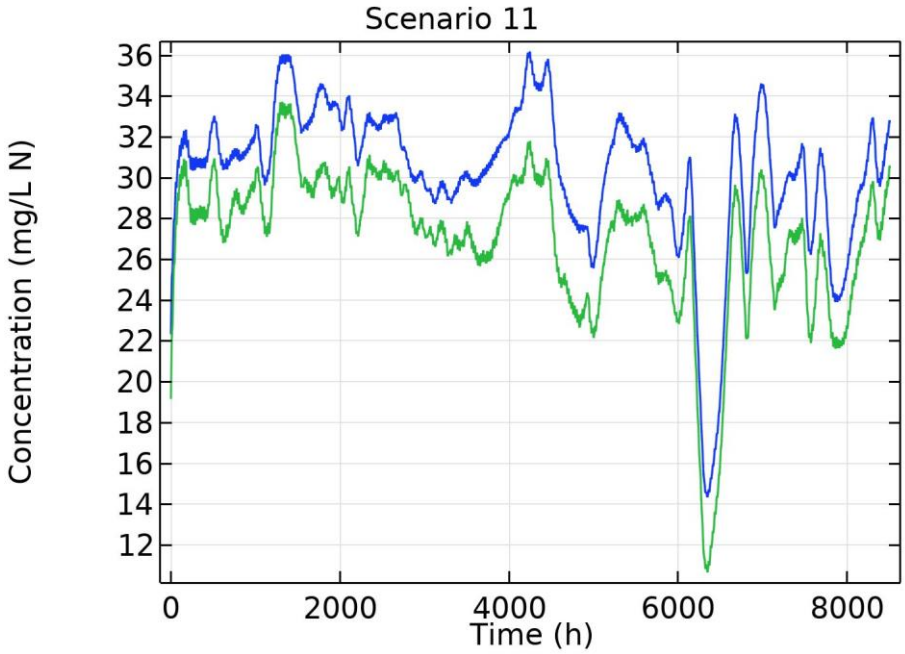
Scenario 11
Concentration (mg/L N)
36
34
32
30
28
26
24
22
20
18
16
14
12
0
2000
4000
6000
8000
Time (h)

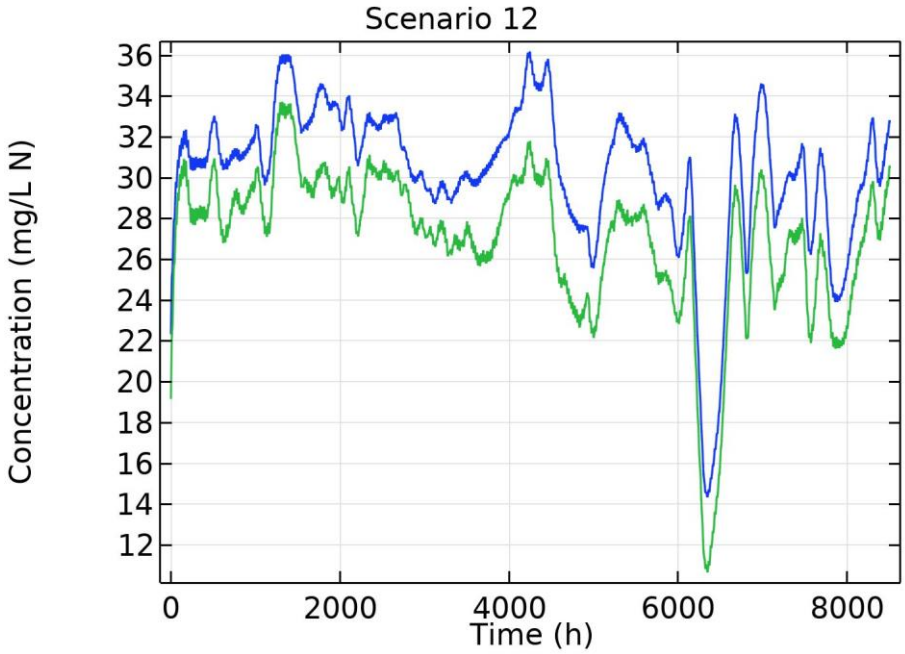
Scenario 12
Concentration (mg/L N)
36
34
32
30
28
26
24
22
20
18
16
14
12
0
2000
4000
6000
8000
Time (h)

Phosphorus

The following graphs show the evolution of the concentration of total phosphorus (which corresponds to phosphate phosphorus). Note that organic phosphorus was not considered.

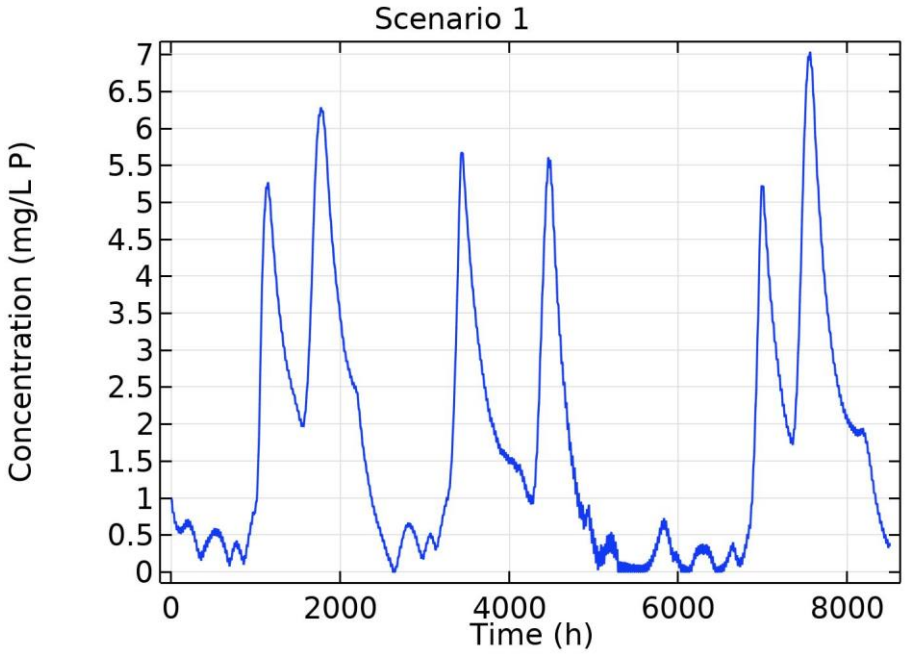

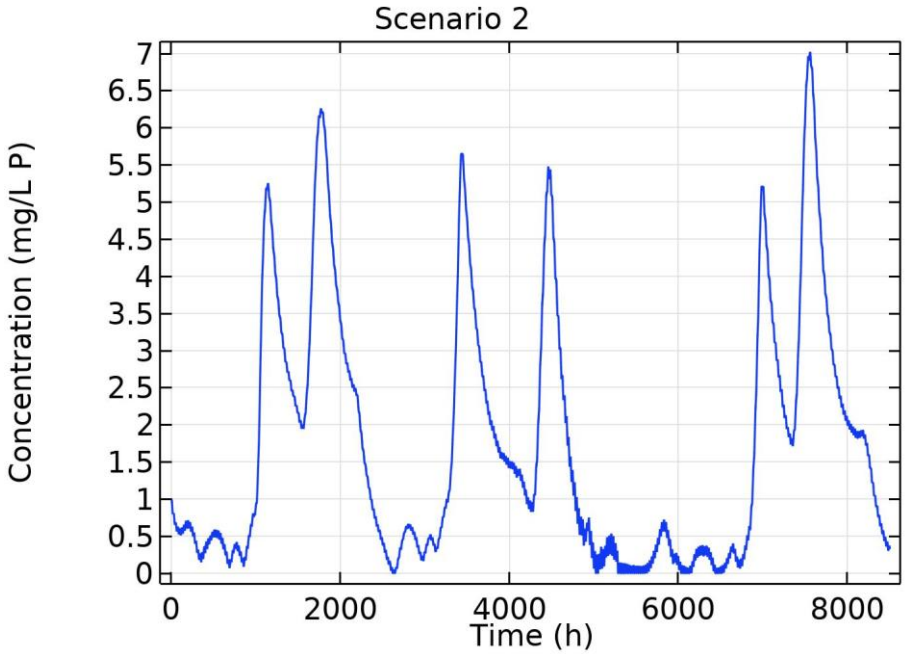

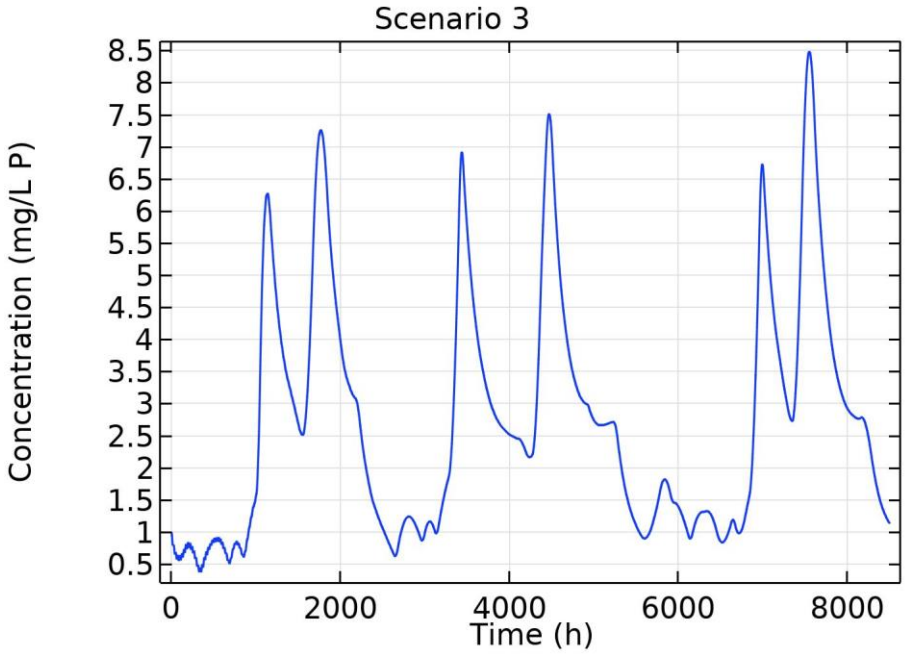
Scenario 3
Concentration (mg/L P)
8.5
8
7.5
7
6.5
6
5.5
5
4.5
4
3.5
3
2.5
2
1.5
1
0.5
0
2000
4000
6000
8000
Time (h)

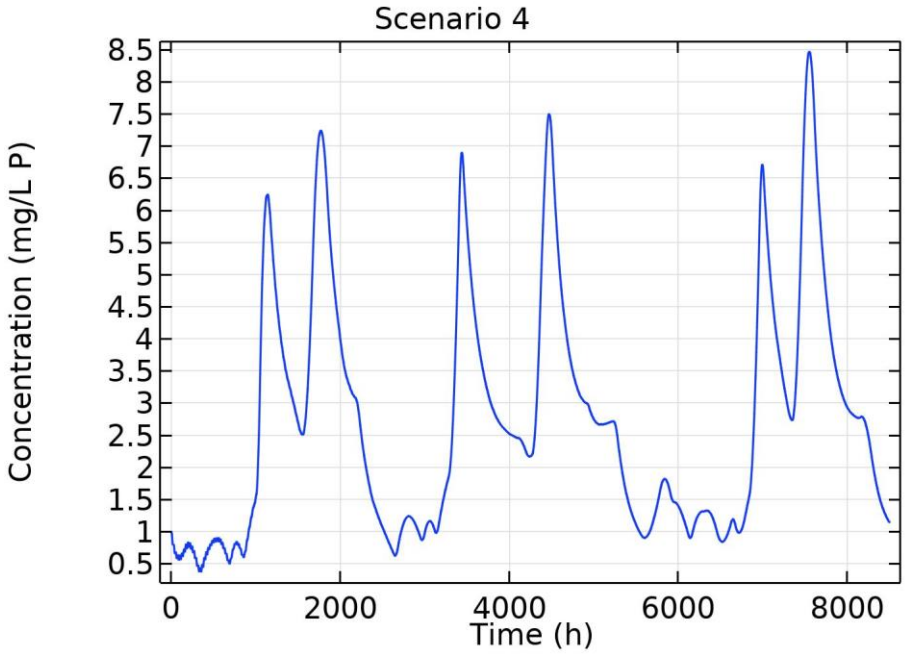
Scenario 4
Concentration (mg/L P)
8.5
8
7.5
7
6.5
6
5.5
5
4.5
4
3.5
3
2.5
2
1.5
1
0.5
0
2000
4000
6000
8000
Time (h)

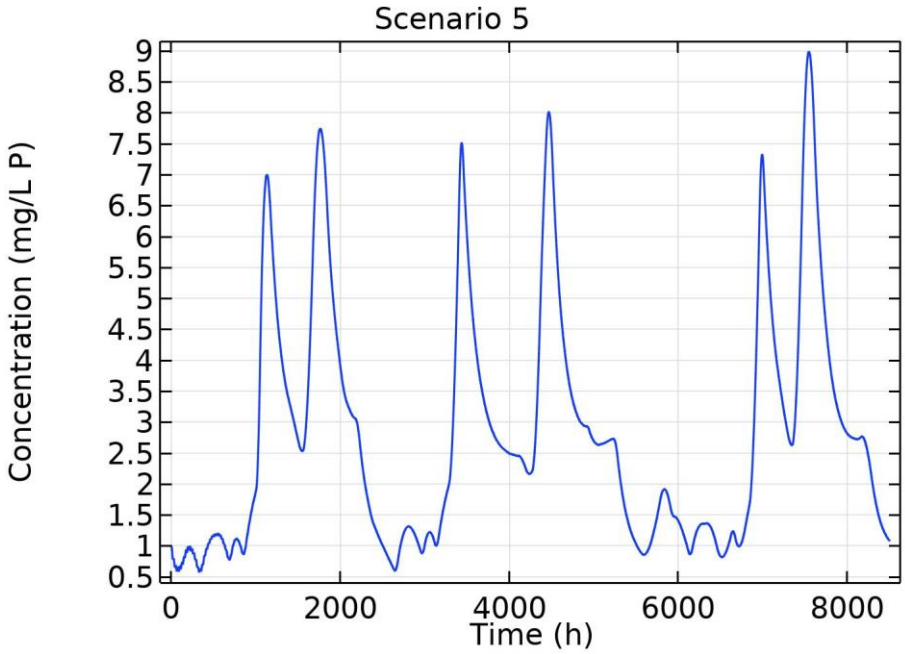
Scenario 5
Concentration (mg/L P)
9
8.5
8
7.5
7
6.5
6
5.5
5
4.5
4
3.5
3
2.5
2
1.5
1
0.5
0
2000
4000
6000
8000
Time (h)

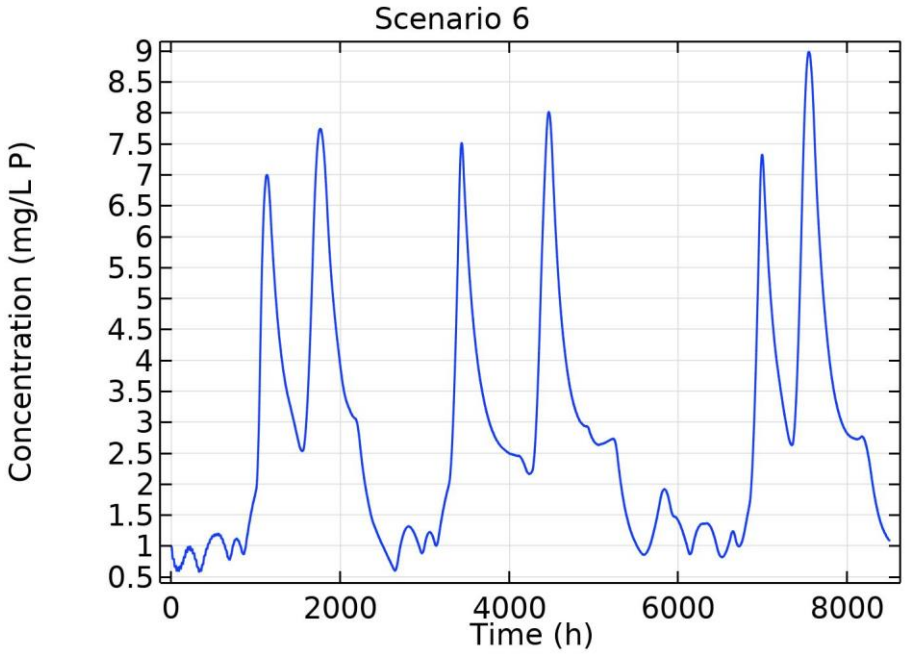
Scenario 6
Concentration (mg/L P)
9
8.5
8
7.5
7
6.5
6
5.5
5
4.5
4
3.5
3
2.5
2
1.5
1
0.5
0
2000
4000
6000
8000
Time (h)

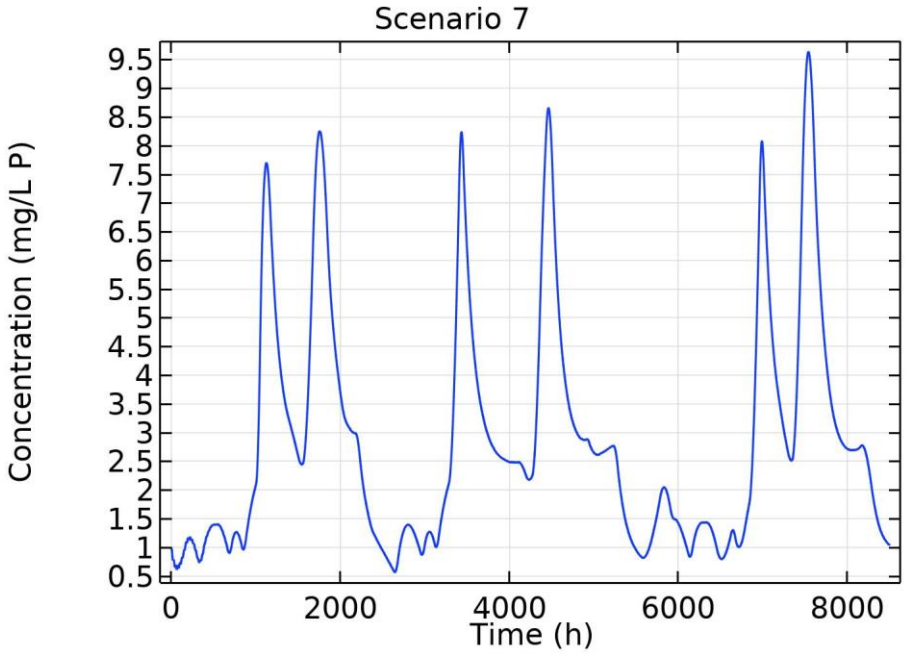
Scenario 7
Concentration (mg/L P)
9.5
9
8.5
8
7.5
7
6.5
6
5.5
5
4.5
4
3.5
3
2.5
2
1.5
1
0.5
0
2000
4000
6000
8000
Time (h)

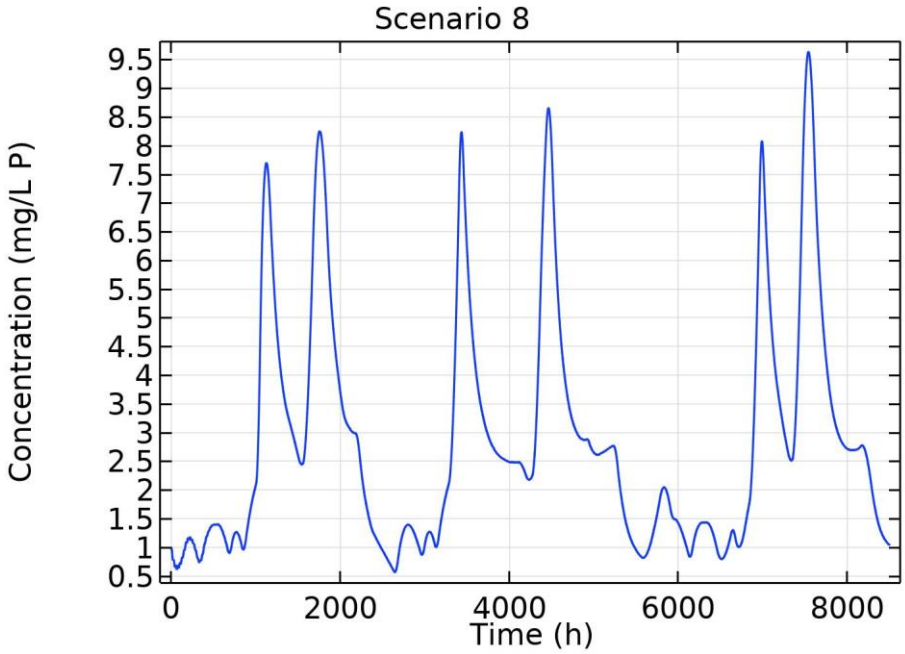
Scenario 8
Concentration (mg/L P)
9.5
9
8.5
8
7.5
7
6.5
6
5.5
5
4.5
4
3.5
3
2.5
2
1.5
1
0.5
0
2000
4000
6000
8000
Time (h)

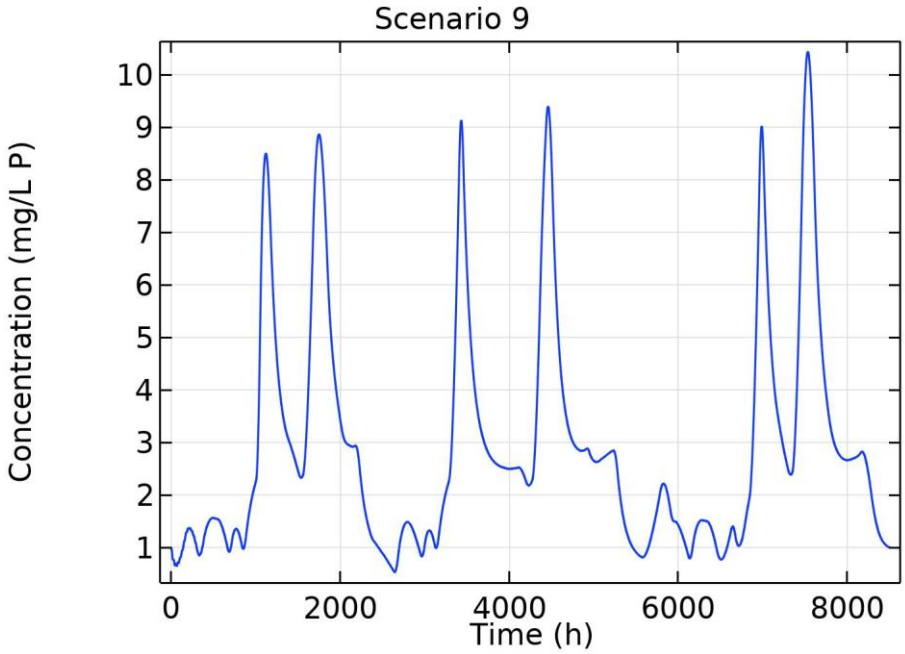
Scenario 9
Concentration (mg/L P)
10
9
8
7
6
5
4
3
2
1
0
2000
4000
6000
8000
Time (h)

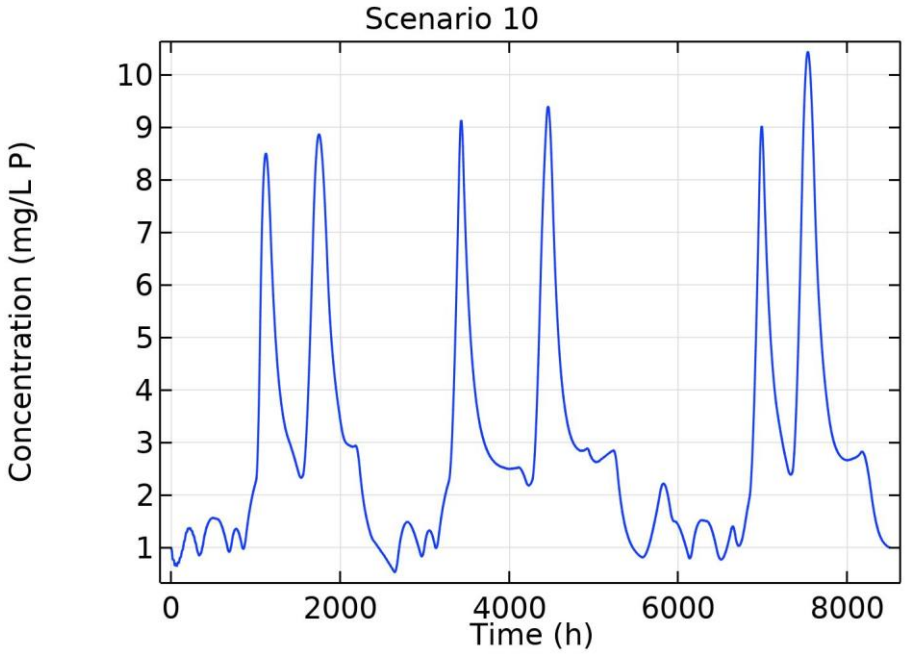
Scenario 10
Concentration (mg/L P)
10
9
8
7
6
5
4
3
2
1
0
2000
4000
6000
8000
Time (h)

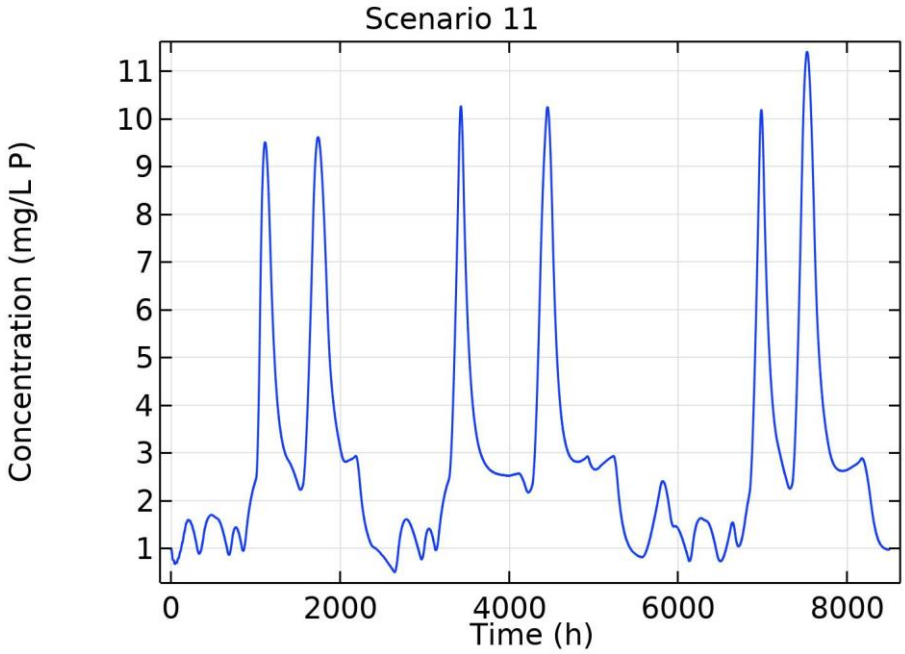
Scenario 11
Concentration (mg/L P)
11
10
9
8
7
6
5
4
3
2
1
0
2000
4000
6000
8000
Time (h)

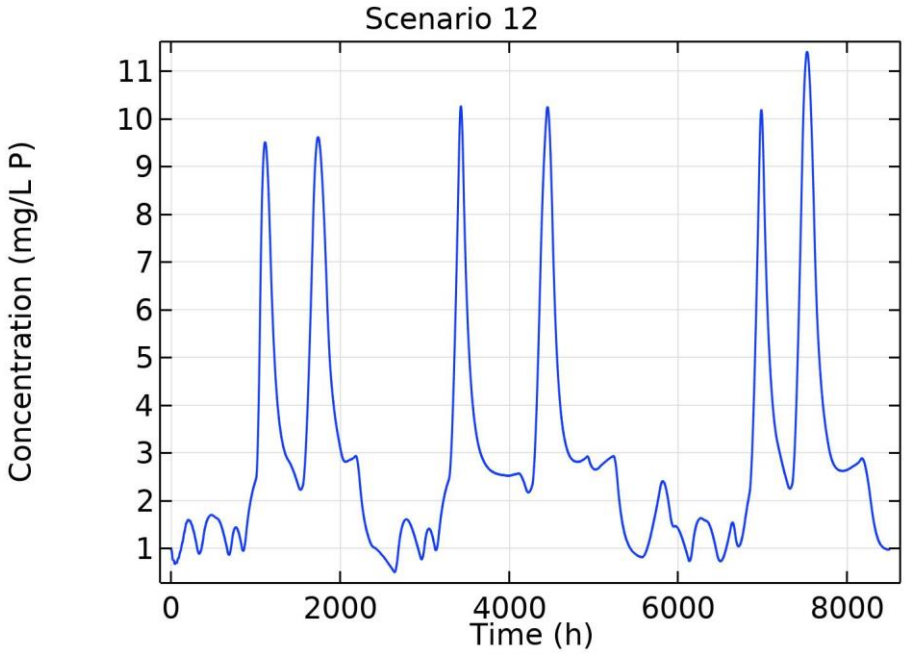
Scenario 12
Concentration (mg/L P)
11
10
9
8
7
6
5
4
3
2
1
0
2000
4000
6000
8000
Time (h)

Annex II. Model components

In the following section, the process rate formulas, the stoichiometric coefficients and their relation are described. This material was extracted from Solimeno et al., 2019 and complemented with the values of the parameters used in this study.

*Values modified during calibration with respect to those originally established by Solimeno et al., 2019 (in parentheses).

Mathematical description of the processes of the model (processes rates)

Processes	**Process rate [M L^{-3} T^{-1}]**
Microalgae (X_{ALG}) processes	
1a. Growth of X_{ALG} on S_{NH4}	$\rho_{1a} = \frac{\mu_{ALG} \cdot {I_{av}}^{n}}{{I_k}^{n} + {I_{av}}^{n}} \cdot \varphi(T_{ALG}) \cdot \eta_{PS}(S_{O2}) \cdot \varphi(pH_{ALG}) \cdot \frac{S_{CO2} + S_{HCO3}}{K_{C,ALG} + S_{CO2} + S_{HCO3} + \frac{{S_{CO2}}^{2}}{I_{CO2,ALG}}} \cdot \frac{S_{NH3} + S_{NH4}}{K_{N,ALG} + S_{NH3} + S_{NH4}} \cdot \frac{S_{PO4}}{K_{P,ALG} + S_{PO4}} \cdot X_{ALG}$
1b. Growth of X_{ALG} on S_{NO3}	$\rho_{1b} = \frac{\mu_{ALG} \cdot {I_{av}}^{n}}{{I_k}^{n} + {I_{av}}^{n}} \cdot \varphi(T_{ALG}) \cdot \eta_{PS}(S_{O2}) \cdot \varphi(pH_{ALG}) \cdot \frac{S_{CO2} + S_{HCO3}}{K_{C,ALG} + S_{CO2} + S_{HCO3} + \frac{{S_{CO2}}^{2}}{I_{CO2,ALG}}} \cdot \frac{S_{NO3}}{K_{N,ALG} + S_{NO3}} \cdot \frac{K_{N,ALG}}{K_{N,ALG} + S_{NH3} + S_{NH4}} \cdot \frac{S_{PO4}}{K_{P,ALG} + S_{PO4}} \cdot X_{ALG}$
2. Endogenous respiration of X_{ALG}	$\rho_2 = k_{resp,ALG} \cdot \varphi(T_{ALG}) \cdot \varphi(pH_{ALG}) \cdot \frac{S_{O2}}{K_{O2,ALG} + S_{O2}} \cdot X_{ALG}$
3. Decay of X_{ALG}	$\rho_3 = k_{death,ALG} \cdot \varphi(T_{ALG}) \cdot \varphi(pH_{ALG}) \cdot X_{ALG}$
Heterotrophic bacteria (X_H) (aerobic and denitrifying activity)	
4a. Aerobic growth of X_H on S_{NH4}	$\rho_{4a} = \mu_H \cdot f_{T,MB}(T) \cdot \varphi(pH_H) \cdot \frac{S_S}{K_{S,H} + S_s} \cdot \frac{S_{O2}}{K_{O2,H} + S_{O2}} \cdot \frac{S_{NH4} + S_{NH3}}{K_{N,H} + S_{NH4} + S_{NH3}} \cdot \frac{S_{PO4}}{K_{P,H} + S_{PO4}} \cdot X_H$
4b. Aerobic growth of X_H on S_{NO3}	$\rho_{4b} = \mu_H \cdot f_{T,MB}(T) \cdot \varphi(pH_H) \cdot \frac{S_S}{K_{S,H} + S_s} \cdot \frac{S_{O2}}{K_{O2,H} + S_{O2}} \cdot \frac{S_{NO3}}{K_{N,H} + S_{NO3}} \cdot \frac{S_{PO4}}{K_{P,H} + S_{PO4}} \cdot X_H$

5. Anoxic growth of X_H on S_{NO2} (denitrification on S_{NO2})	$\rho_5 = \mu_H \cdot \eta_H \cdot f_{T,MB}(T) \cdot \varphi(pH_H) \cdot \frac{S_S}{K_{S,H} + S_s} \cdot \frac{K_{O2,H}}{K_{O2,H} + S_{O2}} \cdot \frac{S_{NO2}}{K_{NO2,H,anox} + S_{NO2}} \cdot \frac{S_{PO4}}{K_{P,H} + S_{PO4}} \cdot X_H$
6. Anoxic growth of X_H on S_{NO3} (denitrification on S_{NO3})	$\rho_6 = \mu_H \cdot \eta_H \cdot f_{T,MB}(T) \cdot \varphi(pH_H) \cdot \frac{S_S}{K_{S,H} + S_s} \cdot \frac{K_{O2,H}}{K_{O2,H} + S_{O2}} \cdot \frac{S_{NO3}}{K_{NO3,H,anox} + S_{NO3}} \cdot \frac{S_{PO4}}{K_{P,H} + S_{PO4}} \cdot X_H$
7. Aerobic endogenous respiration of X_H	$\rho_7 = k_{resp,H} \cdot f_{T,MB}(T) \cdot \varphi(pH_H) \cdot \frac{S_{O2}}{K_{O2,H} + S_{O2}} \cdot X_H$
8. Anoxic endogenous respiration of X_H	$\rho_8 = k_{resp,H} \cdot \eta_H \cdot f_{T,MB}(T) \cdot \varphi(pH_H) \cdot \frac{K_{O2,H}}{K_{O2,H} + S_{O2}} \cdot \frac{S_{NO3} + S_{NO2}}{K_{NO3,H,anox} + S_{NO2} + S_{NO3}} \cdot X_H$
9. Decay of X_H	$\rho_9 = k_{death,H} \cdot f_{T,MB}(T) \cdot \varphi(pH_H) \cdot X_H$
Autotrophic bacteria (nitrifying activity)	
10. Growth of X_{AOB}	$\rho_{10} = \mu_{AOB} \cdot \varphi(T_N) \cdot \varphi(pH_N) \cdot \frac{S_{O2}}{K_{O2,AOB} + S_{O2}} \cdot \frac{S_{NH3} + S_{NH4}}{K_{NH4,AOB} + S_{NH4} + S_{NH3}} \cdot \frac{S_{CO2} + S_{HCO3}}{K_{C,AOB} + S_{CO2} + S_{HCO3}} \cdot \frac{S_{PO4}}{K_{P,AOB} + S_{PO4}} \cdot X_{AOB}$
11. Growth of X_{NOB}	$\rho_{11} = \mu_{NOB} \cdot \varphi(T_N) \cdot \varphi(pH_N) \cdot \frac{S_{O2}}{K_{O2,NOB} + S_{O2}} \cdot \frac{K_{I,NH4}}{K_{I,NH4} + S_{NH4} + S_{NH3}} \cdot \frac{S_{NO2}}{K_{NO2,NOB} + S_{NO2}} \cdot \frac{S_{CO2} + S_{HCO3}}{K_{C,NOB} + S_{CO2} + S_{HCO3}} \cdot \frac{S_{PO4}}{K_{P,NOB} + S_{PO4}} \cdot X_{NOB}$
12. Endogenous respiration of X_{AOB}	$\rho_{10} = k_{resp,AOB} \cdot \varphi(T_N) \cdot \varphi(pH_N) \cdot \frac{S_{O2}}{K_{O2,AOB} + S_{O2}} \cdot X_{AOB}$
13. Endogenous respiration of X_{NOB}	$\rho_{13} = k_{resp,NOB} \cdot \varphi(T_N) \cdot \varphi(pH_N) \cdot \frac{S_{O2}}{K_{O2,NOB} + S_{O2}} \cdot X_{NOB}$
14a. Decay of X_{AOB}	$\rho_{14a} = k_{death,AOB} \cdot \varphi(T_N) \cdot \varphi(pH_N) \cdot X_{AOB}$

14b. Decay of X_{NOB}	$\rho_{14b} = k_{death,NOB} \cdot f_{T,MB}(T) \cdot \varphi(pH_N) \cdot X_{NOB}$
Hydrolysis, Chemical equilibrium and Transfer of gases	
15. Hydrolysis	$\rho_{15} = k_{HYD} \cdot \frac{X_S/X_H}{K_{HYD} + (X_S/X_H)} \cdot X_H$
16. Chemical equilibrium $CO_2 \leftrightarrow HCO_3^-$	$\rho_{16} = k_{eq,1} \cdot (S_{CO2} - S_H S_{HCO3}/K_{eq,1})$
17. Chemical equilibrium $HCO_3^- \leftrightarrow CO_3^{2-}$	$\rho_{17} = k_{eq,2} \cdot (S_{HCO3} - S_H S_{CO3}/K_{eq,2})$
18. Chemical equilibrium $NH_4^+ \leftrightarrow NH_3$	$\rho_{18} = k_{eq,3} \cdot (S_{NH4} - S_H S_{NH3}/K_{eq,3})$
19. Chemical equilibrium $H^+ \leftrightarrow OH^-$	$\rho_{19} = k_{eq,w} \cdot (1 - S_H S_{OH}/K_{eq,w})$
20. S_{O2} transfer to the atmosphere	$\rho_{20} = K_{lal,O2} \cdot (S_{O2}^{WAT} - S_{O2})$
21. S_{CO2} transfer to the atmosphere	$\rho_{21} = K_{lal,CO2} \cdot (S_{CO2}^{WAT} - S_{CO2})$
22. S_{NH3} transfer to the atmosphere	$\rho_{22} = K_{lal,NH3} \cdot (-S_{NH3})$

Matrix of stoichiometric parameters that relates processes and components through stoichiometric coefficients

	S_{NH4}	S_{NH3}	S_{NO3}	S_{NO2}	S_{CO2}	S_{HCO3}	S_{CO3}	S_{PO4}	S_{O2}	S_H	S_{OH}	S_S	S_I	X_{ALG}	X_S	X_I	X_H	X_{AOB}	X_{NOB}
ρ_{1a}	$v_{1,1a}$				$v_{5,1a}$			$v_{8,1a}$	$v_{9,1a}$	$v_{10,1a}$				$v_{14,1a}$					
ρ_{1b}			$v_{3,1b}$		$v_{5,1b}$			$v_{8,1b}$	$v_{9,1b}$	$v_{10,1b}$				$v_{14,1b}$					
ρ_2	$v_{1,2}$				$v_{5,2}$			$v_{8,2}$	$v_{9,2}$	$v_{10,2}$				$v_{14,2}$					
ρ_3	$v_{1,3}$				$v_{5,3}$			$v_{8,3}$	$v_{9,3}$	$v_{10,3}$				$v_{14,3}$	$v_{15,3}$	$v_{16,3}$			
ρ_{4a}	$v_{1,4a}$				$v_{5,4a}$			$v_{8,4a}$	$v_{9,4a}$	$v_{10,4a}$		$v_{12,4a}$					$v_{17,4a}$		
ρ_{4b}			$v_{3,4b}$		$v_{5,4b}$			$v_{8,4b}$	$v_{9,4b}$	$v_{10,4b}$		$v_{12,4b}$					$v_{17,4b}$		
ρ_5				$v_{4,5}$	$v_{5,5}$			$v_{8,5}$		$v_{10,5}$		$v_{12,5}$					$v_{17,5}$		
ρ_6			$v_{3,6}$		$v_{5,6}$			$v_{8,6}$		$v_{10,6}$		$v_{12,6}$					$v_{17,6}$		
ρ_7	$v_{1,7}$				$v_{5,7}$			$v_{8,7}$	$v_{9,7}$	$v_{10,7}$							$v_{17,7}$		
ρ_8	$v_{1,8}$		$v_{3,8}$	$v_{4,8}$	$v_{5,8}$			$v_{8,8}$		$v_{10,8}$							$v_{17,8}$		
ρ_9															$v_{15,9}$	$v_{16,9}$	$v_{17,9}$		
ρ_{10}	$v_{1,10}$			$v_{4,10}$	$v_{5,10}$			$v_{8,10}$	$v_{9,10}$	$v_{10,10}$								$v_{18,10}$	
ρ_{11}			$v_{3,11}$	$v_{4,11}$	$v_{5,11}$			$v_{8,11}$	$v_{9,11}$	$v_{10,11}$									$v_{19,11}$
ρ_{12}	$v_{1,12}$				$v_{5,12}$			$v_{8,12}$	$v_{9,12}$	$v_{10,12}$						$v_{16,12}$		$v_{18,12}$	
ρ_{13}	$v_{1,13}$				$v_{5,13}$			$v_{8,13}$	$v_{9,13}$	$v_{10,13}$						$v_{16,13}$			$v_{19,13}$
ρ_{14a}															$v_{15,14a}$	$v_{16,14a}$		$v_{18,14a}$	
ρ_{14b}															$v_{15,14b}$	$v_{16,14b}$			$v_{19,14b}$
ρ_{15}	$v_{1,15}$				$v_{5,15}$			$v_{8,15}$		$v_{10,15}$		$v_{12,15}$	$v_{13,15}$		$v_{15,15}$				
ρ_{16}					$v_{5,16}$	$v_{6,16}$				$v_{10,16}$									
ρ_{17}						$v_{6,17}$	$v_{7,17}$			$v_{10,17}$									
ρ_{18}	$v_{1,18}$	$v_{2,18}$								$v_{10,18}$									
ρ_{19}										$v_{10,19}$	$v_{11,19}$								
ρ_{20}									$v_{9,20}$										
ρ_{21}					$v_{5,21}$														
ρ_{22}		$v_{2,22}$																	

Values of biokinetic, chemical and physic parameters

Parameters	Description	Value	Unit
Microalgae (X_{ALG})			
μ_{ALG}	Maximum growth rate of X_{ALG}	1,18* (1,45)	d^{-1}
$k_{resp,ALG}$	Endogenous respiration constant	0,1* (0,05)	d^{-1}
$k_{death,ALG}$	Decay constant	0,05	d^{-1}
$K_{C,ALG}$	Saturation constant of X_{ALG} on S_{CO2}	4E-3	$gC\ m^{-3}$
$I_{CO2,ALG}$	Inhibition constant of X_{ALG} on S_{CO2}	120	$gC\ m^{-3}$
$K_{N,ALG}$	Saturation constant of X_{ALG} on nitrogen	0,1	$gN\ m^{-3}$
$K_{O2,ALG}$	Saturation constant of X_{ALG} on S_{O2}	0,2	$gO_2\ m^{-3}$
$K_{P,ALG}$	Saturation constant of X_{ALG} for S_{HPO4}	0,001* (0,02)	$gP\ m^{-3}$
Heterotrophic bacteria (X_H)			
μ_H	Maximum growth rate of X_H	0,3* (1,3)	d^{-1}
η_H	Anoxic reduction factor for X_H	0,8* (0,6)	–
$k_{resp,H}$	Endogenous respiration rate of X_H	0,3	d^{-1}
$K_{O2,H}$	Saturation constant of X_H for S_{O2}	0,2	$gO_2\ m^{-3}$
$K_{N,H}$	Saturation constant of X_H for S_N	0,2	$gN\ m^{-3}$
$K_{S,H}$	Saturation constant of X_H for S_S	20	$gCOD\ m^{-3}$
$K_{NO3,H,anox}$	Saturation constant of X_H for S_{NO3}	1* (0,5)	$gN\ m^{-3}$
$K_{NO2,H,anox}$	Saturation constant of X_H for S_{NO2}	0,62* (0,2)	$gN\ m^{-3}$
$k_{death,H}$	Decay constant of X_H	0,3	d^{-1}
Autotrophic bacteria: ammonia oxidizing bacteria (X_{AOB}) and nitrite oxidizing bacteria (X_{NOB})			
μ_{AOB}	Maximum growth rate of X_{AOB}	0,725* (0,63)	d^{-1}
μ_{NOB}	Maximum growth rate of X_{NOB}	1,8* (1,1)	d^{-1}
$K_{O2,AOB}/K_{O2,NOB}$	Saturation constant of X_{AOB} / X_{NOB} for S_{O2}	0,5	$gO_2\ m^{-3}$
$K_{NH4,AOB}$	Saturation constant of X_{AOB} on S_{NH4}	0,5	$gN\ m^{-3}$
$K_{I,NH4}$	Ammonia inhibition constant of X_{NOB}	40* (5)	$gN\ m^{-3}$
$K_{NO2,NOB}$	Saturation constant of X_{NOB} for S_{NO2}	0,5	$gN\ m^{-3}$
$K_{C,AOB}/K_{C,NOB}$	Saturation constant of X_{AOB} / X_{NOB} for S_{HCO3}	0,5	$gC\ m^{-3}$
$k_{resp,AOB}$/ $k_{resp,NOB}$	Endogenous respiration rate of X_{AOB} /X_{NOB}	0,05	d^{-1}
$k_{death,AOB}$/ $k_{death,NOB}$	Decay constant of X_{AOB} and X_{NOB}	0,2	d^{-1}
Hydrolysis			
k_{HYD}	Hydrolysis rate constant	3,0	d^{-1}
Photorespiration factor of microalgae			
K_{PR}	Inhibition constant of photorespiration	0,03	–

τ	Excess of S_{O2} coefficient	3,5	–
S_{O2}^{SAT}	S_{O2} air saturation	9,07	$gO_2\ m^{-3}$
Light factor of microalgae			
α	Activation rate	1,9E-3	$(\mu E\ m^{-2})^{-1}$
β	Inhibition rate	5,7E-7	$(\mu E\ m^{-2})^{-1}$
γ	Production rate	0,14	s^{-1}
δ	Recovery rate	4,7E-4	s^{-1}
K_I	Biomass extinction coefficient	0,07	$m^2\ g^{-1}$
pH cardinal factor			
$pH_{ALG,max}$	Maximum pH value for X_{ALG}	12,3	–
$pH_{ALG,min}$	Minimum pH value for X_{ALG}	4	–
$pH_{ALG,opt}$	Optimum pH value for X_{ALG}	8,8	–
$pH_{H,max}$	Maximum pH value for X_H	11,2	–
$pH_{H,min}$	Minimum pH value for X_H	2	–
$pH_{H,opt}$	Optimum pH value for X_H	8,2	–
$pH_{N,max}$	Maximum pH value for X_{AOB} and X_{NOB}	11	–
$pH_{N,min}$	Minimum pH value for X_{AOB} and X_{NOB}	2	–
$pH_{N,opt}$	Optimum pH value for X_{AOB} and X_{NOB}	8,5	–
Temperature cardinal factor			
$T_{ALG,max}$	Maximum temperature value for X_{ALG}	46	–
$T_{ALG,min}$	Minimum temperature value for X_{ALG}	7	–
$T_{ALG,opt}$	Optimum temperature value for X_{ALG}	30* (26)	–
$T_{N,max}$	Maximum temperature value for X_{AOB} and X_{NOB}	40	–
$T_{N,min}$	Minimum temperature value for X_{AOB} and X_{NOB}	13	–
$T_{N,opt}$	Optimum temperature value for X_{AOB} and X_{NOB}	31	–
Heterotrophic bacteria thermal factor			
$T_{H,opt}$	Optimum temperature value for X_H	20	°C
θ	Temperature coefficient for XH	1,07	

Parameters	**Equations**
Chemical equilibrium $CO_2 \leftrightarrow HCO_3^-$.	$K_{eq,1} = 10^{17,843-\frac{3404,71}{273,15+T}-0,032786(273,15+T)}$
Chemical equilibrium $HCO_3^- \leftrightarrow CO_3^{2-}$	$K_{eq,2} = 10^{9,494-\frac{2902,39}{273,15+T}-0,02379(273,15+T)}$
Chemical equilibrium $NH_4^+ \leftrightarrow NH_3$	$K_{eq,3} = 10^{2,891-\frac{2727}{(273,15+T)}}$
Chemical equilibrium $H^+ \leftrightarrow OH^-$	$K_{eq,w} = 10^{-\frac{4470,99}{273,15+T}+12,0875-0,01706(273,15+T)}$

Kinetics parameters			
$k_{eq,1}$	Dissociation constant of $CO_2 \leftrightarrow HCO_3^-$	10000	d^{-1}

$k_{eq,2}$	Dissociation constant of $HCO_3^- \leftrightarrow CO_3^{2-}$	1000	d^{-1}
$k_{eq,3}$	Dissociation constant of $NH_4^+ \leftrightarrow NH_3$	1000	d^{-1}
$k_{eq,w}$	Dissociation constant of $H^+ \leftrightarrow OH^-$	1000	$g\ m^{-1}\ d^{-1}$
Transfer of gases to the atmosphere			
$K_{lal,O2}$	Mass transfer coefficient for S_{O2}	16	d^{-1}
$K_{lal,CO2}$	Mass transfer coefficient for S_{CO2}	5	d^{-1}
$K_{lal,NH3}$	Mass transfer coefficient for S_{NH3}	5	d^{-1}

Values of fractions of carbon, hydrogen, oxygen and nitrogen in microalgae and bacteria biomass

Parameters	Description	Value	Unit
Fractions of microalgal biomass (X_{ALG})			
$i_{C,ALG}$	Fraction of carbon in microalgae	0,387	$gC\ gCOD^{-1}$
$i_{H,ALG}$	Fraction of hydrogen in microalgae	0,075	$gH\ gCOD^{-1}$
$i_{O,ALG}$	Fraction of oxygen in microalgae	0,269	$gO_2\ gCOD^{-1}$
$i_{N,ALG}$	Fraction of nitrogen in microalgae	0,065	$gN\ gCOD^{-1}$
$i_{P,ALG}$	Fraction of phosphorus in microalgae	0,01	$gP\ gCOD^{-1}$
Fractions of bacteria biomass (X_H, X_{AOB}, X_{NOB})			
$i_{C,BM}$	Fraction of carbon in bacteria	0,323	$gC\ gCOD^{-1}$
$i_{H,BM}$	Fraction of hydrogen in bacteria	0,060	$gH\ gCOD^{-1}$
$i_{O,BM}$	Fraction of oxygen in bacteria	0,077	$gO_2\ gCOD^{-1}$
$i_{N,BM}$	Fraction of nitrogen in bacteria	0,075	$gN\ gCOD^{-1}$
$i_{P,BM}$	Fraction of phosphorus in bacteria	0,018	$gP\ gCOD^{-1}$
Fractions of slowly biodegradable substrates (X_S)			
$i_{C,XS}$	Fraction of carbon in X_S	0,318	$gC\ gCOD^{-1}$
$i_{H,XS}$	Fraction of hydrogen in X_S	0,045	$gH\ gCOD^{-1}$
$i_{O,XS}$	Fraction of oxygen in X_S	0,077	$gO_2\ gCOD^{-1}$
$i_{N,XS}$	Fraction of nitrogen in X_S	0,034	$gN\ gCOD^{-1}$
$i_{P,XS}$	Fraction of phosphorus in X_S	0,005	$gP\ gCOD^{-1}$
Fractions of inert particulate organics (X_I)			
$i_{C,XI}$	Fraction of carbon in X_I	0,327	$gC\ gCOD^{-1}$
$i_{H,XI}$	Fraction of hydrogen in X_I	0,037	$gH\ gCOD^{-1}$
$i_{O,XI}$	Fraction of oxygen in X_I	0,075	$gO_2\ gCOD^{-1}$
$i_{N,XI}$	Fraction of nitrogen in X_I	0,016	$gN\ gCOD^{-1}$
$i_{P,XI}$	Fraction of phosphorus in X_I	0,005	$gP\ gCOD^{-1}$
Fractions of readily biodegradable substrates (S_S)			

$i_{C,SS}$	Fraction of carbon in S_S	0,318	gC $gCOD^{-1}$
$i_{H,SS}$	Fraction of hydrogen in S_S	0,045	gH $gCOD^{-1}$
$i_{O,SS}$	Fraction of oxygen in S_S	0,078	gO_2 $gCOD^{-1}$
$i_{N,SS}$	Fraction of nitrogen in S_S	0,034	gN $gCOD^{-1}$
$i_{P,SS}$	Fraction of phosphorus in S_S	0,005	gP $gCOD^{-1}$
Fractions of soluble inert organics (S_I)			
$i_{C,SI}$	Fraction of carbon in S_I	0,327	gC $gCOD^{-1}$
$i_{H,SI}$	Fraction of hydrogen in S_I	0,037	gH $gCOD^{-1}$
$i_{O,SI}$	Fraction of oxygen in S_I	0,075	gO_2 $gCOD^{-1}$
$i_{N,SI}$	Fraction of nitrogen in S_I	0,016	gN $gCOD^{-1}$
$i_{P,SI}$	Fraction of phosphorus in S_I	0,005	gP $gCOD^{-1}$
Fractions of inert produced by biomass degradation			
f_{ALG}	Production of X_I in endogenous resp. of X_{ALG}	0,1	gCOD $gCOD^{-1}$
f_{XI}	Production of X_I in endogenous resp. of X_H	0,1	gCOD $gCOD^{-1}$
Yield of biomass			
Y_{ALG}	Yield of X_{ALG}	0,62	gCOD $gCOD^{-1}$
Y_H	Yield of X_H on S_{O2}	0,6	gCOD $gCOD^{-1}$
$Y_{H,NO3}$	Yield of X_H on S_{NO3}	0,5	gCOD $gCOD^{-1}$
$Y_{H,NO2}$	Yield of X_H on S_{NO2}	0,3	gCOD $gCOD^{-1}$
Y_{AOB}	Yield of X_{AOB}	0,13	gCOD $gCOD^{-1}$
Y_{NOB}	Yield of X_{NOB}	0,03	gCOD $gCOD^{-1}$
K_{HYD}	Hydrolysis saturation constant	1	gCOD $gCOD^{-1}$

Mathematical expressions of the stoichiometric coefficients of each process

Stoichiometric coefficients	**Unit**
Growth of X_{ALG} on S_{NH4}	
$v_{1,1a} = -i_{N,ALG}$	gN $gCOD^{-1}$
$v_{5,1a} = -i_{C,ALG}$	gC $gCOD^{-1}$
$v_{8,1a} = -i_{P,ALG}$	gP $gCOD^{-1}$
$v_{9,1a} = (8i_{C,ALG}/3 + 8i_{H,ALG} - i_{O,ALG} - 12i_{N,ALG}/7 + 40i_{P,ALG}/31)/2$	gO_2 $gCOD^{-1}$
$v_{10,1a} = i_{N,ALG}/14 - 2i_{P,ALG}/31$	gH $gCOD^{-1}$
$v_{14,1a} = 1$	gCOD $gCOD^{-1}$
Growth of X_{ALG} on S_{NO3}	
$v_{3,1b} = -i_{N,ALG}$	gN $gCOD^{-1}$
$v_{5,1b} = -i_{C,ALG}$	gC $gCOD^{-1}$

$v_{8,1b} = -i_{P,ALG}$	gP gCOD^{-1}
$v_{9,1b} = (8i_{C,ALG}/3 + 8i_{H,ALG} - i_{O,ALG} + 20i_{N,ALG}/7 + 40i_{P,ALG}/31)/2$	gO_2 gCOD^{-1}
$v_{10,1b} = -i_{N,ALG}/14 - 2i_{P,ALG}/31$	gH gCOD^{-1}
$v_{14,1b} = 1$	gCOD gCOD^{-1}
Endogenous respiration of X_{ALG}	
$v_{1,2} = i_{N,ALG} - f_{ALG}\, i_{N,XI}$	gN gCOD^{-1}
$v_{5,2} = i_{C,ALG} - f_{ALG}\, i_{C,XI}$	gC gCOD^{-1}
$v_{8,2} = i_{P,ALG} - f_{ALG}\, i_{P,XI}$	gP gCOD^{-1}
$v_{9,2} = ((i_{O,ALG} - f_{ALG}\, i_{O,XI}) - 8(i_{H,ALG} - f_{ALG}\, i_{H,XI}) - 8/3\,(i_{C,ALG} - f_{ALG}\, i_{C,XI}) + 12/7\,(i_{N,ALG} - f_{ALG}\, i_{N,XI}) - 40/31\,(i_{P,ALG} - f_{ALG}\, i_{P,XI}))/2$	gO_2 gCOD^{-1}
$v_{10,2} = -1/14\,(i_{N,ALG} - f_{ALG}\, i_{N,XI}) + 2/31\,(i_{P,ALG} - f_{ALG}\, i_{P,XI})$	gH gCOD^{-1}
$v_{14,2} = -1$	gCOD gCOD^{-1}
$v_{16,2} = f_{ALG}$	gCOD gCOD^{-1}
Decay of X_{ALG}	
$v_{1,3} = i_{N,ALG} - (1 - f_{ALG})Y_{ALG}\, i_{N,XS} - f_{ALG}Y_{ALG}\, i_{N,ALG}$	gN gCOD^{-1}
$v_{5,3} = i_{C,ALG} - (1 - f_{ALG})Y_{ALG}\, i_{C,XS} - f_{ALG}Y_{ALG}\, i_{C,ALG}$	gC gCOD^{-1}
$v_{8,3} = i_{P,ALG} - (1 - f_{ALG})Y_{ALG}\, i_{P,XS} - f_{ALG}Y_{ALG}\, i_{P,ALG}$	gP gCOD^{-1}
$v_{9,3} = -((i_{O,ALG} - f_{ALG}\, i_{O,XI}) - 8(i_{H,ALG} - f_{ALG}\, i_{H,XI}) - 8/3\,(i_{C,ALG} - f_{ALG}\, i_{C,XI}) + 12/7\,(i_{N,ALG} - f_{ALG}\, i_{N,XI}) - 40/31\,(i_{P,ALG} - f_{ALG}\, i_{P,XI}))/2$	gO_2 gCOD^{-1}
$v_{10,3} = -1/14\,(i_{N,ALG}\,(1 - f_{ALG})Y_{ALG}\, i_{N,XS} - f_{ALG}Y_{ALG}\, i_{N,XI}) + 2/31\,(i_{P,ALG}\,(1 - f_{ALG})Y_{ALG}\, i_{P,XS} - f_{ALG}Y_{ALG}\, i_{P,XI})$	gH gCOD^{-1}
$v_{14,3} = -1$	gCOD gCOD^{-1}
$v_{15,3} = (1 - f_{ALG})Y_{ALG}$	gCOD gCOD^{-1}
$v_{16,3} = f_{ALG}Y_{ALG}$	gCOD gCOD^{-1}
Aerobic growth of X_H on S_{NH4}	
$v_{1,4a} = i_{N,SS}/Y_H - i_{N,BM}$	gN gCOD^{-1}
$v_{5,4a} = i_{C,SS}/Y_H - i_{C,BM}$	gC gCOD^{-1}
$v_{8,4a} = i_{P,SS}/Y_H - i_{P,BM}$	gP gCOD^{-1}
$v_{9,4a} = -((1 - Y_H)/Y_H)/2$	gO_2 gCOD^{-1}
$v_{10,4a} = -1/14\,(i_{N,SS}/Y_H - i_{N,BM}) + 2/31\,(i_{P,SS}/Y_H - i_{P,BM})$	gH gCOD^{-1}
$v_{12,4a} = -1/Y_H$	gCOD gCOD^{-1}
$v_{17,4a} = 1$	gCOD gCOD^{-1}
Aerobic growth of X_H on S_{NO3}	
$v_{3,4b} = i_{N,SS}/Y_H - i_{N,BM}$	gN gCOD^{-1}
$v_{5,4b} = i_{C,SS}/Y_H - i_{C,BM}$	gC gCOD^{-1}
$v_{8,4b} = (i_{P,SS}/Y_H - i_{P,BM})$	gP gCOD^{-1}
$v_{9,4b} = -((1 - Y_H)/Y_H)/2$	gO_2 gCOD^{-1}
$v_{10,4b} = -1/14\,(i_{N,SS}/Y_H - i_{N,BM}) + 2/31\,(i_{P,SS}/Y_H - i_{P,BM})$	gH gCOD^{-1}
$v_{12,4b} = -1/Y_H$	gCOD gCOD^{-1}

$v_{17,4b} = 1$	gCOD gCOD^{-1}
Anoxic growth of X_H on S_{NO2}	
$v_{4,5} = -(1 - Y_{H,NO2})/(1{,}71Y_{H,NO2})$	gN gCOD^{-1}
$v_{5,5} = (i_{C,SS}/Y_{H,NO2} - i_{C,BM})$	gC gCOD^{-1}
$v_{8,5} = (i_{P,SS}/Y_{H,NO2} - i_{P,BM})$	gP gCOD^{-1}
$v_{10,5} = 1/24\,(i_{O,SS}/Y_{H,NO2} - i_{O,BM}) - 1/3\,(i_{H,SS}/Y_{H,NO2} - i_{H,BM}) - 1/9\,(i_{C,SS}/Y_{H,NO2} - i_{C,BM}) + 1/93\,(i_{P,SS}/Y_{H,NO2} - i_{P,BM})$	gH gCOD^{-1}
$v_{12,5} = -1/Y_{H,NO2}$	gCOD gCOD^{-1}
$v_{17,5} = 1$	gCOD gCOD^{-1}
Anoxic growth of X_H on S_{NO3}	
$v_{3,6} = -(1 - Y_{H,NO3})/(1.14Y_{H,NO3})$	gN gCOD^{-1}
$v_{4,6} = (1 - Y_{H,NO3})/(1{,}14Y_{H,NO3})$	gN gCOD^{-1}
$v_{5,6} = (i_{C,SS}/Y_{H,,NO3} - i_{C,BM})$	gC gCOD^{-1}
$v_{8,6} = (i_{P,SS}/Y_{H,NO3} - i_{P,BM})$	gP gCOD^{-1}
$v_{10,6} = 1/14\,(i_{N,SS}/Y_{H,NO3} - i_{N,BM}) + 2/31\,(i_{P,SS}/Y_{H,NO3} - i_{P,BM})$	gH gCOD^{-1}
$v_{12,6} = -1/Y_{H,NO3}$	gCOD gCOD^{-1}
$v_{17,6} = 1$	gCOD gCOD^{-1}
Aerobic endogenous respiration of X_H	
$v_{1,7} = i_{N,BM} - f_{XI}\, i_{N,XI}$	gN gCOD^{-1}
$v_{5,7} = i_{C,BM} - f_{X1}\, i_{C,XI}$	gC gCOD^{-1}
$v_{8,7} = i_{P,BM} - f_{X1}\, i_{P,XI}$	gP gCOD^{-1}
$v_{9,7} = -(1 - f_{X1})/2$	gO_2 gCOD^{-1}
$v_{10,7} = -1/14\,(i_{N,BM} - f_{XI}\, i_{N,XI}) + 2/31\,(i_{P,BM} - f_{XI}\, i_{P,XI})$	gH gCOD^{-1}
$v_{16,7} = f_{XI}$	gCOD gCOD^{-1}
$v_{17,7} = -1$	gCOD gCOD^{-1}
Anoxic endogenous respiration of X_H	
$v_{1,8} = i_{N,BM} - f_{XI}\, i_{N,XI}$	gN gCOD^{-1}
$v_{3,8} = (f_{XI} - 1)/1{,}14$	gN gCOD^{-1}
$v_{4,8} = (1 - f_{XI})/1{,}14$	gN gCOD^{-1}
$v_{5,8} = i_{C,BM} - f_{XI} i_{C,XI}$	gC gCOD^{-1}
$v_{8,8} = i_{P,BM} - f_{XI} i_{P,XI}$	gP gCOD^{-1}
$v_{10,8} = 1/40\,(i_{O,BM} - f_{XI} i_{O,XI}) - 1/5\,(i_{H,BM} - f_{XI} i_{H,XI}) - 1/15\,(i_{C,BM} - f_{XI} i_{C,XI}) + 1/35\,(i_{N,BM} - f_{XI} i_{N,XI}) - 1/31\,(i_{P,BM} - f_{XI} i_{P,XI})$	gH gCOD^{-1}
$v_{16,8} = f_{XI}$	gCOD gCOD^{-1}
$v_{17,8} = -1$	gCOD gCOD^{-1}
Decay of X_H	
$v_{15,9} = (1 - f_{XI})c$	gCOD gCOD^{-1}
$v_{16,9} = f_{XI} Y_H$	gCOD gCOD^{-1}

$v_{17,9} = -1$	gCOD $gCOD^{-1}$
Growth of ammonia oxidizing bacteria (X_{AOB})	
$v_{1,10} = -1/Y_{AOB} - i_{N,BM}$	gN $gCOD^{-1}$
$v_{4,10} = 1/Y_{AOB} - i_{N,BM}$	gN $gCOD^{-1}$
$v_{5,10} = -i_{C,BM}$	gC $gCOD^{-1}$
$v_{8,10} = -i_{P,BM}$	gP $gCOD^{-1}$
$v_{9,10} = (1 - 3{,}43/Y_{AOB})/2$	gO_2 $gCOD^{-1}$
$v_{10,10} = 2/14Y_{AOB} - 1/14\,(i_{N,BM}) - 2/31\,(i_{P,BM})$	gH $gCOD^{-1}$
$v_{18,10} = 1$	gCOD $gCOD^{-1}$
Growth of nitrite oxidizing bacteria (X_{NOB})	
$v_{3,11} = 1/Y_{NOB} - i_{N,BM}$	gN $gCOD^{-1}$
$v_{4,11} = -1/Y_{NOB}$	gN gCOD-1
$v_{5,11} = -i_{C,BM}$	gC $gCOD^{-1}$
$v_{8,10} = -i_{P,BM}$	gP $gCOD^{-1}$
$v_{9,11} = (1 - 1{,}14/Y_{NOB})/2$	gO_2 $gCOD^{-1}$
$v_{10,11} = -1/14\,(i_{N,BM}) - 2/31\,(i_{P,BM})$	gH $gCOD^{-1}$
$v_{19,11} = 1$	gCOD $gCOD^{-1}$
Endogenous respiration of X_{AOB}	
$v_{1,12} = i_{N,BM} - f_{XI}\, i_{N,XI}$	gN $gCOD^{-1}$
$v_{5,12} = i_{C,BM} - f_{XI} i_{C,XI}$	gC $gCOD^{-1}$
$v_{8,12} = i_{P,BM} - f_{XI} i_{P,XI}$	gP $gCOD^{-1}$
$v_{9,12} = -(1 - f_{XI})/2$	gO_2 $gCOD^{-1}$
$v_{10,12} = -1/14\,(i_{N,BM} - f_{XI}\, i_{N,XI}) + 2/31\,(i_{P,BM} - f_{XI}\, i_{P,XI})$	gH $gCOD^{-1}$
$v_{16,12} = f_{XI}$	gCOD $gCOD^{-1}$
$v_{18,12} = -1$	gCOD $gCOD^{-1}$
Endogenous respiration of X_{NOB}	
$v_{1,13} = i_{N,BM} - f_{XI}\, i_{N,XI}$	gN $gCOD^{-1}$
$v_{5,13} = i_{C,BM} - f_{XI} i_{C,XI}$	gC $gCOD^{-1}$
$v_{8,13} = i_{P,BM} - f_{XI} i_{P,XI}$	gP $gCOD^{-1}$
$v_{9,13} = -(1 - f_{XI})/2$	gO_2 $gCOD^{-1}$
$v_{10,13} = -1/14\,(i_{N,BM} - f_{XI}\, i_{N,XI}) + 2/31\,(i_{P,BM} - f_{XI}\, i_{P,XI})$	gH $gCOD^{-1}$
$v_{16,13} = f_{XI}$	gCOD $gCOD^{-1}$
$v_{19,13}$ = -1	gCOD $gCOD^{-1}$
Decay of X_{AOB} and X_{NOB}	
$v_{15,14a} = (1 - f_{XI})Y_{AOB}$	gCOD $gCOD^{-1}$
$v_{16,14a} = f_{XI} Y_{AOB}$	gCOD $gCOD^{-1}$
$v_{18,14a}$ = -1	gCOD $gCOD^{-1}$

$v_{15,14b} = (1 - f_{XI})Y_{NOB}$	gCOD gCOD^{-1}
$v_{16,14b} = f_{XI}Y_{NOB}$	gCOD gCOD^{-1}
$v_{19,14b} = -1$	gCOD gCOD^{-1}
Hydrolysis	
$v_{1,15} = -(1 - f_{SI})i_{N,SS} - f_{SI}i_{N,SI} + i_{N,XS}$	gN gCOD^{-1}
$v_{5,15} = i_{C,XS} - (1 - f_{SI})Y_{HYD}i_{C,SS} - f_{SI}Y_{HYD}i_{C,SI}$	gC gCOD^{-1}
$v_{8,15} = i_{P,XS} - (1 - f_{SI})Y_{HYD}i_{P,SS} - f_{I,XS}Y_{HYD}i_{P,SI}$	gP gCOD^{-1}
$v_{10,15} = -1/14\left(i_{N,XS} - (1 - f_{SI})Y_{HYD}i_{N,SS} - f_{SI}Y_{HYD}i_{N,SI}\right) + 2/31\left(i_{P,XS} - (1 - f_{SI})Y_{HYD}i_{P,SS} - f_{SI}Y_{HYD}i_{P,SI}\right)$	gH gCOD^{-1}
$v_{12,15} = (1 - f_{SI})Y_{HYD}$	gCOD gCOD^{-1}
$v_{13,15} = (f_{SI})Y_{HYD}$	gCOD gCOD^{-1}
$v_{15,15} = -1$	gCOD gCOD^{-1}
Chemical equilibria $CO_2 \leftrightarrow HCO_3^-$	
$v_{5,16} = -1$	gC gC^{-1}
$v_{6,16} = 1$	gC gC^{-1}
$v_{10,16} = 1/12$	gH gC^{-1}
Chemical equilibria $HCO_3^- \leftrightarrow CO_3^{2-}$	
$v_{6,17} = -1$	gC gC^{-1}
$v_{7,17} = 1$	gC gC^{-1}
$v_{10,17} = 1/12$	gH gC^{-1}
Chemical equilibria $NH_4^+ \leftrightarrow NH_3$	
$v_{1,18} = -1$	gN gN^{-1}
$v_{2,18} = 1$	gN gN^{-1}
$v_{10,18} = 1/14$	gH gN^{-1}
Chemical equilibria $H^+ \leftrightarrow OH^-$	
$v_{10,19} = 1$	gH gH^{-1}
$v_{11,19} = 1$	gH gH^{-1}
Oxygen transfer to the atmosphere	
$v_{9,20} = 1$	–
Carbon dioxide transfer to the atmosphere	
$v_{5,21} = 1$	–
Ammonia transfer to the atmosphere	
$v_{2,22} = 1$	–